University of Southern Queensland

AN INVESTIGATION INTO THE EFFECT OF MATERIAL COMPOSITION ON THE FUNDAMENTAL PROPERTIES OF PERMEABLE CONCRETE

A Dissertation submitted by

Manal Hussin

For the award of Master of

Engineering and Surveying 2012

CERTIFICATION OF DISSERTATION

I certify that the work in this thesis has not been previously submitted for any degree and nor has it been submitted as part of a requirement for a degree except where fully acknowledged within the text.

I also certify that I have written this thesis and that any help that I have received in my research work and in the preparation of this thesis has been acknowledged. I also certify that I have fully referenced all sources of information and literature that I have used in this thesis.

_____ _____

Date

_____ _____

Date

_____ _____

Date

_____ Date _____

ACKNOWLEDGEMENT

I am extremely grateful to my supervisors Dr.Yan Zhuge, Professor Frank Bullen and Dr.Weena Lokuge for their enthusiastic guidance, invaluable help and encouragement in all aspects of this research project. Their numerous comments, criticisms and suggestions during the preparation of this thesis are gratefully acknowledged. Their patience and their willing availability for helping with this heavy workload, whenever needed, was very much appreciated.

I also would to express my gratitude to the technical staff of the Faculty of Engineering and Surveying – Mr. Daniel Eising, Mr. Mohan Trada and Mr. Wayne Crowell, for their generous help and support. My gratitude to Mrs. Jane Eberhardt for her help in editing and proofreading this thesis.

I would also like to thank my fellow postgraduate students in the Faculty of Engineering and Surveying for their discussion, support and social interaction during my study.

I sincerely thank my husband Atef Kadom for his wonderful encouragement and support during this study and my parents Kamil Hussin and Karema Mohamed, my brothers and my children for instilling in me a desire to learn and to pursue knowledge. I may not have achieved all that I have, including this thesis, without their words of wisdom.

ABSTRACT

The use of permeable concrete in the construction industry has been increasing around the world during the last few years. The fundamental properties of permeable concrete must thus be comprehensively evaluated and elucidated in order to obtain the full benefits of this material. This research investigated the effects of material composition on the mechanical properties (compressive strength, stress-strain behaviour and the modulus of elasticity) and on the hydraulic properties (porosity ratio and permeability) of the permeable concrete.

Eight different permeable concrete mix designs were prepared with two aggregate sizes in two different proportions, different sand ratios, two aggregate to cement ratios and a constant water to cement ratio. The target 28-day compressive strength was designed to be between 15MPa and 35MPa. The porosity ratio was designed to be between 25% and 15%, whilst the permeability was designed to be between 12mm/sec to 2mm/sec.

A review of the published literature revealed no standard experimental procedure for determining the stress-strain behaviour and the modulus of elasticity of permeable concrete using the strain gauge method. The only method in use was the platen-to-platen method. This research involved the development of a testing method for determining these properties using the strain gauge method. The results are compared with those that were obtained using the platen-to-platen method. A significant difference was found between the properties that were measured by these two methods.

A semi-empirical equation to represent the complete stress-strain behaviour for unconfined permeable concrete is proposed as part of this research. Various existing models for low-strength concrete and normal-strength concrete were used and

compared with the experimental data. Various parameters were studied and their relationships were experimentally determined. The only parameters needed to run the new model is the ultimate compressive strength and the density. The proposed semi-empirical stress-strain equations were compared with actual cylinder tests results under axial compression; the new model gives a good representation of the mean behaviour of the actual stress-strain response of the permeable concrete.

LIST OF PUBLISHED PAPERS

Hussin, M, Zhuge,Y, Bullen ,F & lokuge, W 2011, 'Laboratory Evaluation of the Stress-Strain relationship of Permeable Concrete', *Advanced Materials Research,* vols. 243-249, pp. 3259-3262, viewed item: DOI: 10.4028/www.scientific.net/AMR.243-249.3259.

Hussin, M, Zhuge,Y, Bullen ,F & lokuge, W 2012, 'Investigation of Some Fundamental Properties of Permeable Concrete', *Advanced Materials Research,* vol. 487, pp. 869-73, viewed item: DOI: 10.4028/www.scientific.net/AMR.487.869.

Hussin, M, Zhuge,Y, Bullen ,F & lokuge, W 2012, 'A mathematical model for complete stress-strain curve prediction of permeable concrete'. Submitted to 22nd AUSTRALASIAN CONFERENCE ON THE MECHANICS OF STRUCTURES AND MATERIALS (ACMSM). ACMSM will be held at the University of Technology Sydney, Australia on 11-14 December, 2012.

TABLE OF CONTENT

LIST OF FIGURES

CHAPTER 1:

CHAPTER2:

CHAPTER 3:

CHAPTER 4

CHAPTER 5

LIST OF TABLES

CHAPTER 3

CHAPTER4

CHAPTER 5

APPENDICES

APPENDIX A

APPENDIX B

APPENDIX C

LIST OF SYMBOLS

P	*Porosity ratio*
M_{dry}	*Oven dry weigh*
M_{sub}	*Submerged weigh*
V_T	*Total volume*
ρ_w	*Density of water*
P_c	*Correct porosity in the site*
P_i	*Porosity in the site*
D_a	*Maximum aggregate size*
D_c	*Core diameter*
P_{min}	*Minimum porosity*
P_{max}	*Maximum porosity*
K	*Permeability coefficient*
a	*Cross-section area of the cylinder pipe*
A	*Cross-section area of the specimen*
L	*Length of the specimens*
t	*Time for water to pass from level h_1 to h_2*
h_1	*Initial water level (290mm)*
h_2	*Final water level (70mm)*
E_{itsg}	*MOE for the strain gauge*
E_{itp}	*MOE for the platen-to-platen*
E_{it}	*Initial tangent modulus of elasticity*
E_o	*Secant modulus of elasticity at peak stress*
β	*Material parameter*
f_c	*Concrete stress*
f'_c	*Maximum stress*
ε_{max}	*Concrete strain when concrete stress is equal to 0.5 f'_c on the descending part of the stress-strain curve*
ε	*Concrete strain*
ε_d	*Strain corresponds to a stress value of 0.3 f'_c in the descending part of the stress-strain curve*
ε_o	*Corresponding strain at maximum stress*
λ	*Power transformation*
d_n	*Number averaged pore size*
$\emptyset_A$	*Area fraction of pores*
d_{MFS}	*Mean free spacing of pores*
S_p	*Specific surface area of pores*

Γ_{3D}	*Three-dimensional of pore distribution density*
$\alpha_0, \alpha_1, \alpha_2$	*Parameters*
ρ	*Dry unit weight*
n	*Parameters*
$P_{area}\%$	*Percentage of the pore area*
A_p	*Total cross-section pores in the specific part of the specimen*
A_t	*Total cross-sectional area of the specific part of the specimen*

CHAPTER 1
INTRODUCTION

1.1 Background

1.1.1 Permeable concrete

Rapid urbanisation has led to an increasing rate of consumption of natural resources and this can cause environmental problems. One such problem is the increase in impervious areas such as in roads and in car parks, which had been previously permeable (Wanielista et al. 2007). These impervious surfaces block the natural process of water infiltration into the soil, and result is increased runoff from such areas after heavy stormwater and snowmelt events. This runoff results in three main environmental problems:

- A decrease in ground water recharge due to the lack of infiltration
- An alteration in the natural flow patterns within a drainage basin
- The transportation of contaminants such as sediments, nutrients, and heavy metals into stream channels via overland water flows

(Wanielista et al. 2007)

Various strategies are thus being investigated by researchers such as Dudley et al. (2011) to help to protect and to restore the natural ecosystems. One of these strategies is using a perm**e**able pavement, which has built-in void spaces to allow water and air to pass through (Wanielista et al. 2007). Ferguson (2005) divided these permeable pavements into nine groups including porous asphalt, permeable concrete, concrete paving blocks, gravel paving systems, and grass paving systems. This research has focused on permeable concrete (or as other

researchers name it pervious concrete or porous concrete), which is a type of concrete that has both a higher porosity and a significantly higher water permeability than normal concrete. Its physical characteristics thus differ greatly to those of conventional concrete (Tennis, Leming & Akers 2004).

Permeable concrete has several advantages including:

- It allows stormwater to infiltrate into a storage basin below the pavement or to the soil and, finally, to recharge the water table.
- It has the capability to capture the first flush of the runoff, which usually carries a significant portion of the pollutants from the pavement (Tennis, Leming & Akers 2004).
- It maintains the quantity of stormwater runoff and leads to an improvement in the water quality (Deo 2011).
- It produces better road safety due to the peculiar macro-texture of the permeable concrete, which increases the skid resistance (Schaefer et al. 2006).
- It dampens road noise from tyre-pavement interactions.
- The open structure of permeable concrete, which allows air and water to flow through it, reduces the urban heat island effect (Brown 2003; Wanielista et al. 2007; Yang & Jiang 2003).
- The use of the pavement for retention decreases the size of, or the need for, rainwater retention facilities in road-works. The labour and maintenance costs associated with implementing stormwater management systems such as retention ponds, pumps, swales, and storm sewers can be possibly reduced,

or even eliminated, with the proper construction of permeable concrete pavements.

- The roots of plants and trees in close proximity to these pavements benefit from better watering and aeration.

Figure1.1 below shows a demonstration of permeable concrete paving.

Figure 1.1 Permeable concrete paving demonstration

(http://en.wikipedia.org/wiki/Permeable_paving)

The use of permeable concrete has thus continued to grow in popularity among civil engineers for a range of different applications. These include: for parking lots, for drive ways and sidewalks, for noise absorption concrete, for thermally

insulated concrete, and for other civil engineering and architectural applications (Chindaprasirt et al. 2008).

Despite these previously mentioned advantages, there are still some concerns about using the permeable concrete in particular areas that are subjected to high traffic volume. Some challenges are highlighted below:

- In a cold weather situation, there is a potential for clogged void spaces that can lead to a reduction in its drainage capacity thus necessitating frequent maintenances during its life circle. Regular inspection and preventative maintenance will however; keep it working for many years.
- The structural capacity of the permeable concrete is dependent on its induced pore structural features and on the interaction between the cement paste and the coarse aggregate (Doe 2011). It may have lower strength and durability due to the absence or minimal quantity of the used sand or due to the existence of large pore volumes. The current use of permeable concrete is thus limited to areas that are subjected to low-traffic volume.

1.1.2 Historical use of permeable concrete

Permeable concrete was originally used in the construction of two storey homes and became more widely used during a period of material shortages in Europe after World War II (Offenberg 2008). Wanielista et al. (2007) noted that cost efficiency was the primary reason for its earliest usage due to the limited amount of cement that was required. It had also been used in the United States in the 1970's where its use began, not as a cheaper substitute for conventional concrete although that was advantageous, but for its permeability

characteristics (Wanielista et al. 2007). Excessive runoff from newly constructed areas was a major problem in the United States at that time. The amount of impervious area had increased as more land development had taken place. This had produced an increase in runoff, which then led to flooding and to an increase in water and soil pollution. This had a negative impact on the environment and caused degradation in the quality of the runoff water (Wanielista et al. 2007).

A large number of projects in United States have been completed over the last few years using this form of concrete and its biggest use has been in landscaping, in building car parks, pedestrian ways and public parking lots, in noise-absorbing concrete and in other civil engineering structures (Chindaprasirt et al. 2008; Tennis, Leming & Akers 2004). There has been Japanese research into permeable concrete for use in road surfaces and to support vegetation along river banks (Aoki 2009). Research into the structural and hydraulic properties of eco-paving has also been undertaken in Australia since 1994. The University of New South Wales (UNSW) began research into permeable concrete paving in 1994 and, more recently, the University of South Australia (UniSA) also became involved in research into this new material (Lian & Zhuge 2010). The research work at UniSA focused mainly on water quality and on pollution control using permeable pavements but only the properties of the base course materials in permeable pavement systems and segmental paving have been studied (Lian & Zhuge 2010).

Although fundamental information about the mechanical and hydraulic properties of permeable concrete including the influence of the water to the

cement ratio (W/C), the cement-paste characteristics, the coarse aggregate, the size, and the type were studied (Chindaprasirt et al. 2008; Ghafoori & Dutta 1995; Lian & Zhuge 2010; Yang & Jiang 2003), several of its performance characteristics are not yet fully understood. Among them is the influence of the material design of the permeable concrete on its structural performance, on its stress-strain behaviour, and on its modulus of elasticity; these are the focus for this research. On the other hand, most of the testing methods that had been used to find the fundamental properties of permeable concrete had been adopted from the conventional concrete standards; the relevance of such methods could be questionable. It is, therefore, very important to develop a proven and relevant testing method that is suitable for permeable concrete rather than just using the traditional standards for normal concrete.

1.2 Objectives of the investigation

The main objectives of this research are as follows:

1. To investigate the fundamental properties of the permeable concrete, which is made with different blends of aggregate sizes and sand ratios.
2. To establish new testing methods for determining the modulus of elasticity and the stress-strain behaviour of permeable concrete rather than just using the simplistic platen-to-platen method.
3. To develop a mathematical model for predicting the stress-strain relationship of the permeable concrete.

1.3 Scope of the investigation

1. To investigate the effect of varying attributes such as the aggregate size, the sand ratio, and the cement paste on the mechanical and hydraulic properties of the permeable concrete.
2. To provide those practitioners that are involved in the testing of permeable concrete with methods for the determination of the static chord modulus of elasticity, focusing on the introduction of the strain gauge for strain measurements of permeable concrete samples under a uni-axial compression test.
3. To determine reliable relationships between the compressive strength, porosity, permeability and the modulus of elasticity for permeable concrete.
4. Proposed a mathematical model for predicting the stress-strain relationship of the permeable concrete having different compressive strength and different porosity ratios.

1.4 Thesis outline

Chapter 1 introduces permeable concrete, examines its historical usage, and highlights the research objectives and scope.

Chapter 2 provides a comprehensive review of the literature, which underpins the present study. This covers a review of the materials used in permeable concrete, their fundamentals properties, and the methods used in testing them.

Chapter 3 outlines the methodologies that were adopted for this research and the experimental details. The experimental procedure for the strain measurement that was developed in this study is also detailed.

Chapter 4 presents the results of the experimental investigations and provides a discussion of the results. The mechanical and hydraulic properties of permeable concretes of different compositions are compared and analysed.

Chapter 5 development of a mathematical model for prediction of the complete stress-strain curve of permeable concrete

Chapter 6 presents the conclusions of this research and provides recommendations for future research.

The thesis concludes with the list of appendixes, references and standards.

CHAPTER 2
LITERATURE REVIEW

2.1 Introduction

Permeable concrete is commonly described as a mixture of Portland cement, uniform coarse aggregate, water, little or no sand, chemical admixtures and/or supplementary cementing materials in some cases (Crouch, Pitt & Hewitt 2007; Huang et al. 2010). The resultant mix is inherently porous with a wide variety and distribution of pore sizes and shapes depending on the mix design adopted. Permeable concrete contains a large number of pore spaces, which range in size from 2mm to 8mm and that vary between 10% and 35% by volume; this allows water to pass through the hardened mass at a rapid rate. This porosity ratio can be achieved by gap-grading the coarse aggregate and by either eliminating, or by minimising, the volume of fine aggregates in the mixture. This creates a network of interconnected pores within the material (Doe 2011).

Permeable concrete is very sensitive to a change in the water content (Obla 2010); too much water will cause paste to drain down to fill the voids and too little water can hinder curing and can lead to premature surface failure. According to Deo (2011), the preferred W/C usually ranges between 0.28 and 0.34, whilst Ghafoori and Dutta (1995) and Tennis, Leming and Akers (2004) recommended a W/C ratio for the permeable concrete of between 0.3 and 0.4.

Other researchers (Ghafoori & Dutta 1995; Tennis, Leming & Akers 2004; Yang & Jiang 2003) have studied the effect of the aggregate-to-cement ratio

(A/C) on the fundamental properties of the permeable concrete. Most of these authors suggested that the A/Cs should range from 4:1 to 4.5:1 by mass, while Ghafoori and Dutta (1995) used four different A/Cs - 4:1, 4.5:1, 5:1 and 6:1. Their results showed that a high proportion of aggregate led to an increase in permeability and to a dramatic decrease in the compressive strength. Permeable concrete can achieve a compressive strength in excess of 20MPa and even more, by using appropriately selected aggregate, by the inclusion of competent structural design, using organic intensifiers, and by special placement techniques. The durability of permeable concrete can also be further enhanced with the use of supplementary cementing materials such as silica fume, fly ash, and blast furnace slag (Yang & Jiang 2003). The load-bearing capacity of a permeable concrete pavement can be further increased by installing sub-grade and sub-base levels of coarse aggregate underneath the pavement. Permeable concrete pavements are expected to have a life cycle of between 20 to 40 years with little maintenance when the preparation, compaction and curing are done properly (Doe 2011).

2.2 Fundamental properties of permeable concrete

The mechanical properties of permeable concrete can be investigated in terms of the compressive strength, the modulus of elasticity, the stress-strain behaviour, and the required testing methods, whilst the hydraulic properties can be studied by considering the porosity, the pore area, and the permeability of the hardened mass.

2.2.1 Compressive strength

The structural characteristics of permeable concrete are different from those of conventional concrete due to its high porosity. Permeable concrete generally has a lower compressive strength, a higher permeability and a lower unit weight, which is approximately 70% of conventional concrete (Wanielista et al. 2007). Laboratory studies have shown that there is a wide range of values for the 28-day compressive strength of permeable concrete. Tennis, Leming and Akers (2004) reported that the compressive strengths of permeable concrete are in the range of 3.5MPa to 28MPa with an average value of 17MPa, whilst Ghafoori and Dutta (1995) reported that the compressive strength could be 21MPa or more. This latter is achievable by adding chemical admixtures, by employing the proper W/C, A/C ratio and compaction method.

Earlier studies have shown that there are several parameters such as the W/C ratio, the amount of fine aggregate, the type and size of the coarse aggregate, the A/C ratio and the compaction energy that affect the compressive strength, the porosity and the permeability of permeable concrete. Chopra and Wanielista (2007) observed that the A/C ratio does have a major effect on the compressive strength of the permeable concrete system. These authors noted that when the A/C ratio increased, the compressive strength also decreased. Yang and Jiang (2003) further observed that use of a smaller aggregate size could improve the strength. The use of smaller aggregate sizes can increase the number of particles per unit volume; this eventually increases the binding area between the aggregate particles and results in an improved strength of permeable concrete. Other researchers have found that the W/C ratio has

another effect on the compressive strength of permeable concrete. Control of the water quantity is necessary to produce a fresh cement paste with a good workability that does not clog up all of the pores. Deo (2011) preferred a very low W/C for use with permeable concrete, which usually ranged from 0.28 to 0.34, to produce the right amount of cement paste to form a thin coating around the coarse aggregate without making the mixture either too dry or too wet. Wang et al. (2006) noted that the cement paste should be just enough to coat the aggregate particles in a thin layer, and recommended that the layer should be 200 μm in thickness. These authors recommended a W/C of 0.27 or lower, but also suggested that it can be further reduced if the workability of the permeable concrete is improved, since the excessive cement paste may seal the voids between the aggregate particles.

Since cement paste in the permeable concrete is minimised to provide a very thin layer for bonding the coarse aggregate together, the concrete thus tends to fail at the binder interface between the aggregates, resulting in a relatively low compressive strength (Lian & Zhuge 2010). Yang and Jiang (2003) suggested that the cement paste should be strengthened by using admixtures to improve the strength properties of the permeable concrete. Lian and Zhuge (2010) and Yang and Jiang (2003) also found that permeable concrete can reach compressive strengths as high as 49.6MPa with a tensile strength about 5.9MPa, respectively, by including the silica fume and super plasticizer; this can, however, reduce the permeability to less than 2mm/sec. Other researchers such as Kevern (2008) and Ghafoori and Dutta (1995) have used chemical additives to improve the strength. Kevern (2008) found that the addition of a

polymer-styrene butadiene rubber (SBR), would significantly improve workability, strength, permeability and freeze-thaw resistance. This produces a higher-strength permeable concrete with relatively lower-cement content and results in a relatively higher porosity.

2.2.2 Modulus of elasticity (MOE)

The MOE is generally defined as a gradient of the linear, elastic section of the stress-strain curve. For concrete, MOE is defined as the slope of the straight line drawn from the "origin" to 40% of the peak strength of that particular concrete according to AS-1012.17 (1997). It is particularly important in concrete from a design point of view since it describes the concrete's mechanical behaviour, reflects the ability of the concrete to deform elastically, and determines the strain distributions and displacements. For that reason, many researchers (Alexander & Milne 1995; Beshr, Almusallam & Maslehuddin 2003; Li & Zheng 2007; Neville 1997; Noguchi et al. 2009; Wu et al. 2001) studied parameters that affect the elastic behaviour of the conventional concrete such as the W/C ratio and the coarse aggregate that was used. Beshr, Almusallam and Maslehuddin (2003) pointed out that, for normal and lightweight concrete (with a compressive strength of less than 41MPa), the properties of the aggregate rarely has an effect on the compressive strength. The weakest components in the concrete within this range are the hardened cement paste film and the transition zones between the cement paste and the coarse aggregate, rather than the coarse aggregate itself. Figure 2.1 shows the modulus of elasticity of the hardened cement and the coarse aggregate.

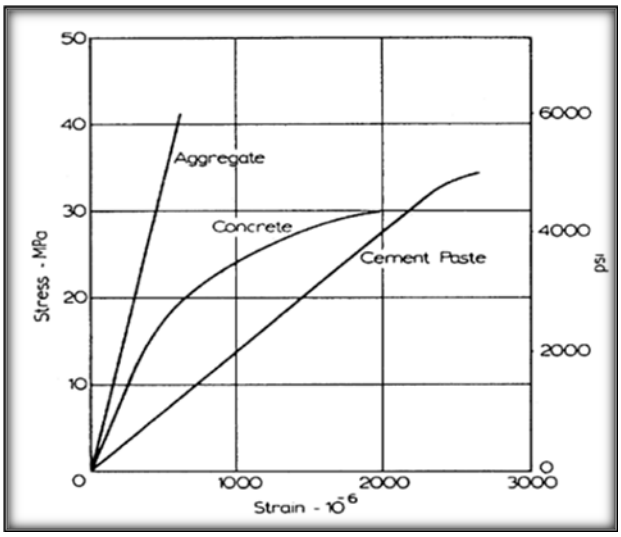

Figure 2.1 Stress-strain relations for cement paste, aggregate and concrete

(Neville 1997, p.72)

By contrast, Wu et al. (2001) pointed out that the coarseness of the aggregate is the main factor affecting the MOE of normal strength concrete. Conventional concrete can be considered as a composition of aggregate that has been bonded together with cement paste so that the voids are completely filled with paste. Such concretes are also often termed dense-graded due to the combined particle size distribution. Concrete with a high, coarse-aggregate ratio thus exhibits a higher MOE since the aggregate is a stiffer material in the concrete. It has been reported that the size of the coarse aggregate has another effect on the MOE of the concrete. Oluokun, Burdette and Deatherage (1991) found that the smaller aggregate size resulted in a higher compressive strength at equal aggregate content but that the opposite is true for the MOE, which increases with larger aggregate sizes.

Cement type also influences the MOE and the compressive strength of the concrete (Alexander & Milne 1995) as mineral additives, which are used to supplement or to replace ordinary Portland Cement such as silica fume, fly ash and slag, change the structure of the tobermorite gel and influence the interfacial zone and bond in the concrete. Larbi (1993) observed that these additives improve the microstructure and reduce the thickness of the transition zone; this can be expected to increase both the strength and the MOE.

The different roles of the paste and the pore network characteristics lead to different compressive strengths and MOE behaviours between conventional and permeable concrete. The factors that affect the MOE of the conventional concrete may thus not work with the permeable concrete. Crouch, Pitt and Hewitt (2007) pointed out that the coarse aggregate is the main factor that affects the MOE of permeable concrete. These authors studied the effects of the aggregate's grading, size, and amount on the MOE. It was found that a more uniform grade of aggregate results in a slightly higher compressive strength and MOE for equal void contents within an optimum void range of 23% to 31%. The compressive strength also decreases and the static modulus of elasticity slightly increases when using larger aggregate sizes with effective void ratios ranging from 26% to 33%. Increasing the size of the aggregates in permeable concrete resulted in an increase in the modulus of elasticity, which was consistent with conventional concrete, whilst increasing the amount of aggregate resulted in a decrease in both the compressive strength and in the MOE.

Researchers such as Crouch, Pitt and Hewitt (2007), Ghafoori and Dutta (1995), and Goede (2009) used different measurements to determine the MOE of the permeable concrete. Crouch (2007) and Goede (2009) determined the MOE according to ASTM C-469 (2002). Crouch, Pitt and Hewitt (2007) found that the MOE ranged from 10GPa to 30GPa for permeable concrete with compressive strength between 5MPa and 45MPa and porosity ranging from 35% to 15 %. Goede (2009) found that in permeable concrete, with a typical compressive strength ranging between 9.2MPa and 11.5MPa and porosity ranging from 28.2% to 25.9%, that the MOE ranged between 9.7GPa and 15.2GPa. Ghafoori and Dutta (1995) also determined that the MOE corresponded to 40% of the ultimate compressive strength, as suggested by the American Concrete Institute (ACI). It was found that the MOE ranged between 9.1GPa to 19.1GPa for permeable concrete with a typical density of 1569 to 1938 kg/cm^3, with a compressive strength of 8.68MPa to 31.3MPa and with a porosity range of between 30% to 10%.

The conclusions drawn from this literature review is that the compressive strength and the elastic behaviour of the permeable concrete are significantly different to those of the conventional concrete. This difference is mainly due to a difference in the paste thickness and characteristics around the aggregate particles, the high porosity, and the larger voids in the permeable concrete.

2.2.3 Stress-strain behaviour

The engineering design of structures using concrete requires a thorough knowledge of the basic principles of stress-strain analysis and measurements.

This behaviour, however, represents a comprehensive response of the concrete to external forces. It can reflect the influence of a damage process, the micro-crack development including random occurrence and localisation, or the formation and propagation of major cracks on a global scale (Jin & Li 2000). Beyond the ultimate strength, the load carrying capacity of concrete under a compressive state of stress progressively reduces along with increasing deformation. The way in which it reduces proves to be an important characteristic of the material's behaviour. An analysis of this behaviour helps to improve the safety, the durability and the reliability of the concrete structure (Doe 2011).

During the testing of a material sample, the resultant stress-strain curve, which is obtained directly or indirectly, is a graphical representation of the relationship between the stress that is derived from measuring the load applied on the sample, and the strain that is derived from measuring the deformation of the sample, that is, the elongation, compression, or distortion. The nature of the curve varies from material to material (Brinson & Brinson 2008) and the following figure 2.2 illustrates the stress-strain behaviour of brittle and ductile materials.

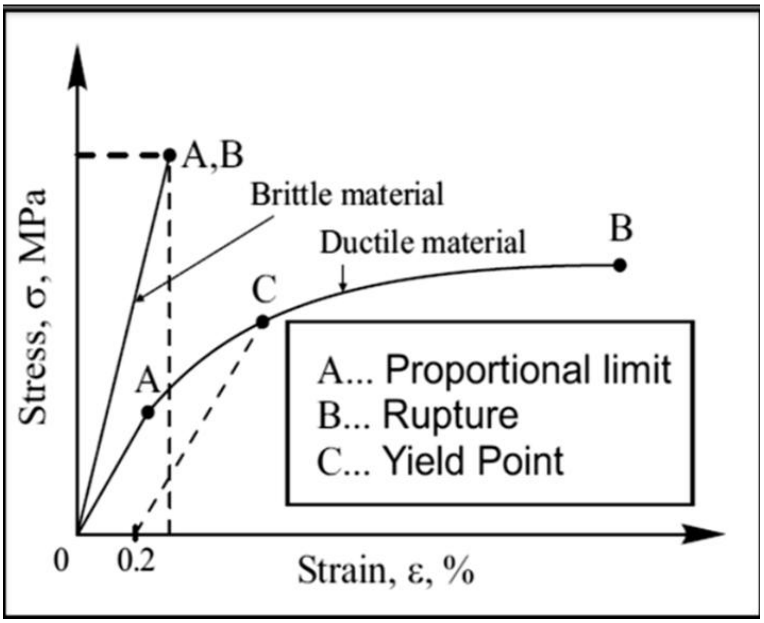

Figure 2.2 Stress-strain diagrams for brittle and ductile materials

(Brinson & Brinson 2008, p.25)

The stress-strain diagram of brittle materials such as for concrete and carbon fibre can divided into three parts:

- The elastic part: The stress-strain curve is linear from the initial loading (origin point) nearly to (point A); it is also known as the "proportional limit ". The response at this part, if the load is released, can be traced back to its original point unless there has been an instance where the loading is extended beyond this limit. The modulus of elasticity can be obtained in this part from the slope of the curve because the transition-zone crack remains stable.
- Beyond the proportional limit, the curve deviates gradually from the straight line up to the critical load beyond which the stress-strain curve begins to bend more sharply to the horizontal until it reaches the peak load at the

rupture point (B). At this point, the crack propagation starts on the interfaces when stress is above the proportional limit and continues beyond the critical load where it penetrates the mortar. This causes a progressive break-down and discontinuity in the internal structure of the concrete.

- The descending branch of the post-peak response starts once the peak stress is reach. This part becomes steeper with an increase in the specimen length, which corresponds to an increase in the brittleness

Khan and Wang (2000) observed that brittle materials do not have a yield point, and do not strain-harden and, as a result, the ultimate strength and the breaking strength are the same; the stress-strain diagram may be non-linear for ductile materials from the initial yield point until the final rupture.

The stress-strain curve of the permeable concrete shows the same brittle behaviour and has the same sections in the stress-strain curve that are observable for the brittle materials even though it does possess a higher porosity. Figure 2.3 below illustrates the stress-strain diagram for the permeable concrete.

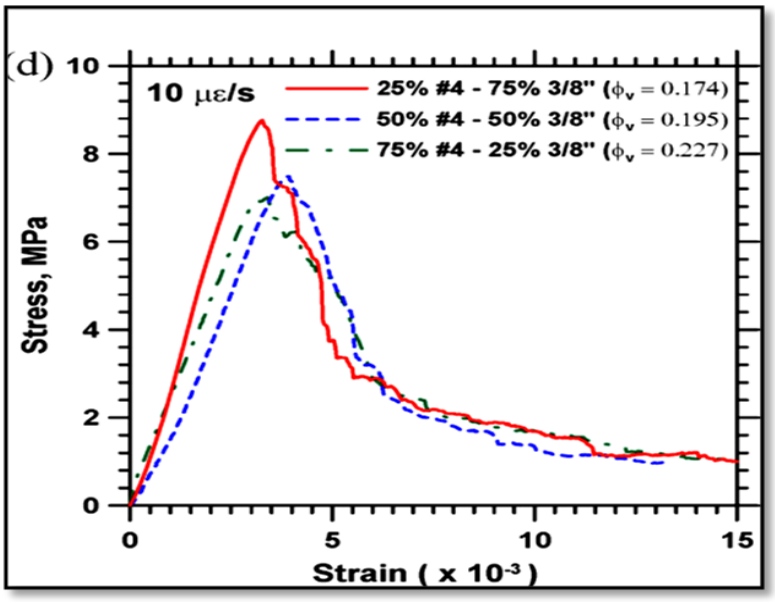

Figure 2.3 Stress-strain curves of the permeable concrete

(Deo & Neithalath 2010, p.4)

The stress-strain response is generally found to be linear at low stress levels for all concrete types and strength levels. It changes, however, to a non-linear response as it approaches the peak stress. This linear and non-linear stress variation corresponds to the elastic and in-elastic deformation that is occurring in the material due to the applied uni-axial load near the peak stress (Deo & Neithalath 2010).

2.2.4 Measurements techniques for the axial deformation (non platen to platen)

Two different measurements are used to measure the axial deformation in the concrete. These are contact and contact-free measurements. The main differences between them are that the contact method measures the deformation in the contact points, whereas the second method avoids the

contact with the specimen. The use of contact-free methods in comparison with the contact one have, however, already been shown to be costly (Šemberk & Kohoutková 2005).

2.2.4.1Contact methods

The common methods that have been used to measure the local axial deformations in the concrete are the compressometer, strain gauges and DEMEC.

2.2.4.1.1 The compressometer

The compressometer is used for evaluating the axial deformation and the strain characteristics of concrete cylinders whilst undergoing compression testing, and this provides the data for a stress-strain diagram. It consists of a set of top and bottom metal rings with a yoke in the centre that moves with the specimen under controlled loading. The deflection gauges register changes in the length of the concrete cylinders as the vertical pressure is increased. The gauge straps are removed after assembly and before any load is applied, thus leaving the specimen positioned in the compression machine. There are two types of compressometers: one with a dial gauge, which consists of two horizontal and parallel rings and one dial gauge, and one with three horizontal and parallel rings and two digital gauges as show in figure 2.4.

1. Compressometer with dial gauge 2. Compressometer with digital indicator

Figure2.4 Compressometer types

http://www.humboldtmfg.com/c-3-p-244-id-3.html#1335

2.2.4.1.2 Strain gauge

There are different types of strain gauges that are used with conventional concrete and other solid materials including the resistive (the common one), the capacitive, the inductive, and the photoelectric types. Figure 2.5 shows a typical strain gauge.

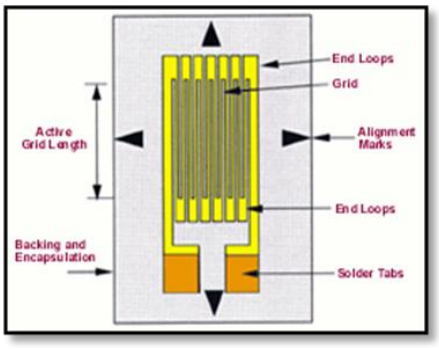

Figure2.5 Strain gauge

http://www.sensorland.com/HowPage002.html

2.2.4.1.3 DEMEC (demountable mechanical strain gauge measurements)

These gauges are simple, reliable, accurate, and are a relatively inexpensive technique for measuring the strain and crack monitoring at different points on a structure (Burland, Standing & Jardine 2001). There are two types of DEMEC - one with a digital dial gauge and one with a normal dial gauge. They consist of an invar main beam with two conical locating-points; one is fixed and the other pivots on a special knife-edge. The pre-drilled, stainless steel discs are attached to the structure with adhesive. The movement of the pivoting point is measured by the strain gauge, which is attached to a base plate on the invar beam. This varies in a length of between 50-200mm depending on the type of the structure. Figure 2.6 shows two different DEMEC gauges.

1. DEMEC with digital indicator

2. DEMEC with dial gauge

Figure2.6 DEMEC types

http://www.ferret.com.au/c/Bestech-Australia/DEMEC-portable-strain-gauges-from-Bestech-Australia-n1826652

2.2.4.2Contact-free methods

These types of measurements are flexible for measuring the displacement in any direction and meet the resolution requirement for structural testing. There are different types of these measurement devices such as the linear variable differential transformers (LVDT), the laser sensors, the charge-coupled-device camera (CCD), and the photogrammetry.

2.2.4.2.1 The LVDT (linear variable differential transformer)

This is a common type of measurement device that meets the resolution requirements for structural testing, and which is used for measuring a displacement in any direction. These types of sensors require a stationary platform as the measurement reference and/or for the sensors to fasten onto The LVDT measurements become, however, prohibitively expensive and are sometimes impossible when a large number of a displacement points are required or desired (Šemberk & Kohoutková 2005). Figure 2.7 shows a LVDT.

Figure 2.7 LVDT

http://www.bing.com/images/search?q=Lvdt+Sensors&qpvt=LVDT+image&FORM=RESTAB

2.2.4.2.2 Laser sensors

This type of sensor sometimes requires markers on the measured point to get a realistic measurement of the axial deformation as shown in figure 2.8. For concrete, sensors have to be able to cope with the effects related to the relatively rough surface at the axial surface of the specimen and which cannot give a precise reading with progressive loading. The change in the properties of the surface of the specimen causes a change in reflection and this thus results in a blurring of the image of the specimen, which makes it difficult to attach markers to the specimen's surface. The measured point also moves with progressive longitudinal deformation, and this needs to reflect by using a mobile attachment (Šemberk & Kohoutková 2005). Figure 2.8 shows the strain measurement using laser sensors.

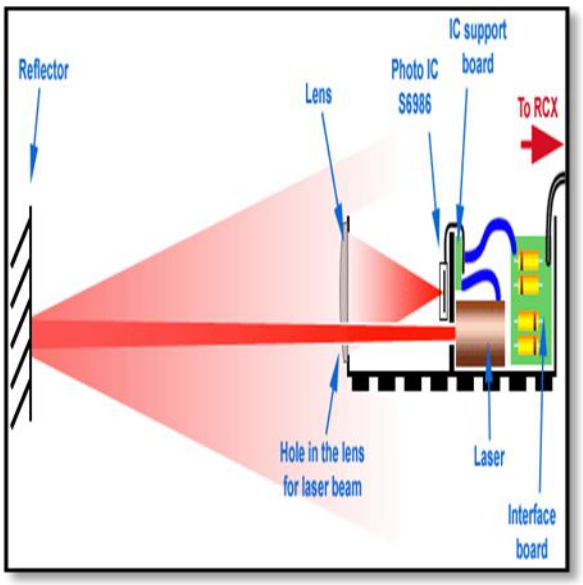

Figure 2.8 Laser sensors

http://www.philohome.com/sensors/laser/laser.gif

2.2.4.2.3 The CCD (charge-coupled-device camera)

This is an optical approach where a high-resolution image is captured. It has a sensor to receive the light signals and then processes these to a digital image. Figure 2.9 shows the CCD technology.

In this method, the number of measure points is limited only by the resolution of the digital camera or of the scanner, which is presently very high and thus does not represent any constraint. The advantages of this method are:

- No sensors need to be attached to the structure, which reduces instrumentation cost.
- A large number of points on the structure can be covered for whichever measurement is obtained. This offers an unprecedented amount of spatially intensive and effective data for enhancing the diagnosis resolution (Šemberk & Kohoutková 2005).

The disadvantages of this method is, however, the high sensitivity to vibration of the testing machine and a low measurement accuracy with laborious post-processing (Choi & Shah 1997).

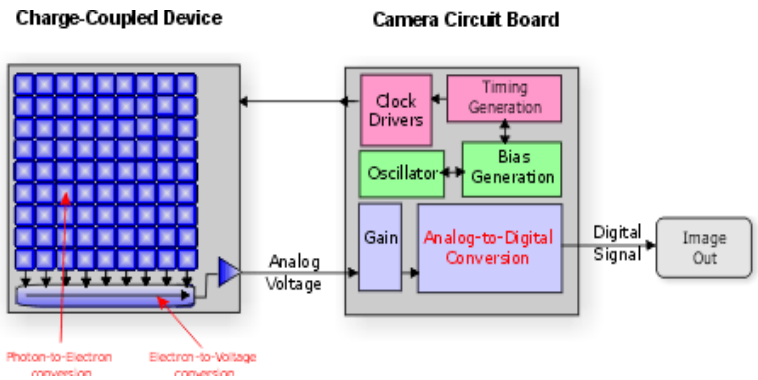

Figure 2.9 CCD technology

(Šemberk & Kohoutková 2005, p.6)

2.2.4.2.4 Photogrammetry

In this type of measurement, the data can be collected during a dynamically developed phenomenon and displacement in three dimensions can be provided; the data processing and the extraction of results will not be time-consuming. Figure 2.10 showed the photogrammetric set-up.

Figure 2.10 Photogrammetric technology

2.2.5 Porosity

The main quality of the permeable concrete is its high porosity, which allows the water to flow through it. This characteristic is achieved by limiting or by eliminating, the fine aggregate such as sand from the mix and by modifying the level of compaction. With no or little sand in the mix, the coarse aggregate is bonded together by only a thin layer of cement paste; this then creates continuous air voids inside the permeable concrete. This composition creates an open-void structure, which allows the water to percolate from the surface down through the effective voids. The effective voids are those that are

accessible from the surface, and these play a major role in the hardened properties of the permeable concrete (Crouch, Pitt & Hewitt 2007).

The relationship between porosity and strength is that porosity is inversely proportional to strength. Higher porosity, in particular, will generally produce a lower strength, whilst higher porosity leads to high permeability for the permeable concrete. This ranges from 15% to 35% and is extremely dependent on several factors such as aggregate gradation, cement amount, W/C and compaction energy (Crouch, Pitt & Hewitt 2007). Yang and Jiang (2003) observed that blended aggregate of different sizes typically result in a higher accessible porosity when compared with mixes made using a single aggregate size. These authors also found that an increase in the aggregate size resulted in a reduction of flexural and compressive strength due to an increase in total porosity and pore size. Deo and Neithalath (2010) further noted that using a single aggregate size in the mixture roughly produces a similar porosity for all the specimens, but results in different pore volumes when aggregate sizes are increased. These authors also found that smaller aggregates would produce a homogenous composition with a more random pore structure than would the bigger aggregates.

Aoki (2009) divided the pores in the permeable concrete into three different types:

- Pores in cement paste: these pores consist of gel pores and capillary pores. Capillary pores are affected by (W/C) ratio and they are either connected or unconnected.

- Air voids: these are bigger in size and may be connected and are responsible for water permeability.
- Aggregate voids: these are influenced by the aggregate's grading and by the degree of compaction. They vary in size, however, and may or may not be connected; this depends upon the types of aggregate used.

Figure 2.11 illustrates the types of pores in permeable concrete. Figure 2.12 illustrates the two-dimensional images of the permeable concrete specimens.

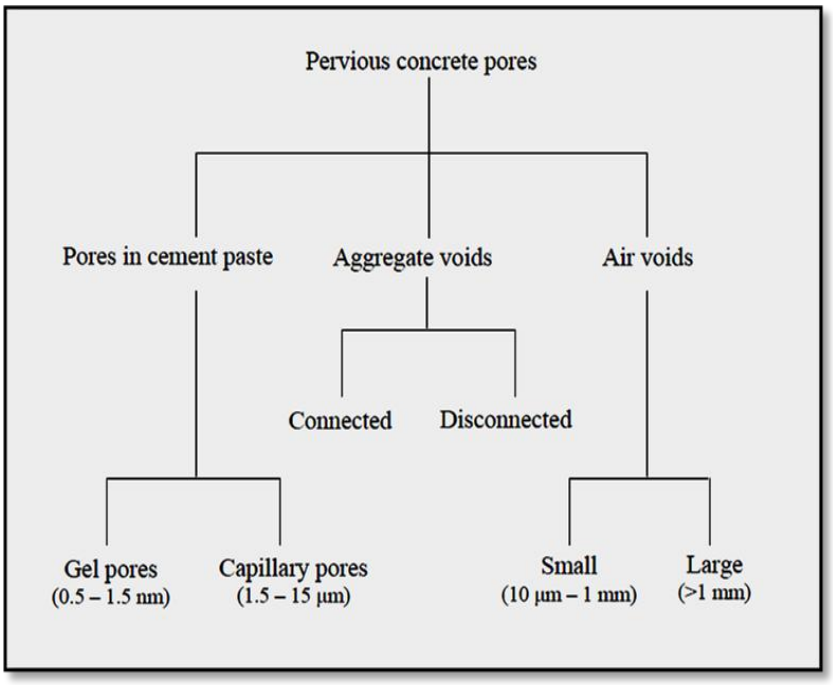

Figure 2.11 Types of pores of permeable concrete

(Aoki 2009, p. 7)

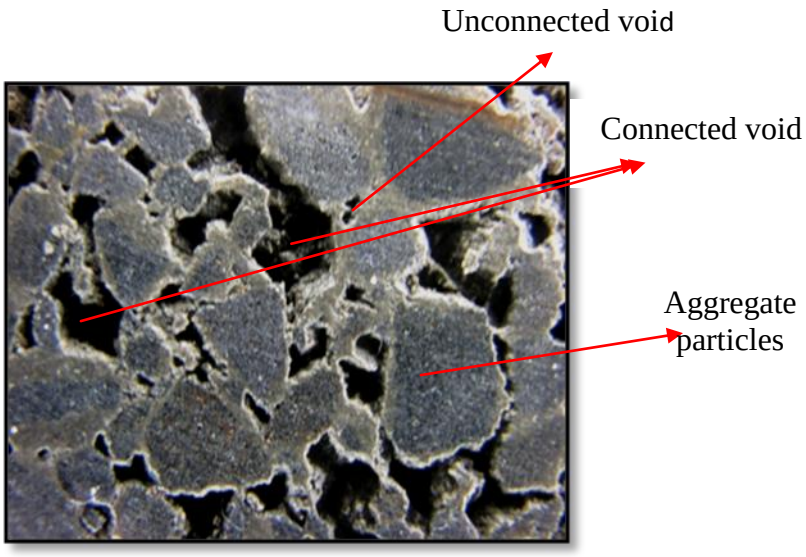

Figure 2.12 Two-dimensional images of a permeable concrete sample

2.2.6 Porosity measurements

Porosity is a ratio of the voids' volume to the total volume of the specimen. It is a very important factor for storm-water management and for design calculations. There are currently no standards for determining the voids content of hardened permeable concrete. The ASTM standards recently introduced the ASTM C1688/C1688M (2012) method, which provides the determination of bulk density and void content of permeable concrete mixtures in their fresh condition only. The determination of hardened porosities is still carried out on the basis of methods adopted in previous studies (Doe 2011).

There are different methods used to determine the porosity; some of them only calculate the effective voids, which are active in transporting water through the material, while others measure all the voids whether they are connected or disconnected. Montes, Valavala and Haselbach (2005) recommended a water displacement method for determining the porosity of the permeable concrete. These authors defined porosity as the volume of all voids (connected and

disconnected) divided by the total volume of the test specimen. This method is based upon the Archimedes' Principle of Buoyancy, which states that the buoyant force is equal to the weight of the fluid displaced. The void content is determined using this method, which is given by the following equation 2.1:

$$P = \left[1 - \left(\frac{M_{dry} - M_{sub}}{\rho_{\omega} * V_T}\right)\right] 100\ \% \qquad (2.1)$$

Where

P = porosity ratio

M_{dry} = oven dry weigh after 24 hours

M_{sub} = submerged weigh under water

V_T = total volume of the sample

ρ_w = density of water

(Montes, Valavala & Haselbach 2005)

Neithalath, Weiss and Olek (2006) used volumetric methods to determine the porosity of the permeable concrete specimen. The porosity was expressed as the ratio of the volume of water required to fill the pore volume of the specimen to the percentage of the total volume of the specimen. In this method, the cylinder was sealed using a latex membrane and water was filled up to the surface of the specimen. Marolf et al. (2004) used an image analysis method to determine the area fraction of the permeable concrete specimens' pores where the specimens were filled with a low viscosity epoxy, and then were sectioned into different depths. The surface of each section was then

scanned, and an image analysis procedure was next employed to distinguish between the connected and the disconnected pores.

In the case of drilled cores a correction was needed to relate the measured porosity to the actual in-situ porosity because some materials were knocked off the surface of the core during the core process. Haselbach and Freeman (2007) used the following equation 2.2 to determine the correct porosity (P_c) as a function of the samples' in-site porosity (P_i).

$$P_{c=}\ P_i\ + (1 - P_i) * \left\{\frac{D_a}{D_c} - \left(\frac{D_a}{2*D_c}\right)^2\right\} * \left\{\frac{P_i - P_{min}}{P_{max} - P_{min}}\right\} \quad (2.2)$$

Where

P_c = correct porosity in the site

P_i = porosity in the site

D_a = maximum aggregate size

D_c = core diameter

P_{min} = minimum porosity

P_{max} = maximum porosity

(Haselbach & Freeman 2007)

2.2.7 Permeability

The permeability of porous concrete has a direct relationship with the porosity; a higher porosity normally leads to a higher permeability and to a lower compressive strength. A permeable structure is created by carefully controlling the amount of water and cementation materials, by limiting or eliminating the

sand ratio, and by minimising the compaction energy. Wide ranges of permeability values for permeable concrete have been reported. Some researchers have reported that the water permeability of permeable concrete was between 2.1mm/sec to 5.43mm/sec and values higher than 11.6mm/sec were also measured in the laboratory (Tennis, Leming & Akers 2004), whilst the field permeability was reported to be in the range of 1.69mm/sec to 19.5mm/sec (Bean, Hunt& Bidelspach 2007).

2.2.8 Permeability measurements

Permeability is also expressed as the water permeability coefficient, as the intrinsic permeability, and as the hydraulic conductivity. There is no standard test method for determining the permeability of permeable concrete. The permeability test, which is usually used for the conventional concrete, does not work with the permeable concrete because of the interconnected pore network. Neithalath, Weiss and Olek (2006) employed the falling head method to determine the permeability of permeable concrete.

These authors observed that the permeability is not a function of porosity or of pore size alone, but rather, is a function of the pore connectivity and of the distribution inside the concrete. This method is relatively easy and quick to set up and yields results that are easy to work with. Figure 2.13 illustrates the falling head method for the permeability test as illustrated by Neithalath, Weiss and Olek (2006). The falling head method measures the time taken by the water level to fall from the initial water head to the final water head, and

water permeability is then calculated using Darcy's First Law as in the following equation 2.3.

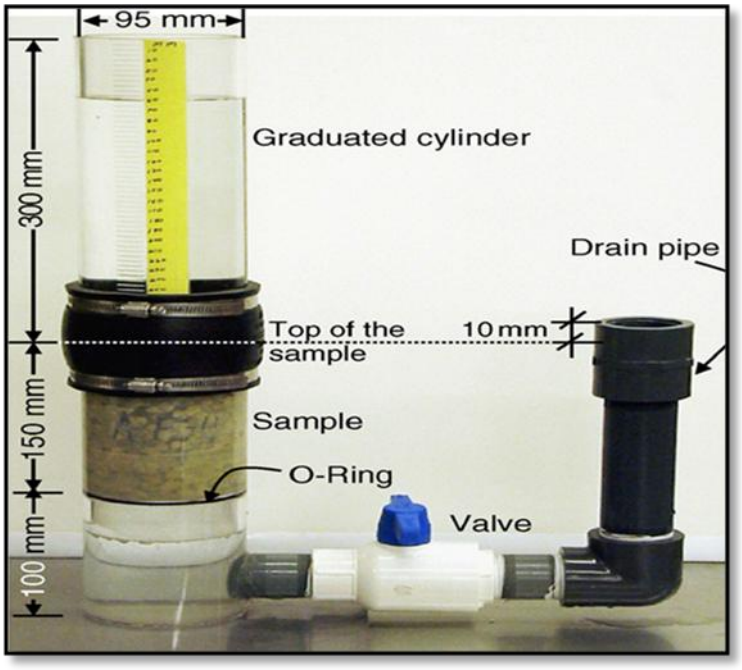

Figure 2.13 Falling head permeability test set-up

(Neithalath, Weiss & Olek 2006, p 2076)

$$K = \frac{aL}{At} ln \frac{h_1}{h_2} \quad (2.3)$$

Where

K = permeability coefficient

a = cross-section area of the cylinder pipe

A = cross-section area of the specimen

L = length of the specimens

t = time for water to pass from level h_1 to level h_2

h_1 = initial water level (290mm)

h_2 = final water level (70 mm)

McCain and Dewoolkar (2009) and Montes, Valavala and Haselbach (2006) used the falling head method to measure the permeability of the permeable concrete. Montes, Valavala and Haselbach (2006) found that the permeability varied between 0.14mm/sec to 11.9mm/sec and increased exponentially with increasing porosity. McCain and Dewoolkar (2009) also used this method for different sizes of specimens with sand-salt mixtures on the top surface as a simulation of a winter surface. Their results showed that the permeability ranged between 6.8mm/sec to 9.8mm/sec and that the results were not affected by any variation in the size of the specimen.

Other researchers (Matsuo et al. 2005; Ravindrarajah & Aoki 2008) used a constant head test method as suggested by the Japan Concrete Institute (2004) to measure the permeability of the permeable concrete. Figure 2.14 illustrates the test set-up. Matsuo et al. (2005) found that the average water permeability of permeable concrete was 20mm/sec for 20% voids content, and this was increased to 40mm/sec for a 30% void content. Darcy's First Law was used to calculate the water permeability in the constant head method as shown in equation 2.4.

$$K_T = \frac{l}{h} * \frac{Q}{A(t_2 - t_1)} \tag{2.4}$$

(Matsuo et al. 2005)

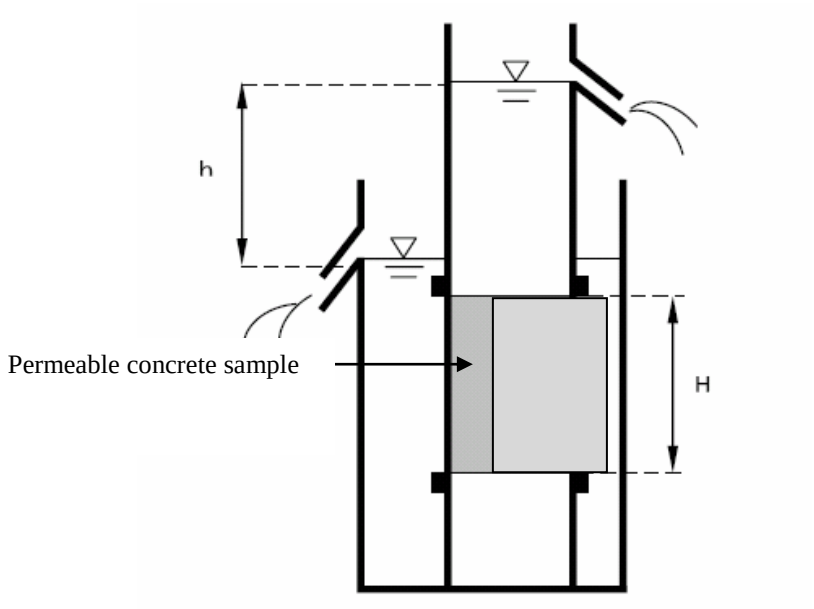

Figure 2.14 Constant head method set-up

(Matsuo et al. 2005)

2.2.9 Relationship between compressive strength and porosity

The relationship between the porosity and the compressive strength of the permeable concrete was investigated by several researchers (Aoki 2009; Chindaprasirt et al. 2008; Hussin et al. 2012; Lian, Zhuge & Beecham 2011; Schaefer et al.2006) and they found that there is an inverse relationship between these parameters. Permeable concrete with a high porosity generally produces a lower compressive strength.

Schaefer et al.(2006) found that the relationship between these two parameters is generally linear as can be observed in the following figure 2.15. These authors demonstrated a relationship between the 7-day compressive strength and the porosity as shown in the following equation 2.5, which was later modified by Aoki (2009) to the MPa units.

$$Compressive\ strenght\ (MPa) = 4762.1 - 97.16 * (porosity\ \%) \qquad (2.5)$$

(Aoki 2009, p. 14)

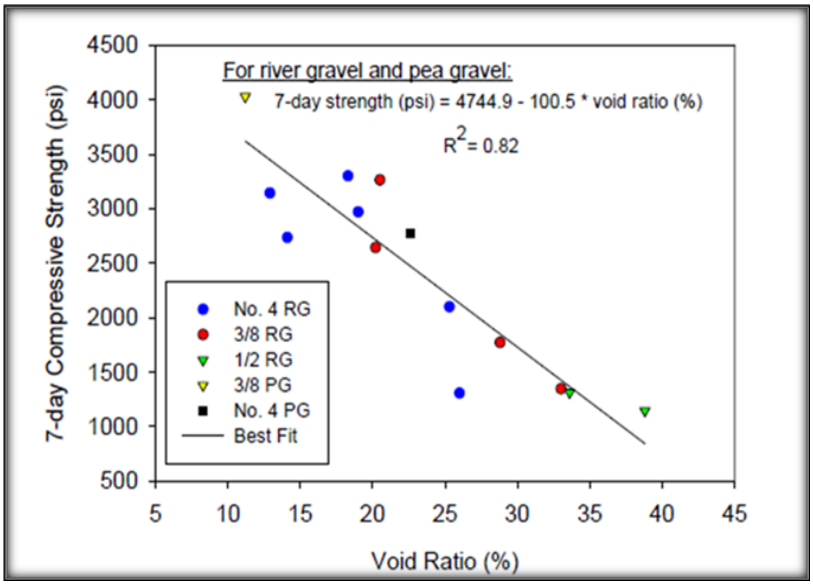

Figure 2.15 Relationship between the 7-day compressive strength and the porosity

(Schaefer et al. 2006, p. 27)

Chindaprasirt et al. (2008) considered that permeable concrete consisted of a coarse aggregate covered by a cement paste under the compression loading, while the pores act as a weakness zone in the cement matrix and produce a concentration of stress and crack formation (Griffiths 1921; Goodier 1933). As a result, Chindaprasirt (2008) demonstrated that the equation suggested by Duckworth (1953) for porous material was valid for describing permeable concrete. Figure 2.16 illustrates the relationship between the compressive strength and the porosity.

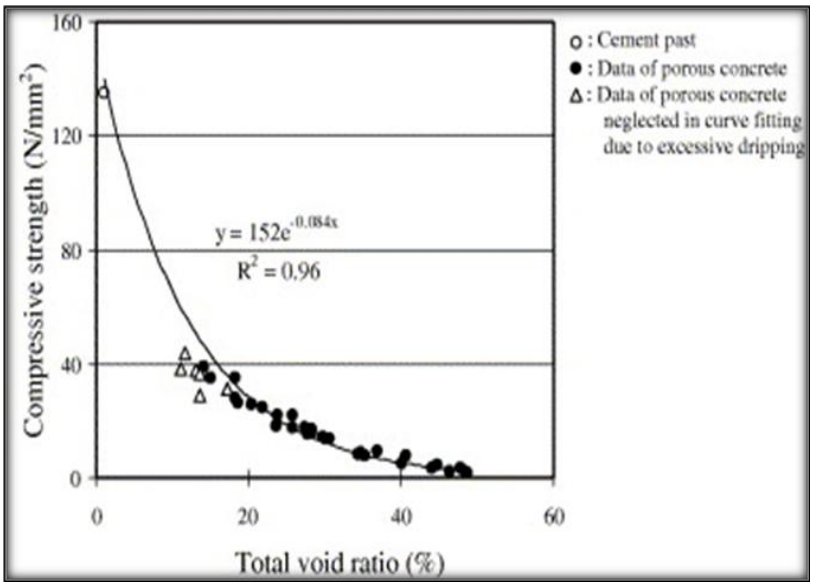

Figure 2.16 The exponential relationship between the compressive strength and the porosity

(Chindaprasir et al. 2008, p.900)

Lian, Zhuge and Beecham (2011) proposed equation 2.6 with R^2 equal to 0.9 to find the relationship between the compressive strength and the porosity ratio. Figure 2.17 illustrates the relationship between the compressive strength and the porosity.

$$compressive\ strenght = 231.44e^{-0.09\ porosity} \quad (2.6)$$

(Lian, Zhuge & Beecham 2011)

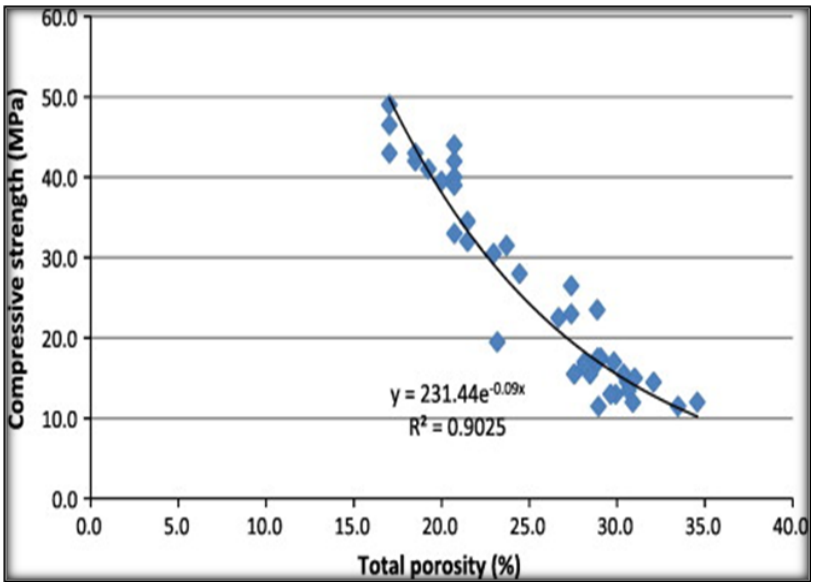

Figure 2.17 Relationship between the compressive strength and the porosity

(Lian, Zhuge & Beecham 2011, p.4296)

2.2.10 Relationship between the permeability and the porosity

The relationship between the porosity and the water permeability has been studied by some researchers (Schaefer et al. 2006; Wang et al. 2006). They found that the water permeability could be related to the porosity as shown in figure 2.18, and that the following equation 2.7, which was modified by Aoki (2009), demonstrates that the permeability in mm/sec can increase exponentially with an increasing porosity ratio.

$$K = 13.74 * e^{13.68*p} \qquad (2.7)$$

Where:

K = water permeability in mm/sec

P = porosity ratio

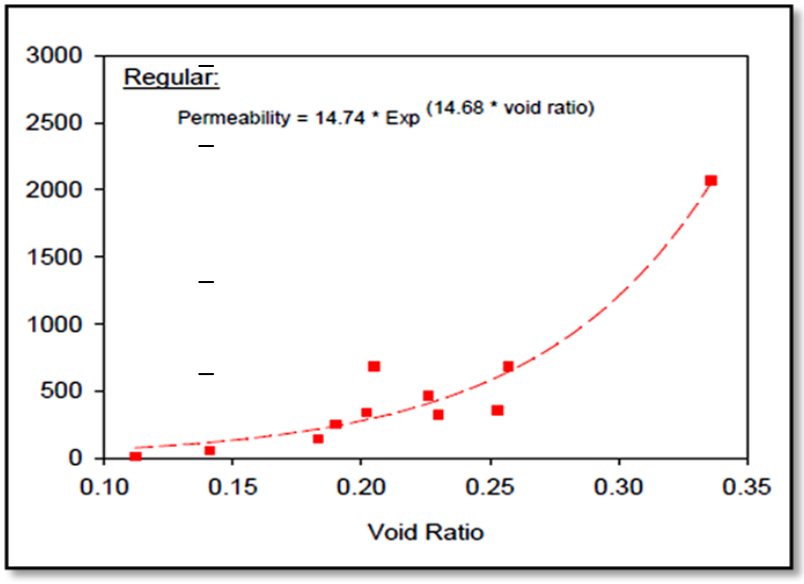

Figure 2.18 Relationship between the permeability and the porosity

(Schaefer et al. 2006, p.30)

A similar exponential relationship was found by Wang et al. (2006), as can be observed below in figure 2.19.

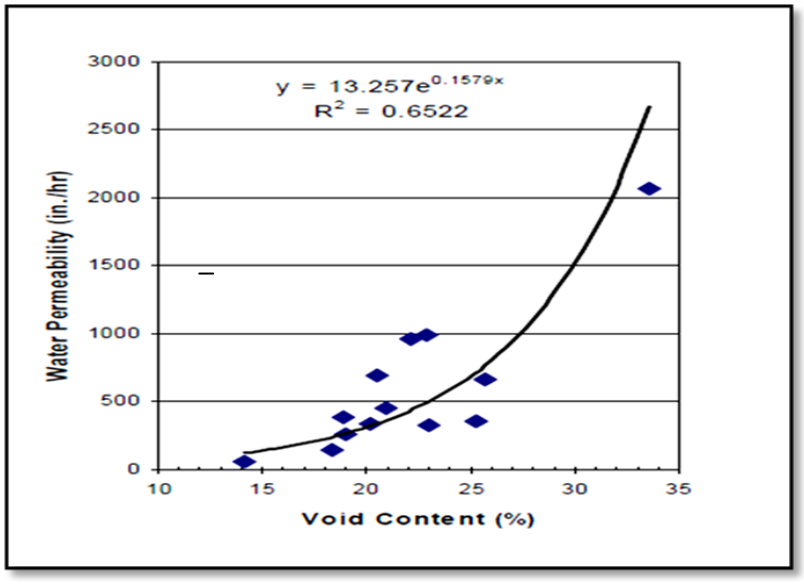

Figure 2. 19 An exponential relationship has been found between the water permeability and the porosity ratio

(Wang et al. 2006, p.8)

2.3 The cost of permeable concrete

The use of permeable concrete will most probably be limited, regardless of its numerous environmental and structural benefits, if its cost cannot compete with that of conventional concrete. There are many factors, however, that affect the cost of permeable concrete such as the need to improve sub-base soils and the availability of the materials in the construction area.

Wanielista et al. (2007) noted that the initial cost of the permeable concrete pavement could be up to 1.5 times that of other conventional pavements. This rise in cost can be attributed to the fact that:

- Permeable concrete is a special product requiring experienced and skilled labour to install the concrete properly. This requirement of specific experience, when accompanied with a low demand, drives up the price.
- The thickness of the permeable concrete pavement must be increased due to its lower compressive strength. This helps to distribute vehicle loading to the soil sub-grade and allows for extra rainfall storage within the concrete layer.
- The maintenance cost: a permeable concrete pavement must be cleaned to keep it working properly and to avoid it clogging up. This extra cost can be recouped when using permeable concrete pavement by decreasing the area required for storm water management. It also provides better traction (macro texture) during wet weather because it is a free-draining pavement.

(Wanielista et al. 2007).

McMillan (2007) collected data on the performance of traditional and permeable concrete pavements according to their durability, maintenance requirements and consequent long–term savings, and then compared these to

the installation costs of traditional and permeable concrete for different construction areas as shown in figure 2.20. This author estimated the installation cost of the traditional concrete at $32.60 to $122.20 per square metre, whilst the installation cost ranged from $43.50 to $97.80 per square metre for permeable concrete; McMillan found that the average cost of traditional and permeable concrete is quite similar. It should be noted, however, that the cost comparisons in figure 2.20 do not include the cost of storm-water management, so the final cost would be lower for permeable concrete. When the two concrete types are compared across the criteria of cost, availability of skilled workers and future outcomes such as durability, maintenance, and long-term savings, the cost for the permeable concrete is clearly less than the cost of the traditional concrete if it is used properly.

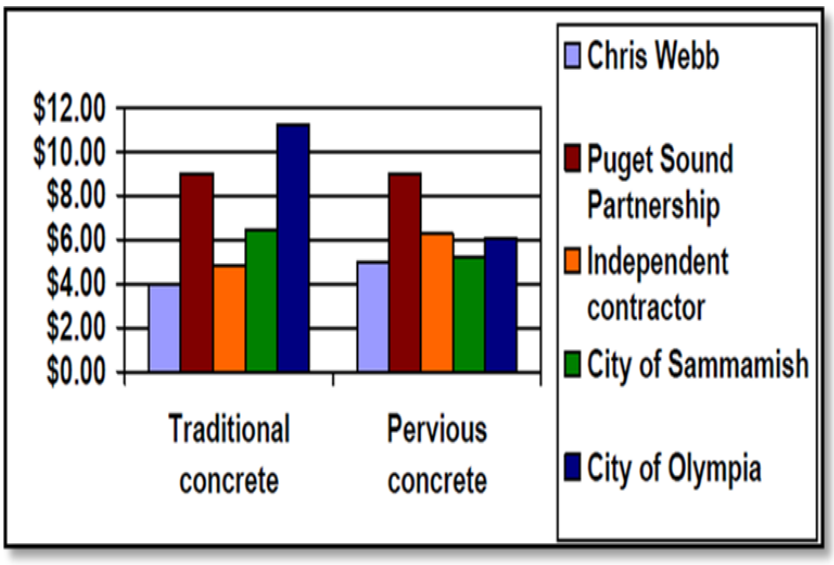

Figure 2.20 Cost per square metre for traditional and permeable concrete

(McMillan 2007, p.16)

According to the Centre for Watershed Protection (2000), the installation of traditional curbs, gutters, storm-drain inlets, piping and retention basins can cost two to three times more for handling water runoff than does the low-impact strategy of permeable concrete pavement. Projects that use permeable concrete typically do not need storm-sewers, and the cost of the installation of underground piping and storm drains can be eliminated. Grading requirements for the pavement are also reduced because there is no need to slope from the parking area to the storm drains.

2.4 Maintaining the permeable concrete pavement

There are certain maintenance requirements that should be carried out regularly in order to maintain the efficiency of the permeable concrete system. These are:

- The site must be inspected once a month for about 4 to 6 months after installation and then inspected annually; this is particularly required after there has been some rain or a storm as the drain voids can become clogged with organic residues.
- The permeable concrete surface may need to be swept or vacuumed every three months in order to clean out the voids in the system and to restore permeability. In the event that sedimentary clogging occurs, the important step in effective pavement return is vacuuming, because vacuuming takes sedimentary particles out of the porous surface. Sweeping is, however, only useful when combined with immediate vacuuming.

- A high pressure hosing should be applied after sweeping and vacuuming in order to check that the voids are still well-filled with aggregate and, if this is not the case, then they may have to be regularly re-filled using a clean aggregate. Low-pressure washing may help to mobilise sediment before it is removed by vacuuming.

(Chopra et al. 2007)

2.5 Conclusion

Permeable concrete is a special type of concrete that has a relatively high porosity and permeability with a low compressive strength, modulus of elasticity and density. The literature review has revealed that:

- The selection of a W/C ratio equal to 0.34 has the best aggregate coating and paste stability without having excess amounts of paste draining through the pores of the material.
- Using blends of 4.75mm and 9.5mm sized aggregates produces a homogenous composite with both acceptable porosity and permeability. As a result, the recommended W/C ratio is equal to 0.34 and the blend of these aggregate sizes will be used to prepare the permeable concrete mixtures in this research.
- Since there has been limited structural design research conducted on permeable concrete, there is no official standardised test procedure for measuring the stress-strain behaviour and the MOE except for that published by Deo & Neithalath (2010). These authors used the platen-to-platen displacement method, which is an easy and quick method to apply. This

method is suitable for measuring the global strain of the permeable concrete specimens including the effect of the capping material, and of the hydraulic testing machine. It is useful for comparative measurement but is of little use in determining fundamental properties such as the MOE. An attempt will thus be made to use different, technological measurements to measure the local strain and to find the relationship between these two methods.

CHAPTER 3
MATERIALS AND EXPERIMENTAL PROCEDURES

3.1 Introduction

This chapter provides descriptive information about the materials and procedures that were utilised to achieve the objectives of this study. Since permeable concrete mixtures must be carefully designed, it is important to characterise the mix components of aggregate, sand, water, and cement. Whilst some of the testing techniques that were adopted to study the properties of permeable concrete were based on accepted standards, some particular tests were adapted from the literature. An experimental investigation was thus carried out to define the characteristics of the hardened permeable concrete and to investigate some of its fundamental properties such as compressive strength, modulus of elasticity, stress-strain relationships, porosity, and permeability.

3.2 Materials

The materials used for the preparation of the permeable concrete mixtures for this research were obtained from a single source in order to limit any variation in their physical and chemical properties.

3.2.1 Aggregate

1. 10mm Basalt aggregates from local quarries in Toowoomba were used as the coarse aggregates for all mixtures in this study. The flakiness index is

about 15 to 25%, the water absorption is about 0.5 to 2% and the crushing value is about 9 to 11%.

The 10 mm aggregate size was separated into two groups according to their size as follows:

- 4.75mm (passing through a 9.5mm sieve and retained on 4.75mm sieve)
- 9.5mm (passing through a 12.5mm sieve and retained on a 9.5mm sieve)

2. Allora medium sand with a bulk density of 1494 kg/m^3 and particle size smaller than 425 µm was used in different proportions as a fine aggregate.

Figure 3.1 shows the basalt aggregate in two different sizes and the sand used in this research.

(A) (B)

Figure 3.1 Basalt aggregate and the sand used for the preparation of the permeable concrete mixes

3.2.2 Cement

Ordinary Portland Cement General-purpose Type 1 was used for the preparation of all of the permeable concrete mixtures in this study. The typical oxide compositions of this cement type are provided by Cement Australia Company in table 3.1 below.

Table 3.1 Chemical composition of the Ordinary Portland Cement

Chemical composition	Average percentage
LOI	2.6
SO_3	2.5
CaO	64.6
SiO_2	19.7
Al_2O_3	5.03
Fe_2O_3	3.42
MgO	1.08
K_2O	0.37
Na_2O	0.22
P_2O_5	0.06
Mn_2O_3	0.08
Cr_2O_3	0.01
SrO	0.03

The method of preparation of the 100 × 200 mm cylindrical samples followed the Australian Standard AS 1012.2 (1994). The sieving, washing, and drying of the various aggregate sizes was carried out according to AS 1141.11.1 (2009). All of the 10 mm aggregate was sieved using the vibration machine and standard sieve sizes to distribute the aggregate into two different group sizes of 4.75mm and 9.5 mm. The aggregates of each group were washed using sufficient clean water to remove all materials such as clays and impurities, which might have prevented bonding between the aggregate particles and the cement paste. The aggregates were then oven-dried for 24 hours at 105^{o}C.

Four different sand proportions, which were started from 0 to 15% with an increment of 5%, were used. These mixtures were prepared using blends of 4.75mm and 9.5mm sized aggregates. These blends were prepared by replacing 25% and 50% of the weight of the smaller sized aggregate by the

larger sized aggregate. Table 3.2 illustrates the mixture proportions for the permeable concrete mixes.

Table 3.2 Mix proportions for the permeable concrete mixes by weight

Mix Name	A/C	W/C	Aggregate		Cement (kg)	Sand	
			4.75mm (kg)	9.5mm (kg)		Weight (kg)	Ratio %
GA5%	4.5	0.34	4.3	4.3	2	0.45	5
GA10%	4.5	0.34	4	4	2	0.9	10
GA15%	4.5	0.34	3.8	3.8	2	1.35	15
GB5%	4.75	0.34	6.7	2.25	2	0.47	5
GB10%	4.75	0.34	6.41	2.13	2	0.95	10
GB15%	4.75	0.34	6	2	2	1.42	15
GC1	4.75	0.34	4.75	4.75	2	-	-
GC2	4.75	0.34	7.13	2.38	2	-	-

3.3 Mixing of the permeable concrete and the casting and curing of the test specimens

The mixing procedures proposed by Wang et al. (2006) were used to help to ensure a good bond between the aggregate particles and the cement paste. The required amount of aggregate and sand was first added to the mixer (pan-type) and mixed for 30 seconds; this was followed by the addition of 5% of the cement. The dry materials were then mixed for one minute or until the aggregate was visually noted to be fully coated by a thin layer of dry cement. The remaining cement and water were next added to the mixer and the mass was mixed for approximately a further three minutes. At the end of

this time, the sides and the bottom of the mixer were scraped using a hand-held metal scraper. Mixing was undertaken for a further three minutes, after which, the mix was then removed into the mixing pan using a metal scoop. The ball test was performed as recommended by Tennis, Leming and Akers (2004) for the workability assessment of the concrete mix. A handful of material was taken from the mixer in the ball test to establish the mouldability of the permeable concrete. Figure 3.2 illustrates the workability assessment of the permeable concrete with different amounts of water. Since the mouldability of permeable concrete is quite sensitive to water content, the amount of water must be carefully controlled.

The next step involved the placement of the fresh concrete into 100 × 200 mm cylindrical steel moulds in three equal layers. The specimens were compacted by tamping; 25 strikes of the tamping rod were distributed evenly over the entire cross-section of the concrete in the mould. The mould was then placed on a vibration table for compaction for approximately 5 to 7 seconds. This was followed by the addition of concrete over the preceding layer. The tamping and vibration tables were then used again for the next two layers. The vibration table was used to provide a consistency to the method of compaction. A small quantity of fresh concrete was also added onto the top of the three compacted layers and levelled using a hand-held strike-plate as required. The moulds were then covered with a plastic wrap and kept for 24 hours in the room environment. The samples were next removed from the mould, labelled, and placed in a fog room with an 86.5% relative humidity and a temperature of 26.3^{o}C until the day of their testing. Two samples were

prepared for each batch for the porosity and permeability tests, and five samples were prepared for the compressive strength test at 28-days.

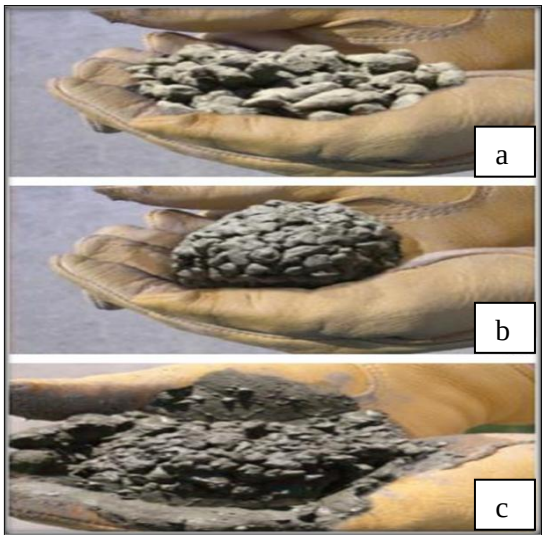

(a) Too little water (b) Proper amount of water (c) Too much water

Figure 3.2 Workability assessments for the permeable concrete

(Tennis, Leming & Akers 2004, p.8)

3.4 Dry density of the permeable concrete

The samples were weighed prior to the compressive strength test; the diameter and height dimensions were measured at three different locations on the cylinder, the averages were determined, and the volume was calculated. The dry density of each specimen was calculated according to the following equation 3.1:

$$Dry\ density\ \frac{kg}{m^3} = \frac{weight}{total\ volume} \qquad (3.1)$$

3.5 Tests methods

3.5.1 Compressive strength

The compressive strength was determined by breaking the permeable concrete samples in a compression-testing machine according to the requirements of AS 1012.9(1999).

Five cylinders of size 100 × 200mm were used to calculate the compressive strength and the average of the five results was reported. Since the ends of the concrete specimens are required to be parallel to within 2^{o} to the axis, the cylinders were capped with sulphur capping on both loading surfaces to ensure the correct loading. A study by Harber (2005) demonstrated that the sulphur capping eliminated the problem of sloping ends and the premature failure that was caused by dislodging aggregate. This researcher also concluded that the (apparent) compressive strength of permeable concrete would increase dramatically and be more representative of its true characteristics with the use of the sulphur capping, since this effectively restrains the aggregates on the top and prevents premature failure. Figure 3.3 illustrates the samples (A) during and (B) after capping with sulphur.

(A)

(B)

Figure 3.3 Permeable concrete samples (A).during and (B).after capping with sulphur

An Avery 500kN hydraulically-powered machine was used to determine the compressive strength as shown in figure 3.4. A data acquisition system was connected to the computer to record the load and the displacement data. The upper bearing-block was fixed, whilst the lower bearing-block was moved up to compress the specimens. The machine's surfaces were wiped clean prior to testing. The samples were placed on the lower bearing-block and centred as illustrated in figure 3.5. The load was applied at a rate that corresponded to a strain increase of 10μm per second and the sample was loaded until failure, which was characterised by visible fractures. The maximum load applied was then recorded.

Figure 3.4 An 500kN Avery machine used for the compression strength test

Figure 3.5 The sample's central location in the machine during the test

3.5.2 Strain and Modulus of Elasticity (MOE) measurements

Key factors in a permeable concrete's structural performance are the stress-strain behaviour and the MOE. Three different methods were used in this research to measure the strain and the MOE; namely the platen-to-platen (p-to-p), the strain gauge (sg), and photogrammetry methods. The platen-to-platen method is only suitable for measuring the global strain of the permeable

concrete specimens including the strain of the capping material, and the compliance of the hydraulic testing machine. True sample strains cannot be measured using this method and the MOE, which is calculated using the other methods (sg, photogrammetry and strain gauge), is thus only approximate at best.

The global stress-strain relationships and the related MOE were determined using the p-to-p method. Local stress-strain behaviours and the related MOE in the middle sections of the permeable concrete specimens were determined using the strain gauge and the photogrammetry. Figure 3.6 illustrates the difference between the global and the local strain in a concrete specimen.

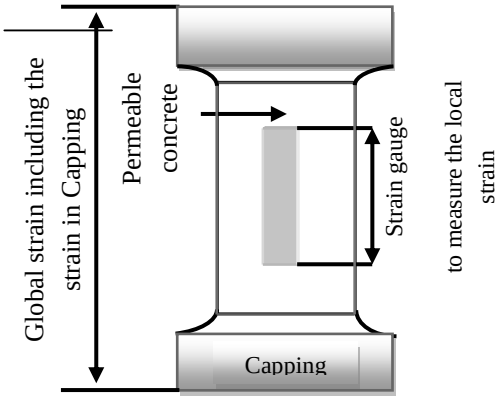

Figure 3.6 The local and the global strain in the concrete samples

3.5.3 Strain gauging

In order to fix the strain gauges onto the uneven, rough, porous surface of the permeable concrete specimens, it was necessary to fill the voids and to seal the surface with a suitable pre-coating material before the gauge was bonded onto it. An area that was adequate for affixing the strain gauges was prepared by using the following treatment steps:

1. Surface treatments: underlying pores were located and opened by lightly striking the small surface pores with a small sharp nail and any loose material was removed from the gauge installation area. The prepared area was about 20-30 mm larger than the strain gauge.
2. Filling: Sulphur was used to flatten the permeable concrete surface and to provide a surface on which the strain gauge would be readily bonded.
3. Sanding the area: The cured sulphur was first abraded with a sanding machine, and then with sand paper until its thickness was between 0.5mm to 1mm.
4. Normal strain gauging procedures were followed for bonding the gauge to the prepared surface.
5. Two strain gauges 60 mm long of type PL-60-11 (single element), which were five times the largest aggregate size, were then bonded to the permeable concrete specimens using a quick-curing adhesive.

Figure 3.7 illustrates the preparation and the process of fixing the strain gauge onto the permeable concrete; this process has been developed as part of this research.

Figure 3.7 Steps in preparing and fixing the strain gauge onto the permeable concrete samples

3.5.4 Photogrammetry

The hardware of the measurement system consisted of a pair of calibrated and synchronized high-resolution digital cameras types 2 JVC HD Everio camcorders. These were placed in a stable position, and then these took photos from different directions off reflective targets on a permeable concrete specimen. The reflective targets, which were appropriate for the achievement of the most accurate geodetic distance measurements, were placed as control points on the specimens.

An Avery 500kN machine that was connected to the data logged system was used with this type of testing. Figure 3.8 showed the photogrammetric testing set-up.

The results of the photogrammetric calculations were the coordinates of the targets at different load steps of the test. Displacements were computed as the difference between the coordinates of the same targets in two load steps. These displacements contained the absolute deformation of the permeable concrete

specimen. The relative movements in the vertical direction were determined by the difference of the displacements between two neighbouring targets. This test method was utilised in this research but, due to the poor quality of the cameras used, the results were not reliable and thus could not be adopted.

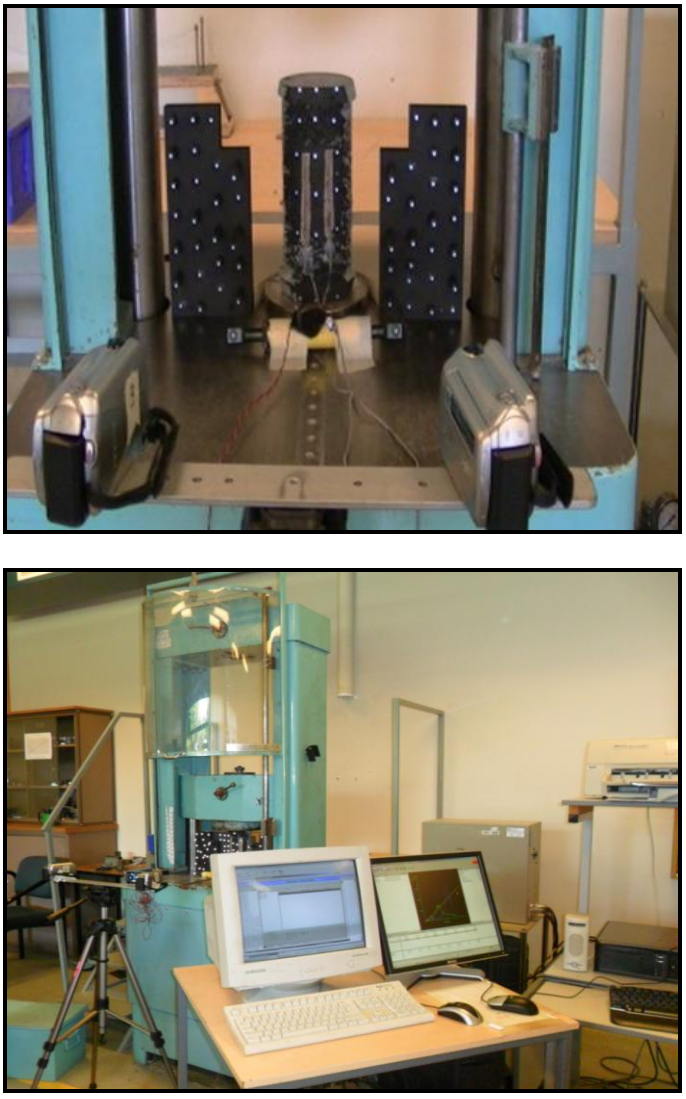

Figure 3.8The strain measurement set-up using photogrammetry technology

3.5.5 Porosity test

The porosity was found for all the mixtures using the water displacement method as previously developed by Montes, Valavala and Haselbach (2005). This method is based on Archimedes' Principle of Buoyancy, which states that the buoyancy force is equal to the weight of the fluid displaced. It can be utilised to find the total porosity according to the following equation 3.2:

$$P = \left[1 - \left(\frac{M_{dry} - M_{sub}}{\rho_{\omega} * V_T}\right)\right] 100\ \% \tag{3.2}$$

(Montes, Valavala & Haselbach 2005, p.4)

The total volume was found by measuring the height and the diameter of the samples at three different locations and the average was calculated using equation 3.3:

$$V_T = \left(D_{avg}\right)^2 \times \pi \times \frac{H_{avg}}{4} \tag{3.3}$$

The dry mass was measured twice by placing the sample in the oven for 24 hours at 110^{o}C in accordance with the recommendations of Montes, Valavala and Haselbach (2005), and by measuring the dry mass at room temperature. A comparison of the two methods is described in Chapter 4. The submerged mass was measured by submerging the sample in water for at least 30 minutes to allow water to penetrate into all connected pores in the specimen. After 30 minutes and while the specimens were still submerged, each specimen was tapped against the side of the tank five times to allow any air bubbles that were

trapped in the pores to escape. The submerged mass of the samples was measured using a wire-mesh basket (used to support the specimen under water) that was connected to a digital scale. Since the fluid used in this test was water, the temperature of the water was thus taken and its true density was used. The following figure 3.9 shows the submerged weight measurement in the porosity test.

Figure 3.9 Porosity test equipment

(To measure the submerged weight)

3.5.6 Determination of the porous area using image analysis

It is recognised that the properties and the performance of any porous material are strongly dependent upon its pores characteristics and structures (Sumanasooriya & Neithalath 2009). The total pore volume, size, the distribution of the pores and the interconnectivity of the pores in permeable concrete affect its performance characteristics such as the compressive strength, stress-strain behaviour, MOE and the permeability. Variations in the voids along the height of a concrete cylinder was expected since surface

vibration was used; this was due to a randomness in the porous material structure (Chindaprasirt et al. 2008). It was thus important to view the porosity in each section of the permeable concrete cylinder.

To measure the fraction of pores, the distribution of the voids along the height of concrete cylinder must be evaluated in order to determine the 3-dimensional matrixes of voids that will allow water to flow through the concrete. A 10mm slice was thus removed from the top of the 200 × 100mm specimen, and the remaining portion was cut into three equal slices using a laboratory concrete-cutting machine. By using the inside surface of the top, centre and bottom faces, three faces were available for the determination of porosity in each part of the permeable concrete specimen. The surfaces were washed with a stiff brush using sufficient clean water to remove any deficiencies that might have accrued during the cutting process. After drying, the portions were painted with black colour and were left until dry, while the voids were filled with white gypsum powder to identify voids and the solid parts. Three images corresponding to each mixture were obtained for features analysis. Each image was cropped and then processed using Earth Resources Data Analysis Systems (ERADS) software, which is used in geospatial image processing and analysis, to identify the voids (white) and the solid areas (black). Figure 3.10 illustrates the steps of the image analysis procedure.

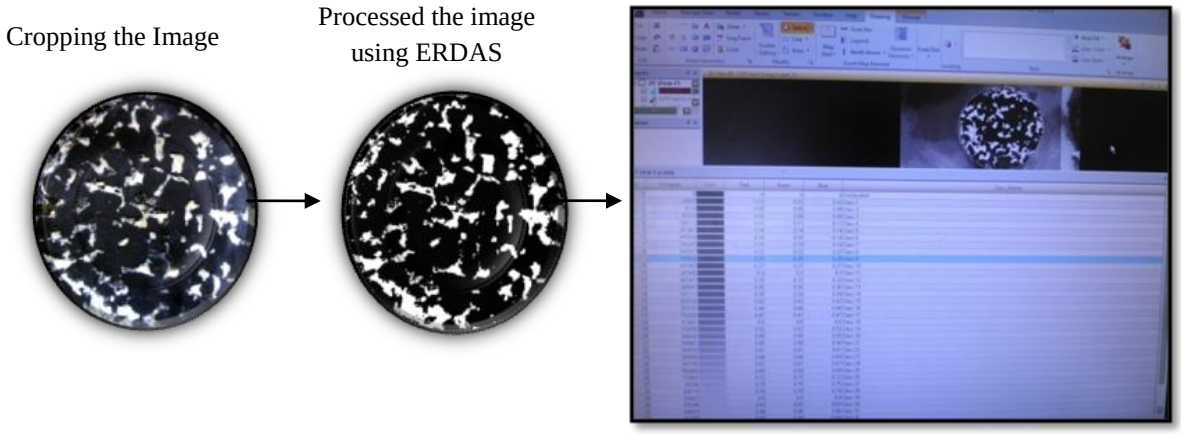

Figure 3.10 Image-analysis procedures to determine the pore voids area

The pore area fractions of these images were obtained as a fraction of total white area A_p to the total area of the circle's binary image A_t. This was calculated for the three planar sections of each specimen, (top, centre and bottom), and the average value was reported as a pore area fraction P_{area}% as shown in equation 3.4.

$$P_{area}\% = \frac{\sum A_p * 100}{\sum A_t} \tag{3.4}$$

3.5.7 Water permeability test

One of the most important tests used for permeable concrete is, of course, the permeability test. The lack of standard specifications for this test has left some allowance for the introduction of innovative techniques for measuring this criterion. The literature review revealed that it was common practice to use a falling-head apparatus to measure the water permeability for the permeable

concrete (Neithalath, Sumanasooriya & Deo 2010) and this approach was adopted in this research. Figure 3.11 shows the permeability test set-up.

The samples were wrapped using cling wrap prior to performing the falling-head test. The cling wrap prevented the water leakage out of the sides of the samples; it also provided an edge on top of the samples so that a sufficient head could be maintained as shown in figure 3.12.

Figure 3.11 Permeability test set-up

Figure 3.12 Permeable concrete specimen wrapped with cling wrap

The specimens were placed in the plastic pipe, then tightened and sealed using circle clamps. Water was allowed to flow through the specimens by opening the valve and the time required to obtain a drop in the water level from the initial water level h_1 to the final water level h_2 was recorded. The coefficient of permeability was then calculated using Darcy's law as given in equation 3.5:

$$K = \frac{aL}{At} ln \frac{h_1}{h_2} \tag{3.5}$$

(Neithalath, Sumanasooriya & Deo 2010, p.803)

3.6 Conclusion

This chapter has provided extensive information about the permeable concrete mix proportions, which were adopted to achieve the aims of this research. The effect of composition materials on the mechanical and hydraulical properties of the permeable concrete mixes were investigated using standard testing methods and some of the adopted testing from the literature review. The experimental program included the compressive strength test, the strain measurements, the porosity test, measurements of the pore area and the permeability test.

CHAPTER 4
EXPERIMENTAL RESULTS AND ANALYSIS

4.1 Introduction

Eight permeable concrete mixtures were prepared with two aggregate sizes in two different proportions, different sand ratios, two aggregate to cement ratios (A/C) and a constant water to cement ratio (W/C). The target 28-day compressive strength was designed to be between 10MPa and 35MPa. The porosity ratio was designed to be between 25% and 15%, whilst the permeability was designed to be between 11.5mm/sec and 1.5mm/sec to provide a good spectrum for the investigation. An investigation into the effects of the aggregate size, sand ratio and aggregate to cement ratio on the mechanical properties (compressive strength, stress-strain behaviour and the modulus of elasticity) and on the hydraulic properties (porosity ratio and permeability) of the permeable concrete was undertaken and the relationships between these parameters were analysed.

4.2 Permeable concrete testing results and analysis

4.2.1 Density

The densities of the permeable concrete mix specimens (with and without sand), their mean values, their standard deviations, and their coefficients of variation are provided in table 4.1 below. The mean densities for the permeable concrete specimens in this research varied between 1965kg/m^3 and 2300kg/m^3. The aggregate sizes had a significant effect on the densities. These

were increased with an increase in the ratio of the large aggregate size (9.5mm) as in GC1* when compared with GC2* (with no sand added). This can be attributed to the fact that the larger aggregates have a higher bulk specific density than do the smaller aggregates.

Since the aggregate's specific gravity is lower than for that of the Portland cement, reducing the A/C ratio to 4.5 as in GA* resulted in an increase in the mix density due to a reduction in the aggregate, and to an increase in the amount of the Portland cement. An increase in the A/C ratio to 4.75 as in GB* resulted in an increased specific area and a reduced mix density; in this case, the amount of the cement paste was just enough to coat the aggregate particles, to produce connected voids and to create a good porosity and permeability but with a low compressive strength.

The sand ratio had another effect on the density; it increased with an increase in the sand ratio. This outcome can be attributed to the fact that the sand filled the voids between the aggregate particles and caused a reduction in the porosity ratio and an increase in mix density.

GC1 was made with a combination of 4.75mm and 9.5mm aggregates in 50%-50% proportions with no sand added.

GC2 was made with a combination of 4.75mm and 9.5mm aggregates in 75%-25% proportions with no sand added.

GA was made with a combination of 4.75mm and 9.5mm aggregates in 50%-50% proportions and different sand ratios.

GB was made with a combination of 4.75mm and 9.5mm aggregates in 75%-25% proportions and different sand ratios.

Table 4.1 Densities of the permeable concrete mixes

Sample no.	15% sand		10% sand		5% sand		No sand	
	GA15	GB15	GA10	GB10	GA5	GB5	GC1	GC2
1	2260	2255	2267	2068	2255	2068	2077	1985
2	2315	2267	2255	2079	2211	2068	2050	1977
3	2321	2300	2298	2220	2237	2052	2095	1976
4	2323	2208	2208	2211	2224	2078	2070	1936
5	2315	2210	2285	2220	2235	2220	1991	1966
Mean(kg/m^3)	2306.8	2248	2262.6	2159.6	2232.4	2097.2	2056.6	1968
Standard deviation	26.40	39.24	34.69	78.78	16.33	69.28	40.05	19.12
Coefficient of variation %	0.011	0.017	0.015	0.036	0.007	0.033	0.019	0.010

4.2.2 Compressive strength

Compressive strength tests were conducted on five specimens from each permeable concrete mix. Table 4.2 lists the 28-day compressive strength of each specimen, the mean values, the standard deviations, and the coefficients of variation of each set. The mean compressive strength of the range of permeable concrete mix designs ranged from 12MPa to 36.8MPa. The low compressive strengths can be attributed to the presence of larger pore voids between the aggregate particles, which act as a weakness zone inside the concrete.

An examination of the crack patterns of the failed permeable concrete specimens after compressive strength testing revealed that the crack surfaces almost always passed through the cement paste between the aggregate particles. Different failure behaviour was also observed between GA and GB specimens due to a change in the A/C ratio as will be discussed in section 4.2.6.

In the ‘No sand’ category, when using the same compaction energy, the same A/C and W/C ratios and different proportions of 4.75mm and 9.5mm aggregate as listed in table 4.2, both GC1 and GC2 had approximately similar compressive strengths (13MPa and 12MPa) although GC1 had a higher density.

A reduction in the A/C had a significant effect on the GA specimens’ tests results with A/C ratio equal to 4.5 compared with GB specimens with A/C ratio equal to 4.75. Ghafoori and Dutta (1995) noted that a reduction in the A/C ratio to 4 led to an increase in strength; a possible reason for this was related to a reduction in the aggregate amount, which resulted in an increase in the amount of cement paste around the aggregate particles, and, finally to an improvement in the compressive strength.

Table 4.2 Results of the 28-day compressive strength tests for the permeable concrete mixes

Sample no.	15% sand		10% sand		5% sand		No sand	
	GA15	GB15	GA10	GB10	GA5	GB5	GC1	GC2
1	35	29.2	28	17.1	23	17.1	12.64	12.7
2	38	27	29	19.95	20.22	14.3	12	12
3	36.6	31	26.5	24	24.6	13	12.3	9.8
4	38.6	25.7	26	21	26.8	16	17	12.3
5	36	27.5	30	20	25.3	17.7	10.6	12.8
Mean(MPa)	36.84	28.08	28	20.41	24.0	15.62	13	12
Standard deviation	1.47	2.06	1.67	2.48	2.51	1.95	2.42	1.23
Coefficient of variation %	0.04	0.07	0.06	0.12	0.10	0.13	0.19	0.10

Changing the sand ratio resulted in an increase in the compressive strength with an increasing sand ratio for the GA and the GB specimens. For example, increasing the sand ratio from 5% to 10% caused an increase in the compressive strength from 24MPa to 28MPa for the GA specimens, whilst this increase in the sand ratio caused an increase in the compressive strength from 15.6MPa to 20.4MPa for GB specimens. With the same A/C and W/C ratios and the same proportions of 4.75mm and 9.5mm (75%-25%), the compressive strength increased from 12MPa for the mix GC2 (with no sand added) to be 15.8MPa for GB5% with 5% sand (around 4MPa with each 5% increasing in sand ratio). The cement paste and the sand combined to increase the contact area between the aggregate particles and to improve the bonding between them. The increased strength was accompanied by an increase in density and by a reduction in porosity. Figure 4.1 shows a best-fit linear relationship between the increases in compressive strength and an increase in the sand ratio.

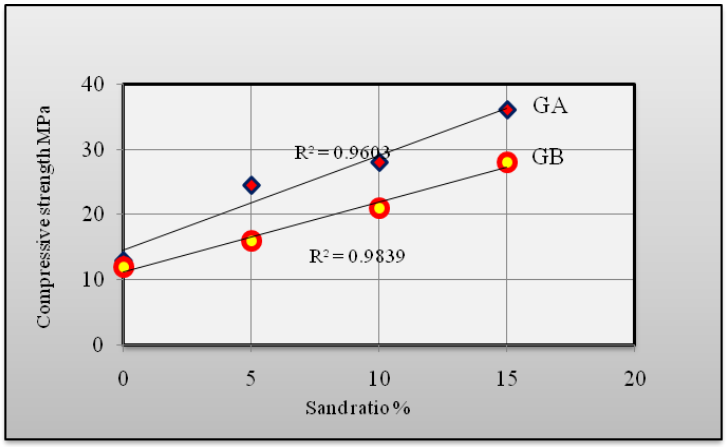

Figure 4.1 The development of compressive strength with an increase in sand ratio in permeable concrete for GA and GB mixes

4.2.3 Modulus of elasticity (MOE)

The MOE was determined for the test specimens using a regression analysis in Microsoft Excel 2007 software. This analysis was conducted on the linear part of the compression stress-strain curve of the permeable concrete specimens using the platen-to-platen and strain gauge methods. Data derived from the compressometer method was adopted from Goede (2009) and has been superimposed in figure 4.2.

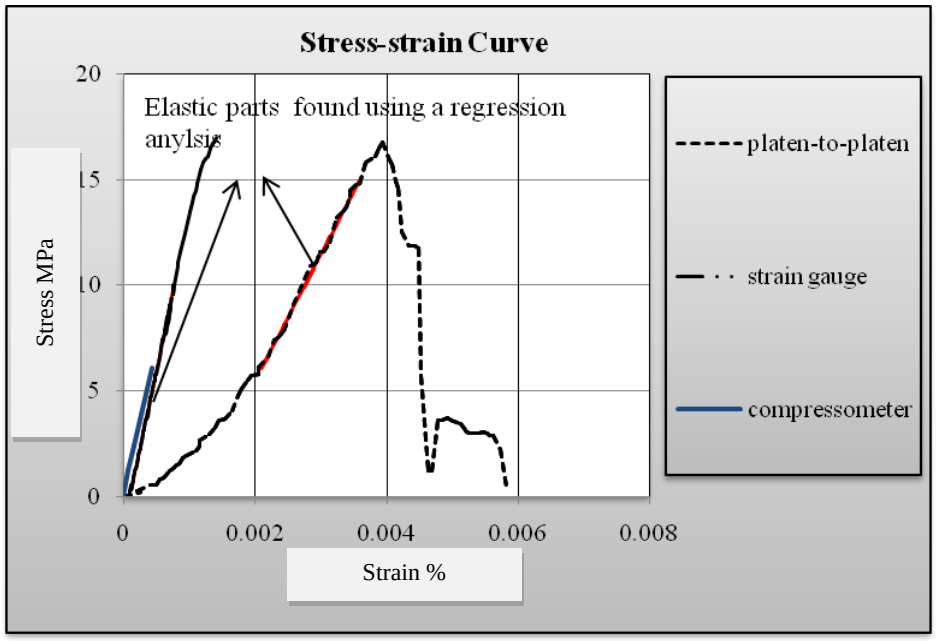

Figure 4.2 The stress-strain curves of the permeable concrete

4.2.3.1 The platen-to-platen method results

The MOE were determined for five specimens from each permeable concrete mixture using the platen-to-platen method. The results for each specimen, the mean values, the standard deviations, and the coefficients of variation are listed in table 4.3 below.

Since the modulus of elasticity is correlated to compressive strength, it is logical that the MOE would be lower for permeable concrete than for traditional concrete due to the lower compressive strength. The use of the platen-to-platen method demonstrated that the MOE of the permeable concrete varied between 3GPa and 9GPa and the compressive strength varied between 12MPa to 36.8MPa.

Table4.3 MOE results (platen-to-platen method) for permeable concrete mixes

Sample no.	15% sand		10% sand		5% sand		No sand	
	GA15	GB15	GA10	GB10	GA5	GB5	GC1	GC2
1	10.5	7.1	8.5	6.3	5.5	4.96	5.5	3.5
2	9.5	7	9	5.5	5.8	4.86	4.5	3
3	8.7	9	7	7	6.5	4.42	3.2	4
4	8.2	7	7.5	5.5	7.3	4.75	5.5	2
5	9.4	5.88	8	4.8	6	6.4	4.5	3.2
Mean(GPa)	9	7	8	6	6	5	4.5	3
Standard deviation	0.87	0.9	0.8	0.84	0.7	0.76	0.95	0.74
Coefficient of variation %	0.093	0.13	0.10	0.14	0.11	0.15	0.20	0.24

4.2.3.2 The strain gauge method results

Three specimens were utilised from each mix design to measure the MOE in the central part of the permeable concrete specimens using a strain gauge method. The results for each specimen, the mean values, the standard deviations, and the coefficients of variation are listed in table 4.4. The MOE of the permeable concrete specimens, which were measured using the strain

gauge method, varied between 27.8GPa and 8.4GPa. These values were significantly higher than for those that were measured using the platen-to-platen method.

Table 4.4 MOE results (strain gauge method) for permeable concrete mixes

Sample no.	15% sand		10% sand		5% sand		No sand	
	GA15	GB15	GA10	GB10	GA5	GB5	GC1	GC2
1	28	27	23.05	15.6	26.6	19	15	7.8
2	25.4	18.4	26.6	17.25	22	15	13	7.6
3	30	17.88	19.5	19.55	18.6	9.7	9	9.7
Mean (GPa)	27.80	21.09	23.05	17.47	22.40	14.57	12.33	8.37
Standard deviation	2.31	5.12	5.02	1.98	4.01	4.67	3.06	1.16
Coefficient of variation %	0.08	0.24	0.15	0.11	0.18	0.32	0.25	0.14

The tests results for the two testing methods, which were conducted on the eight permeable concrete mixes, reveal the major influence that the larger aggregate size will exert on the MOE of the permeable concrete mixes, since the MOE increased when a 9.5mm aggregate was combined with a 4.75mm aggregate in a 50%-50% proportion. This behaviour is similar to that of conventional concrete in which larger aggregate sizes result in higher MOE values. The larger aggregate particles have the effect of reducing the contact areas between the particles, which have been previously considered to be the weakest zone inside the concrete; the internal MOE is thus increased by the adding of the larger size of aggregates.

The test results listed in tables 4.3 and 4.4 demonstrated that the MOE of the permeable concrete mixes was enhanced by increasing the sand ratio and by reducing the A/C. This can be attributed to an increase in the thickness of the cement paste around the aggregate particles and the interfacial transition zone (ITZ) where the cracks usually occurred.

4.2.3.3 Compressometer method results

The compressometer method was used by Ghafoori and Dutta (1995) and by Goede (2009) to measure the MOE according to the ASTM C-469 (2002). Table 4.5 summarises the test results of Goede (2009).

Table 4.5 MOE results (compressometer method) for permeable concrete mixes,Goede (2009)

Sample name	MOE GPa	Compressive strength MPa	Porosity ratio %
WE1	12.99	11.35	27.7
WE2	12.86	9.25	28.1
WE3	15.19	11.45	28.1
WE4	13.44	11.52	27.1
WE5	12.06	9.67	27
WE6	12.57	11.34	27.1
WE7	9.75	9.81	28.2
WE8	14.99	11.14	25.9
WE9	12.99	10.69	25.9
WE10	12.18	9.95	26.4

A considerable difference was found for the MOE, which were measured using the strain gauge or compressometer methods, and the MOE, which were measured using the platen-to-platen method. The platen-to-platen method

consistently gave a lower value than did other methods. This can be attributed to the softness of the sulphur-mortar capping components, the interface between the specimen and the platens and the overall machine compliance (Hussin et al. 2012). The high porosity in the top section of the permeable concrete specimen also had an additional effect on lowering the MOE that were determined using the platen-to-platen method.

The results that were found using the strain gauge and the compressometer methods were approximately similar. This was expected and can be explained by the fact that these two methods measured the MOE in the central part of the specimens. The measurements were not affected by the sulphur-capping material, the overall machine compliance, or by any changes in the porosity from within the end sections of the specimen.

4.2.4 Evaluation of the MOE along the permeable concrete from top to bottom

Since vibration and rodding methods were used during the preparation of the permeable concrete specimens, a variation in the area of the voids along the height of the permeable concrete cylinder can be expected. These porous characteristics and their distribution inside the specimens affected some of the fundamental properties of the permeable concrete such as the MOE.

To highlight this characteristic, three strain gauges were fixed to the same specimens in three different locations (top, centre, and bottom) using the same procedure that was outlined in Chapter 3. Figure 4.3 shows the location of the three strain gauges. The MOE was measured from the stress-strain curve of

each strain gauge using regression analysis as previously utilised in section 4.2.3. Figure 4.4 shows the stress-strain curves derived for the specimens with these three strain gauges. Figure 4.4 demonstrates that the MOE changed from section to section throughout the same specimen. The MOE of the top section was also lower in value. This can be attributed to a higher porosity in this section and due to the fact that the contact area between the particles was reduced.

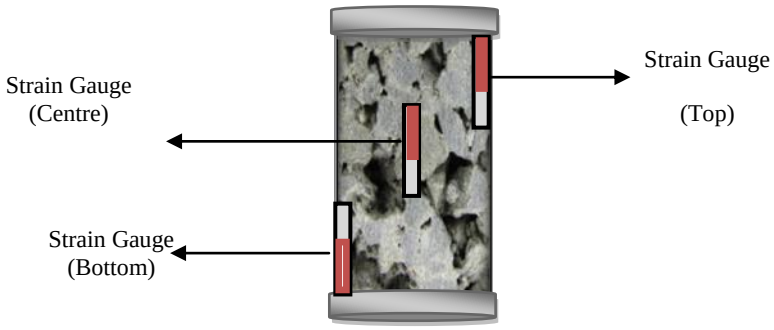

Figure 4.3 A permeable concrete mix sample showing the location of the three strain gauges.

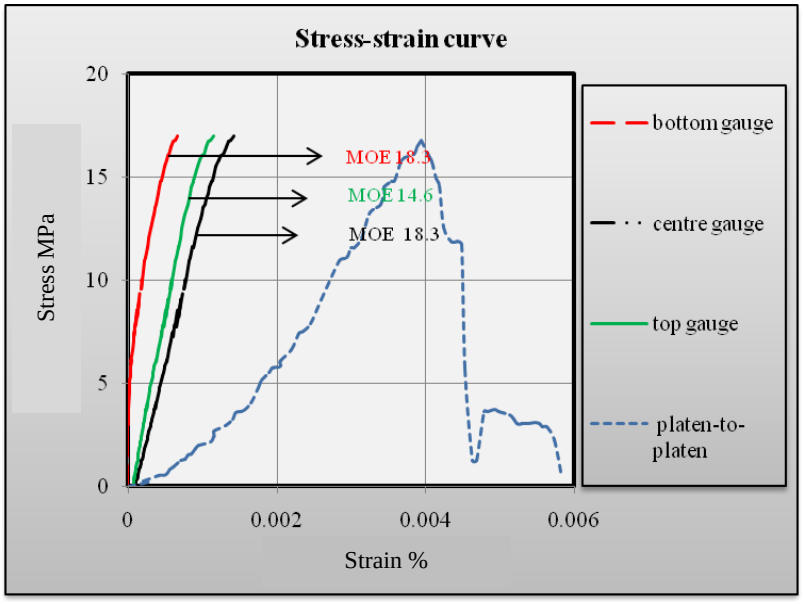

Figure 4.4 Stress-strain curves for specimens measured with three strain gauges

The deformation in the bottom section was very low in the initial stages of testing and, as a result, the strains were less and this was due to the increased mass and fewer voids as shown in figure 4.5

Porosity 25%	Porosity 23%	Porosity 20%
Top part	Central part	Bottom part

Figure 4.5 The difference in porosity that was measured using ERADS IMAGINE 2011 software

During the preparation of the specimens, the concrete mix was placed in three layers and each layer was subjected to vibration. This procedure resulted in the bottom part of each specimen undergoing more compaction and vibration than the higher sections thus resulting in an increase in the contact area between the coarse aggregate particles. With continued vibration for the central and the top sections, a large number of the smaller sized and coarse aggregate moved downwards to fill most of the voids in the bottom section. A relatively high, downward flow of cement paste and sand particles also clogged the voids. The result was a reduction in the porosity ratio in the bottom section of the specimen. The middle section was, however, only subjected to two vibration durations and the top section was subjected to only one. This change in the porosity characteristics throughout the permeable concrete specimens had an effect on the MOE results from section to section.

4.2.5 The stress-strain behaviour

For all tests, the axial stress and strain could be measured simultaneously by the platen-to-platen method, which provided a global strain measurement, whilst the local strain could be measured either by the axial strain gauge or by the compressometer methods. These three measurements allowed the effective evaluation of the specimen's strain homogeny during testing. Figures 4.6, 4.7 and 4.8 demonstrate the stress-strain curves for the three groups GA, GB and GC, respectively, which were measured using the platen-to-platen and the strain gauges method.

The strain at peak stress for a given rate of loading usually increases with an increase in the peak stress and decreases with an increase in the rate of loading for traditional concretes of similar strengths (Deo & Neithalath 2010). Other parameters such as porosity characteristics, void distributions and the testing method will influence the peak stress and the corresponding strain for permeable concrete (Deo & Neithalath 2010).

The test results indicated that the effect of aggregate size and the sand ratio on both the global and local strains were insignificant. It can be seen from the following figures that there was a major difference between the local strain, which was measured by the strain gauge, and the global strain, which was measured by the platen-to-platen method. In all cases, the local strain was much less than the global strain. This is not unexpected because there are two fractions in the permeable concrete; one fraction of the strain was used to close up the pores, while the other fraction was used to deform the particles in the specimen. The strain distribution will be uniform throughout the deformed material for normal concrete due to the absence of voids. The results obtained from each measurement would thus be very similar. Due to the volume change during the compression test, the lateral deformation and Poisson ratio for the permeable concrete specimens would, however, be less than for the normal non-permeable concrete.

The softness of the sulphur-mortar capping components, the interface between the specimen and the platens, the overall machine compliance and changing porosity along the permeable concrete specimen played another effect on the

displacement measured using the platen-to-platen method and the one measured using the strain gauge's method.

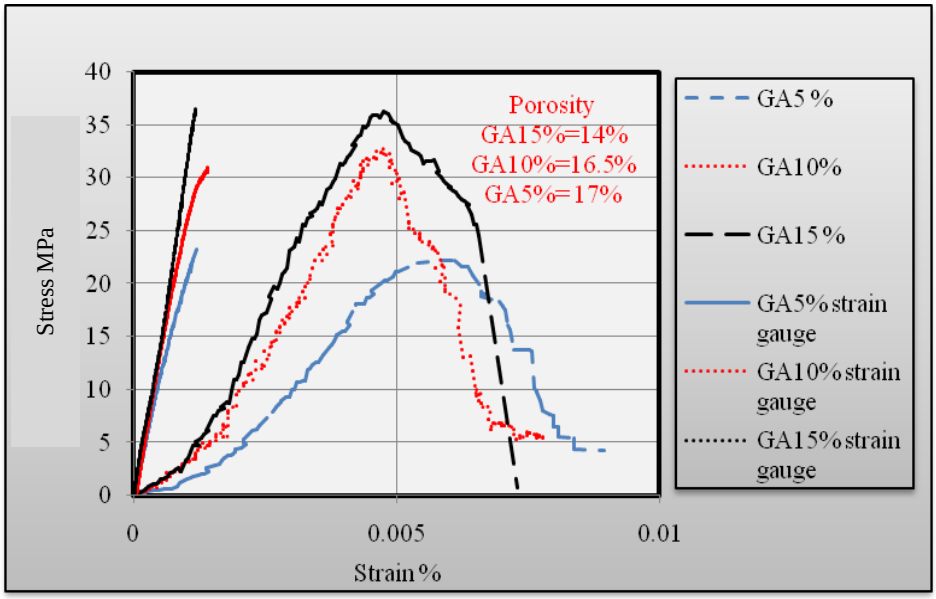

Figure 4.6 The stress-strain curves for GA

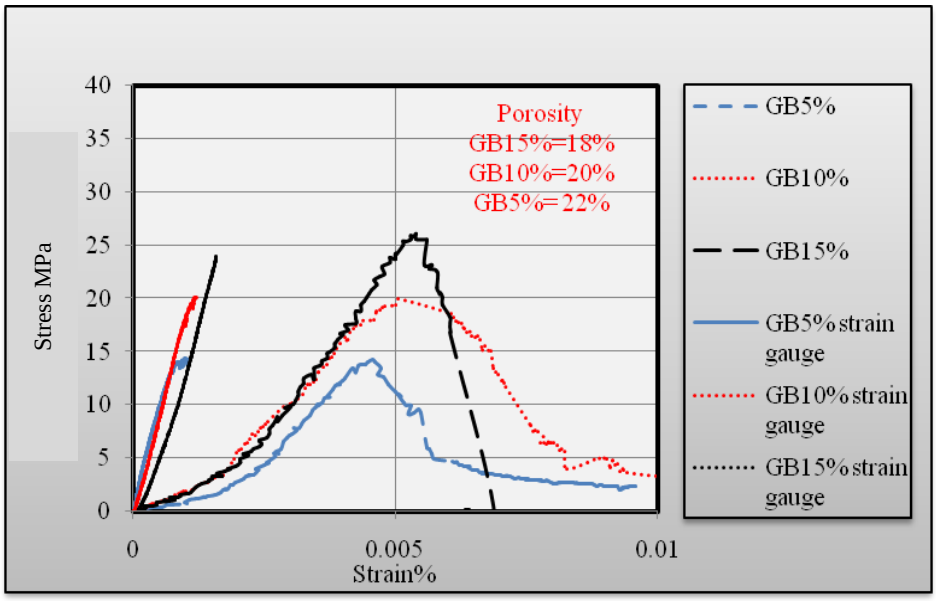

Figure 4.7 The stress-strain curves for GB

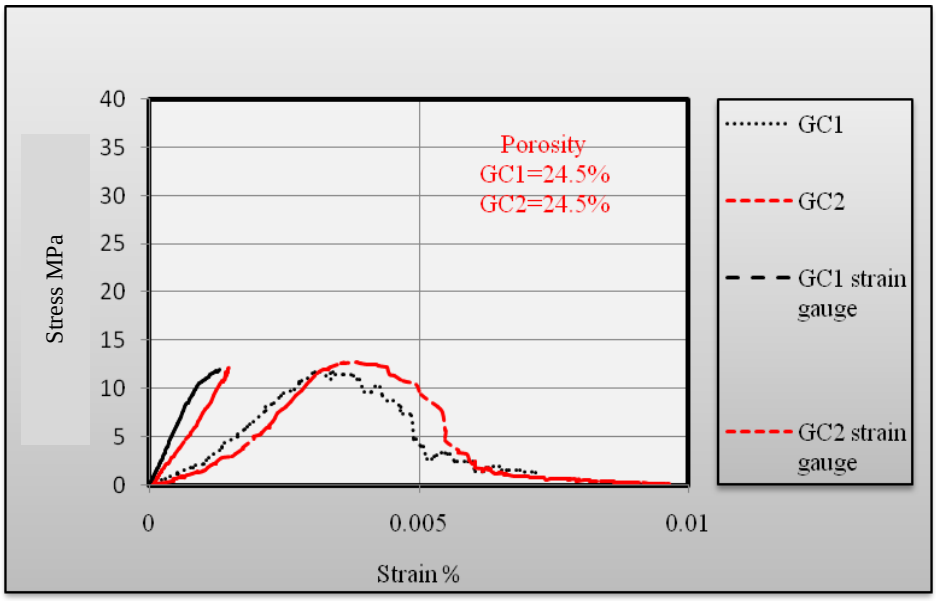

Figure 4.8 The stress-strain curves for GC

For comparison purposes, the same scale was used in figures 4.6, 4.7 and 4.8. GA permeable concrete specimens showed higher compressive strengths and lower porosities ratios. GB specimens showed both acceptable compressive strengths and porosities ratios, while GC with (no sand added) showed lower compressive strengths and higher porosities ratios.

With an increase in the sand ratio, the larger aggregate size and a reduced A/C ratio, the permeable concrete specimen exhibited a higher compressive strength and a reduction in the porosity. As a result, the ascending branch of the stress-strain curve began to be steeper and more linear due to a reduction in bond cracking and this resulted in less internal micro-cracking for a given imposed axial strain. The higher the compressive strength, the larger is the decrease in the descending rate after the maximum strength is reached. In other words, the descending part of the stress-strain curve exhibits more ductile

behaviour and gradual cracking with an increasing porosity ratio and a reduction in the compressive strength.

The peak strain in the conventional concrete increases slightly with an increase in the compressive strength (Hsu & Hsu 1994), while the relationship between these two parameters in the permeable concrete is fairly weak due to the pore characteristics inside the specimens; this is the same result as that found by Deo and Neithalath (2010). The tests results demonstrate that the strain of the permeable concrete specimen is higher than that of the traditional concrete under the same loads; this is mainly due to the lower elastic modulus of the permeable concrete. It was, however, observed that beyond the peak stress, the strain that was measured by the gauge was very low while the strain that was measured by the platen-to-platen method was very high. This loss of strain homogeny at peak stress levels is visible in the results of most tests; it reveals strain localisation and strain characteristics of the concrete damage behaviour. The strain thus increases at a faster rate than does the applied stress and so the curvature of the strain-stress curve decreases with an increase in the porosity ratio.

Investigations into the stress-strain behaviour of the permeable concrete is still very limited. Deo and Neithalath (2010) found that the stress-strain relationship for permeable concrete is similar in shape to that of conventional concrete. The stress-stain curve of the permeable concrete is generally divided into four different parts as shown in figure 4.9.

- The first part of the stress-strain curve for the platen-to-platen method was between 0 and 5% of the peak stress; this part was affected to a high degree

by the sulphur-capping, which produced a non-standard result. This was due to the rough interface between the concrete and the capping material, which produced a non-standard stress distribution within the top portion of the cylinder during testing (Richardson 1991). This was not, however, observed from the stress-strain curve of permeable concrete, which was tested by Deo and Neithalath (2010) (these authors used the same mix design as for the GC group in this thesis). This is because the sulphur capping was not used during the compression test that was carried out by Deo and Neithalath (2010) as it can be observed in figure 4.10. The only recorded effect was coming from the pore voids inside the whole specimens. The curve was not affected by the sulphur-capping material or by the voids in the top and bottom part of the specimens for the strain gauge method; it just gave the stress-strain curve for the middle section.

- Using the platen-to-platen method, the elastic behaviour started after reaching approximately 5% of the peak stress between points A and B as shown in figure 4.9. The stress-strain plot started to become linear and the static MOE could then be found from the slope of the curve or by using a regression analysis in Excel software. At this elastic section, the specimen could return to its original shape when the applied load was removed because the transition zone crack in the permeable concrete specimen remained stable. For the strain gauge method, the elastic part started from point zero because it was not affected by any other external affects such as by the sulphur capping or by other, internal factors such as the voids in the top and the bottom parts of the permeable concrete specimen.

- The plastic part started when the stress-strain curve deviated gradually from a straight line up to the critical point (point B), beyond which the stress-strain curve began to bend more sharply to the horizontal until it reached the peak stress. At this point, the crack (s) began to increase in length, width, and numbers so that the stress-strain curve became non-linear and, thus, the material would not return to its original shape when the applied load was removed.

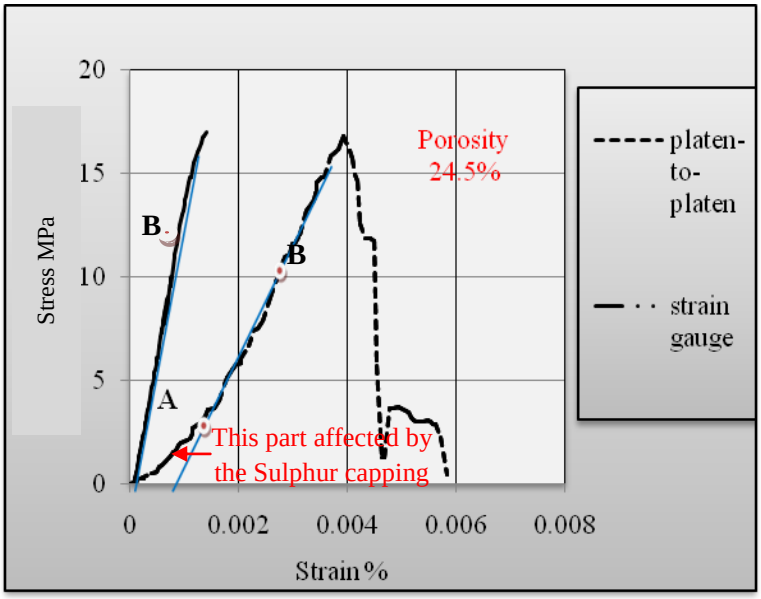

Figure 4.9 General stress-strain curves for the permeable concrete

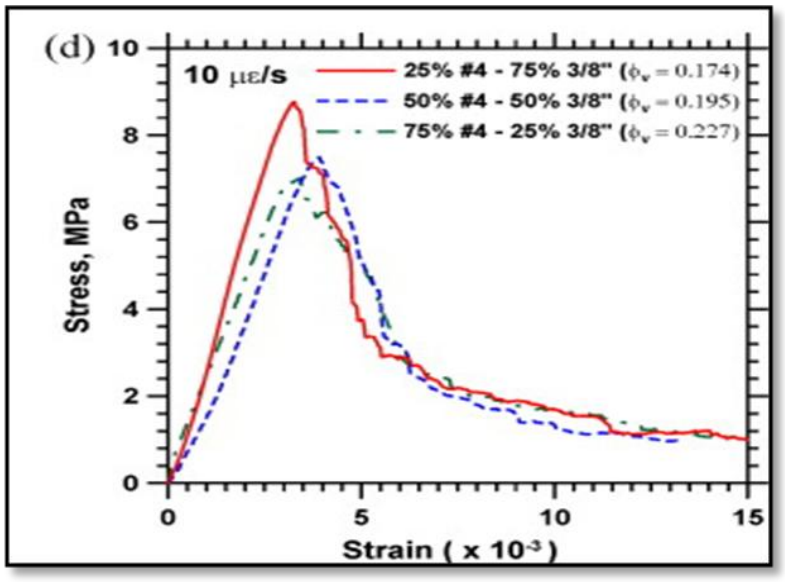

Figure 4.10 Stress-strain curves for permeable concrete

(Deo & Neithalath, 2010, p.4)

- The descending branch started after reaching the peak stress and the specimens started gradually to deform until they failed. The test results showed a different failure pattern for the permeable concrete and it was generally dependent on the porosity. The slope of the descending branch thus decreased as the porosity increased.

The conclusion can thus be drawn that an increase in the porosity leads to a possible change in the stress-strain response. This change is generally characterised by a significant decrease in the curvature of the stress-strain curve and by an increase in the ductility of the permeable concrete as described by the descending portion of the stress-strain curve.

4.2.6 Failure behaviour of permeable concrete

The failure mode of the permeable concrete that was observed during the testing was clearly different from that of the conventional concrete. In general, the permeable concrete gradually failed after reaching the peak load (whereas the conventional concrete underwent a rapid brittle type of failure at the peak load).

When failure of the permeable concrete commenced at peak stress, the applied load started to decrease slowly and several continuous, short vertical cracks appeared and then coalesced into inclined macro-cracks. The cracks in the interfacial transition zone became unstable and crack propagation in the matrix increased. The test specimen was, however, supported by the fraction between the cracks. As the strain was effectively controlled, some of the GC specimens with high porosity did not spall and maintained their completeness until the end of the test. The inclination angles of the macro cracks with respect to the vertical loading plumb were between 65^{o} and 80^{o}. The tests results also demonstrated that the specimens with high compression strength, lower porosity and a higher MOE demonstrated a more brittle behaviour (shown by a sudden drop in post-peak stress level) as in GA15%, GA10% and GB15%. It was observed that an uniform increase in load that was applied within several seconds caused no cracks but, rather, a sudden sharp, explosive break occurred when the peak load was reached, and the piece partly disintegrated into small pieces as shown in figure 4.11.

With increased porosity and a reduction in the sand ratio, the test specimens being gradually compressed revealed a ductile behaviour as shown in figure

4.12. Figure 4.13 demonstrates the crack pattern in a permeable concrete specimen and the inclination angles of the macro-cracks with a high porosity ratio. It can be observed that the broken surface passed through the cement paste; the broken surface thus exhibited a rough surface. This indicates that the strength of the cement paste was lower than for that of the aggregate particles (which means not enough cement in the mix) and this phenomenon was thus different from the behaviour of the conventional concrete.

Figure 4.11 The sudden crack in the permeable concrete specimen with low porosity

Figure 4.12 The gradually developed crack in the permeable concrete specimen with high porosity

Figure 4.13 The failure pattern through the cement paste in the permeable concrete specimen

4.2.7 Volumetric porosity

The porosity ratio in permeable concrete is much greater than in conventional concrete. Mixes with a higher porosity exhibit a lower compressive strength due to the reduction in the support between the coarse aggregate particles. Several of the GA specimens produced much higher compressive strengths of approximately 38MPa but had a porosity of less than 15%. The porosity tests were undertaken after the specimens had been aged for 14-days. The volumetric porosities, the mean values for the specimens were also reported.

The volumetric porosity of the permeable concrete was estimated using two different procedures. In the first procedure, the dry weights of the specimens were measured at room temperature and humidity, while the specimens were oven-dried in the second procedure at 110^{o}C for 24 hours. For both procedures, the specimens were then submerged in water for 30 minutes and the porosity was measured in the manner as described in Chapter 3 section

3.5.5. Table 4.6 lists the porosity ratio results, which were measured at room temperature. Table 4.7 lists the porosity ratio results, which were measured after storing the specimens in the oven. The test results calculation procedures are in Appendix A. Considerable differences were found between the porosity ratios, which were determined by these two different procedures. Researchers such as Montes, Valavala and Haselbach (2005) used an oven-dried weight for measuring the porosity ratio but the dry-weight was, however, measured at room temperature in this research because this researcher believed that such a porosity measurement is more representative of the porosities encountered inside the construction area. The results from that procedure were thus used in this research.

Table 4.6 The porosity ratios at room temperature

Sample no.	15% sand		10% sand		5% sand		No sand	
	GA15	GB15	GA10	GB10	GA5	GB5	GC1	GC2
1	13.5	19.1	17.0	21.3	16.2	22.4	25.3	24.3
2	14.9	17.1	15.6	18.6	17.4	21.7	24.1	24.9
Mean %	14	18	16.5	20	17	22	24.5	24.5

Table 4.7 The porosity ratios after storing specimens in the oven

Sample no.	15% sand		10% sand		5% sand		No sand	
	GA15	GB15	GA10	GB10	GA5	GB5	GC1	GC2
1	26.9	29.2	29.1	32.1	28.4	31.8	30.2	32.3
2	23.1	27.2	25.6	30.1	28.6	33.5	31.8	32.7
Mean %	25	28	27.4	31	28.5	32.5	31	32.5

The laboratory test results demonstrated that the porosity ranged from approximately 14% to 24% and that it corresponded to the values of porosity as reported in the literature review. With reference to the volumetric porosity for the GC specimens (without any sand added) in table 4.6, the aggregate size did not appear to have any effect on the test results, which were distinguished by the effect of increasing the amount of the 9.5mm aggregate in the permeable concrete mixture. Increasing the A/C ratio produced a direct effect on the porosity ratio; an increase in the ratio resulted in an increase in the aggregate amount and an increase in the specific surface area. Extra cement paste would thus be required for coating a larger specific surface, and would have resulted in no excess paste clogging the voids. The results also showed that the sand ratio has a significant influence in reducing the porosity of both the GA and the GB permeable concrete mixes due to it filling the voids between the aggregate particles.

4.2.8 Determination of the porous area

The pore spaces were measured in three sections (top, middle and bottom) to quantify pore continuity in a specimen. The method employed was to first image each section and then, to measure the pore areas using the ERADS IMAGINE 2011 software as described in chapter 3 section 3.5.6. The results are presented in terms of porous area percentage index (P_{area}%). The equation for calculating P_{area} % is expressed as follows:

$$P_{area}\% = \frac{\sum A_p * 100}{\sum A_t} \quad (4.1)$$

Where

P_{area}% = percentage of the pore area

A_p = total cross-section pores in the specific part of the specimen

A_t =total cross-sectional area of the specific part of the specimen

The pore areas for the different sections of the permeable concrete specimens are listed in table 4.8. Figure 4.14 demonstrates the sequential development of the pore areas through the permeable concrete specimen.

Table 4.8 Solid and pore areas for different sections through the permeable concrete specimens

Mix name	Top part		Centre part		Bottom part		Average
	Solid areas	Pore areas	Solid areas	Pore areas	Solid areas	Pore areas	
GA15%	84.9	15.1	87	13	88.14	11.86	13.31
GA10%	83	16.93	84	16	89.27	10.73	14.56
GA5%	79.03	20.97	84.24	15.76	88.59	11.41	16
GB15%	75.60	24.40	80.81	19.19	81.61	18.39	20.66
GB10%	68.42	28.58	80.7	19.3	82.43	17.57	21.80
GB5%	73.64	26.36	78.13	21.87	79.64	20.36	22.87
GC1	68.68	29.32	78.14	21.86	78	17.35	22.84
GC2	75.4	24.6	78.22	21.78	78.5	21	22.46

GA15% Top part

GA15%Centre part

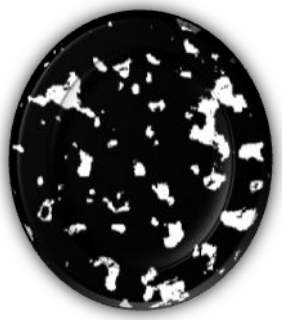

GA15% Bottom part

GA10% Top part

GA10%Centre part

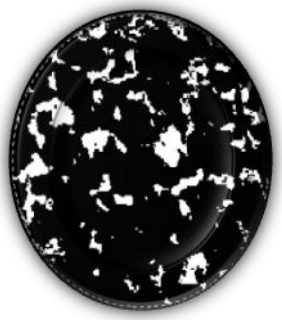

GA10% Bottom part

GA5% Top part

GA5%Centre part

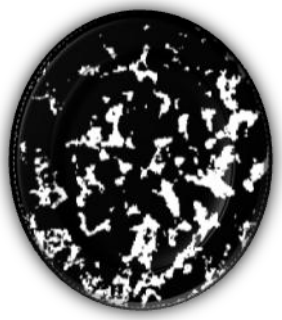

GA5% Bottom part

GB15% Top part

GB15%Centre part

GB15% Bottom part

GB10% Top part

GB10%Centre part

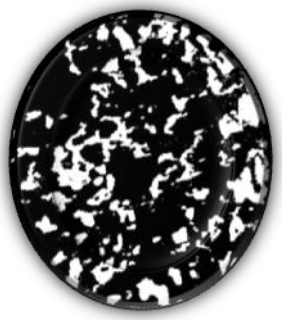

GB10% Bottom part

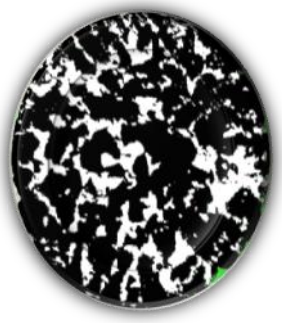

GB5% Top part

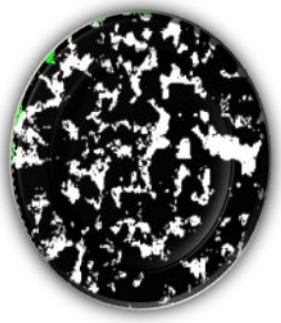

GB5%Centre part

GB5% Bottom part

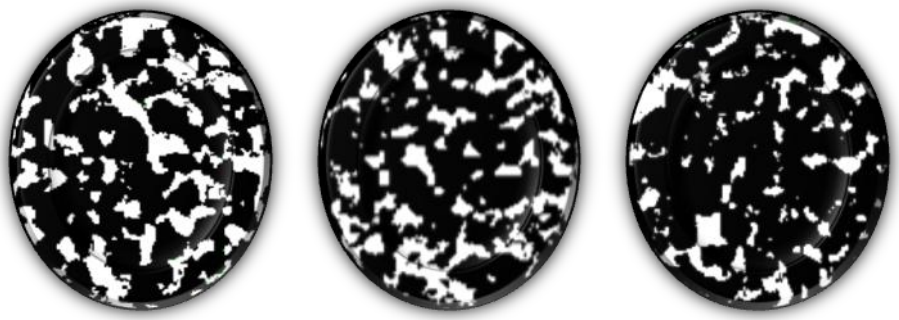

GC1% Top part GC1%Centre part GC1% Bottom part

GC2% Top part GC2%Centre part GC2% Bottom part

Figure 4.14 The development of the pore areas through the permeable concrete specimen

The tests results demonstrate that the aggregate size did not show any effect on the averge pore area, which were approximately similar for GC1 and GC2. It can, however, be observed from the results in table 4.8 that there was a reduction between the porosities in the different parts of the permeable concrete specimen itself. It was observed that, for the specimen produced by using a blend of 4.75mm and 9.5mm aggregate in equal ratio, there was a big reduction in the porosity area and especially in the bottom part of the specimen. This can be attributed to the fact that the smaller aggregate filled most of the pores during the three periods of vibration used in the preparation of the specimen. The pores in the GC2 specimen also showed more

homogeneity in the distribution throughout the cross section and large numbers of pores were unconnected in the bottom section.

The average pore areas along the permeable concrete specimen (see table 4.8) demonstrated approximately a similar result to those demonstrated when using the volumetric porosity tests (see table 4.6). That can attributed to the fact that both of these methods measured the conected and unconnecteded voids within the permeable concrete.

4.2.9 Permeability

The primary function of a permeable concrete mixture is the construction of a structure that can adequately support the required load and can also ameliorate excessive storm-water discharge. The mixtures that were expected to possess the best permeability were those with a high porosity. The permeability tests were undertaken when the specimens were 14-days old. The permeability test results included the mean values, which are listed below in table 4.9. The calculations for these results can be found in Appendix B.

These test results demonstrate that the specimens that exhibited the highest permeability had neither the highest porosity, nor the largest pore area connectivity. This indicates that permeability is not directly a function of the porosity but, rather, of the pore connectivity. Figure 4.15 shows a two-dimensional permeable concrete specimen with connected and unconnected voids. It can be observed from this figure that this specimen contained a high percentage of pore areas, but a large number of these voids were unconnected

to the process of transferring the water through it. Its permeability would thus be very low even with a high porosity.

Table 4.9 The results of the permeability tests

Sample no.	15% sand		10% sand		5% sand		No sand	
	GA15	GB15	GA10	GB10	GA5	GB5	GC1	GC2
1	1.50	3.97	1.55	4.28	1.97	7.71	5.50	13.67
2	1.67	2.72	1.93	3.45	1.94	7.04	7.05	9.10
Mean mm/sec	1.6	3.5	1.75	4	2	7.5	6.3	11.58

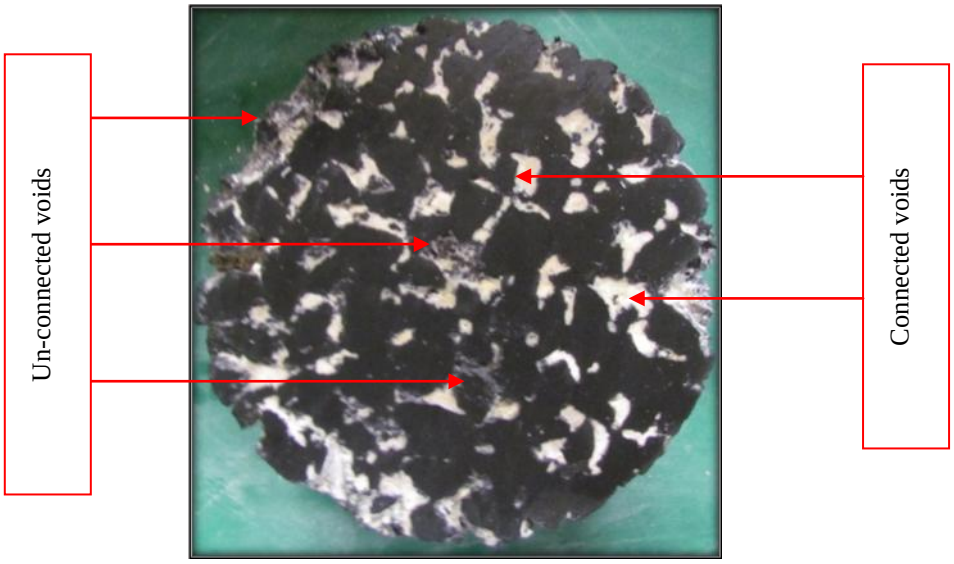

Figure 4.15 Two-dimensional permeable concrete's specimen with connected and un-connected voids

The laboratory tests results demonstrate that the aggregate size does have a significant effect on the permeability. With the same A/C ratio, the same compaction energy and with no sand added, the concrete mixes, which were

made with blends of the highest ratio of the 4.75mm aggregate, exhibited the highest permeability. This can be explained by the fact that the smaller aggregates produced more homogenous and connected voids rather than those produced by the larger aggregates. The smaller aggregate appears to have filled the voids between the larger aggregate (especially in the bottom part) during the vibration that was used during the preparation of those specimens, and which were made with a combination of 4.75mm and 9.5mm aggregate in equal ratio. A reduction in the A/C also corresponded to another reduction in the permeability coefficient and this was due to a reduction in the amount of the aggregate and to an increase in the amount of the cement paste, which resulted in the clogging of the voids (especially in the bottom part) due to the use of vibration. Increasing the sand ratio also appears to have reduced the water permeability since it combined with the cement paste and with the smaller aggregate to fill the voids left inside the permeable concrete.

4.3 Relationships among the fundamentals properties of the permeable concrete

4.3.1 Density and compressive strength

The testing results for the density and the compressive strength from this research and from Yang and Jiang (2003) are shown in Figure 4.16

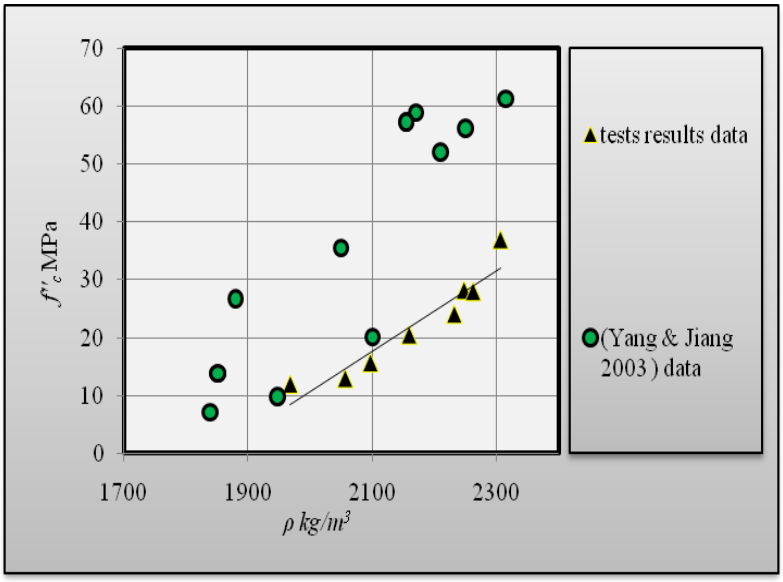

Figure 4.16 The relationship between the density and the compressive strength

As can be observed from Figure 4.16, a significant linear relationship (as shown in equation (4.2) was found between the density and the compressive strength (Coefficient of Determination R^2 =0.899) based on the testing data from this research; the strength increased with an increase in the density for all permeable concrete mixes and this trend was expected. The results of this research were observed to conform to the results of Yang and Jiang (2003) when the compressive strength was less than 20MPa and the density was less than 2100 kg/m^3. The strength results from this research were shown to be lower with a higher density by comparison to the results that were derived from the permeable concrete mixes of Yan and Jiang (2003); the compressive strength of the latter's was higher than 20 MPa. That can be attributed to the fact that those authors used different additives to enhance the compressive strength such as silica fume (SF)*, superplasticiser (SP)*, vinyl acetate-ethylene emulsion (VAE)* and polyvinyl alcohol formaldehyde hydrosol (PAF)*. All of these additives greatly enhanced the strength, while the authors

controlled the pressing force to keep the unit weight between 1900-2100 kg/m^3 even as they increased the strength. Although the strength results of Yang and Jiang (2003) reached 57.2 MPa, the permeability was reduced to 1.7mm/sec.

$$f'_c = 0.069\,\rho - 129. \qquad (4.2)$$

Where:

f'_c =the compressive strength in MPa

ρ =the permeable concrete density in kg/m^3

4.3.2 Compressive strength and the MOE

Generally, the tests results showed that the MOE increased with an increased compressive strength for all permeable concrete mixtures even when using different methods to measure it. The MOE tests results for the permeable concrete mixtures using the platen-to-platen and strain gauge methods, the data from Goede (2009) in table 4.5, and the results that were calculated by equation 4.3 below as suggested by Ghafoori & Dutta (1995) are shown in the following figure 4.17.

SF, the Sio_2 content is 92.45%, and specific surface area is about 18,000 m^2/kg.
SP, the SP is liquor of the phenolic aldehyde. Its density is 1.1g/cm3 and has 31% solid content.
VAE emulsion is fluid milk-white dispersions of copolymers of vinyl acetate and ethylene in water. The solid content of the emulsion is 55%. Its pH value is 4.5 and density is 1.07gm/cm^3.
PAF hydrosol is a limped solution of polyvinyl alcohol formaldehyde. The solid content of the hydrosol is 8% and the density is 1.04g/cm^3.

(Yang & Jiang 2003, p. 382 and 383)

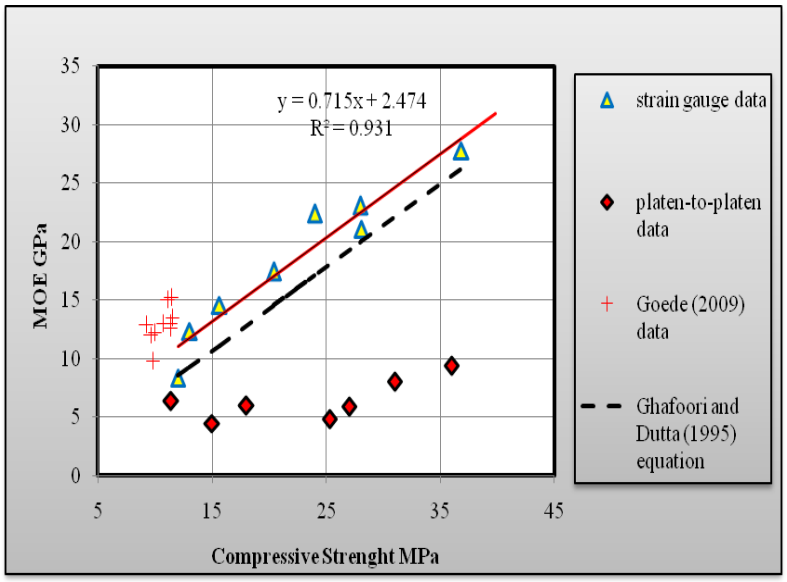

Figure 4.17 The relationship between the compressive strength and the MOE

$$E_{it} = 0.7134 * f'_c 2 \quad (4.3)$$

Where:

E_{it} = MOE GPa

f'_c = compressive strength MPa

(Ghafoori & Dutta 1995)

It can be observed from figure 4.17 that the equation that was proposed by Ghafoori & Dutta (1995) mirrored the strain gauge data and gave approximately the same trend. These authors used the compressometer method to find the MOE of the permeable concrete; the test results demonstrated slightly higher results than those predicted by equation 4.3. The test results from the platen-to-platen method did not, however, show any correlations with either the strain gauge or the compressometer method since the specimens were affected by the sulphur capping. A fitted linear equation (4.4) with R^2

=0.93 to find the MOE (strain gauge method) using the compressive strength data where:

$$E_{it} = 0.715f'_c + 2.474 \quad (4.4)$$

This relationship is very important on the construction site where the concrete specimens are just available for the compressive strength tests.

In order to avoid the difficulties of fixing the gauge onto the rough surface of the permeable concrete, it is very important to find a relationship of the MOE, which is determined using the strain gauge (sg), and by using the platen-to-platen (p-to-p) method. This would enable the designer to use the p-to-p method and then to apply a simple relationship for finding a much more representative MOE of the permeable concrete. Figure 4.18 shows the relationship between the MOE that have been derived from these two testing methods.

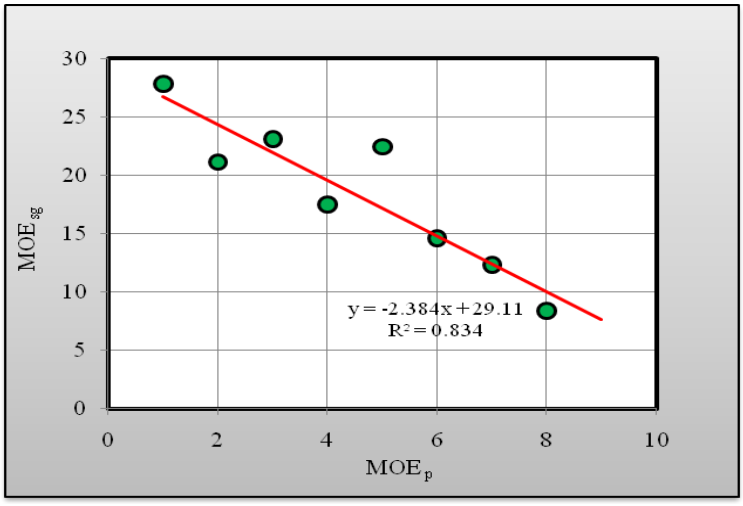

Figure 4.18 The relationship between the MOE derived from the two testing methods

The fitted linear relationship yields equation (4.5), with R^2 =0.834.

$$E_{itsg} = -2.384\ (E_{itp}) + 29.11 \quad (4.5)$$

Where:

E_{itsg} = MOE for the strain gauge

E_{itp} = MOE for the platen-to-platen

4.3.3 Porosity and compressive strength

Figure 4.19 shows the relationship between the porosity and the compressive strength for the eight permeable concrete mixtures. The results from Goede (2009) in table 4.5 and the results calculated by equation (4.6) as suggested by Lian, Zhuge, and Beecham, (2011) have also been included.

$$f'_c = 231.44\ e^{-0.09P} \quad (4.6)$$

(Lian, Zhuge, & Beecham 2011)

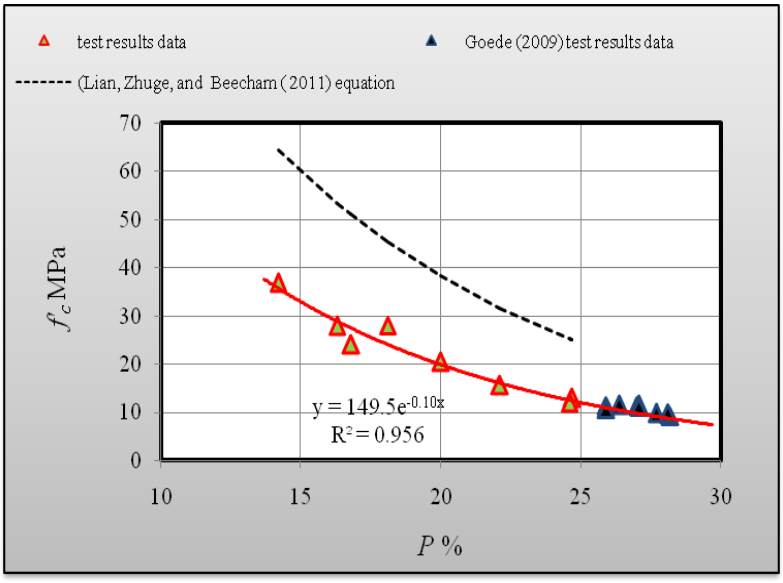

Figure 4.19 The relationship between the porosity and the compressive strength

The tests results demonstrate that the compressive strength drops exponentially as the volumetric porosity increases as presented in equation (4.7) with R^2=0.95. It can be observed from figure 4.19 that the results of Goede (2009) are well matched with the trend line of these research results. This may be partially attributed to the fact that this author used the same volumetric porosity measurement procedure as was used in this study. The equation that was suggested by Lian, Zhuge, and Beecham (2011) gave a higher prediction of compressive strength but with a result that followed a similar trend. This can be explained by the fact that those authors measured the volumetic porosity after drying the specimen in the oven for 24 hours and that caused a higher porosity result.

The porosity range of permeable concrete is between 15% to 25 % ,while the range of its compressive strength is between 35MPa to 10MPa. This range has been noted by several researchers as previously discussed in Chapter 2.

$$f'_c = 149.5e^{-0.10P} \quad (4.7)$$

Where

f'_c =compressive strenght MPa

P =porosity ratio%

4.3.4 Porosity and permeability

Figure 4.20 shows the relationship between porosity and water permeability for the eight permeable concrete mixes. The test results demonstrate that the coefficient of permeability (K) increases exponentially when the porosity is

increased. The water permeability results in figure 4.20 are calculated using equations (4.8) and (4.9) as suggested by Montes and Haselbach (2006) and by Schaefer et al. (2006), respectively.

$$K = 18\left[\frac{p^3}{1-p^2}\right] \tag{4.8}$$

(Montes & Haselbach 2006)

$$K = 0.10406 * e^{(14.68*p)} \tag{4.9}$$

(Schaefer et al. 2006)

Where:

K = coefficient of water permeability (mm/sec)

P = porosity ratio (%)

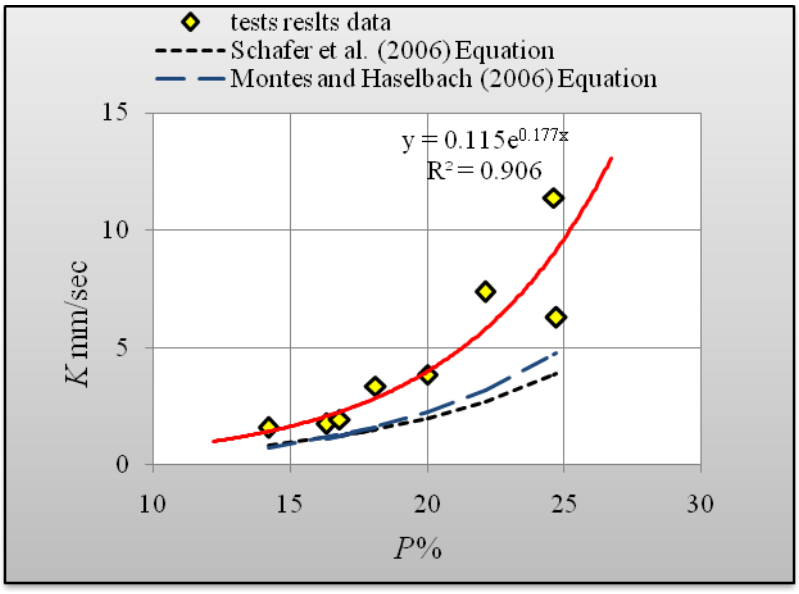

Figure 4.20 The relationship between the porosity and the permeability.

It can be observed that the experimental results have good correlation with other researchers' equations when the porosity is less than 20% but predict higher permeability for porosities higher than 20%. An exponential relationship was found between the porosity and the coefficient of permeability as presented in equation (4.10) with R^2=0.906.

$$K = 0.1156e^{0.1771*P} \quad (4.10)$$

4.4 Conclusion

The experimental results from the testing of eight permeable concrete mixtures are summarised below in table 4.10. These averaged results include the density, the compressive strength (CS), the MOE (E_{itsg} and E_{itp}), the porosity and the permeability.

Table 4.10 The properties of the permeable concrete specimens

Property	15% sand		10% sand		5% sand		No sand	
	GA15	GB15	GA10	GB10	GA5	GB5	GC1	GC2
Density kg/m^3	2306.8	2248	2262.6	2159.6	2232.4	2097.2	2056.6	1968
CSMPa	36.84	28.08	28	20.41	24.0	15.62	13	12
E_{itp}GPa	9	7	8	6	6	5	4.5	3
E_{itsg}GPa	28.25	25.75	26.6	18.8	21.65	15.9	13.25	8.75
Porosity %	14	18	16.5	20	17	22	24.5	24.5
Permeability mm/sec	1.6	3.5	1.75	4	2	7.5	6.3	11.58

These tests results were experimentally determined; the compressive strength is expressed as a function of the density and the porosity. The MOE are expressed as a function of the compressive strength, while the water permeability is expressed as a function of the volumetric porosities.

The density of permeable concrete is lower than the density of the conventional concrete. The lowest density was found for mix GC2, which was produced using a combination of 4.75mm and 9.5mm aggregates in proportions of 75%-25%, with no added sand and with the A/C ratio equal to 4.75. By contrast, the highest density was found for the mix GA15%, which was produced using a combination of 4.75mm and 9.5mm aggregates in proportions of 50%-50% with a sand ratio of 15% and the A/C ratio equal to 4.5. In the case of compressive strengths, mixes GC1 and GC2 exhibited the lowest compressive strengths of 13MPa and 12MPa, respectively, while the mixes GA15% and GB15% exhibited the highest compressive strengths due to the higher use of sand in the 15% category.

A significant difference was found between the MOE as measured by the platen-to-platen and by the strain gauges methods, even though the mixes GC1 demonstrated the lowest MOE in both methods; these were equal to 3GPa and 8.75GPa. The porosities ratios for the mixes GC1 and GC2 were approximately similar, being equal to 24.5%, even though mix GC1 exhibited the higher density. In contrast, mix GA15% demonstrated a very low porosity that was equal to 14% and it thus cannot be considered to be permeable concrete.

The water permeability of mix GC2 at 11.58 mm/sec was higher than for mix GC1, which was equal to 6.3mm/sec, despite the similar porosity of these two mixes. This lower permeability can be attributed to smaller and more disconnected pore structures in the bottom section of the GC1 specimen. Mixes GA15% and GA10% demonstrated a very low permeability, which was equal to 1.6mm/sec and 1.75 mm/sec, respectively, and these also cannot be considered to be permeable concrete.

Considering all the fundamental properties of the tests results, a permeable concrete combination of 75% of 4.75mm aggregate and 25% of 9.5mm aggregate with 5% of sand and an A/C ratio equal to 4.75 is the best mix design for permeable concrete. This mix produces an acceptable compressive strength and MOE as shown in table 4.10. The volumetric porosity and the permeability values of this mix are also within the acceptable values as outlined in the literature review and can be used for a design purpose.

CHAPTER 5
DEVELOPMENT OF A MATHEMATICAL MODEL FOR PREDICTION OF THE COMPLETE STRESS-STRAIN CURVE OF PERMEABLE CONCRETE

5.1 Introduction

A series of compression tests were conducted during the study using100 x 200mm cylindrical samples a modified testing method to determine the complete stress-strain behaviour of permeable concrete. Various existing models for low strength concrete and normal strength concrete were reviewed and compared with the experimental data. Various parameters were studied and their relationships were experimentally correlated. This has allowed the development of a semi-empirical equation for predicting stress-strain behaviour of unconfined permeable concrete with compressive strength between 10MPa-35MPa and porosities ranging between 25%-15%.

As indicated earlier there has been an increasing use of permeable concrete in the civil engineering and building construction industries in recent years. However, its use is currently limited to low trafficked areas such as pavements in car parks and footpaths, largely due to its low strength and stiffness. It is a timely concern to investigate the stress-strain behaviour of permeable concrete to help enable its wider use in more structural applications. An understanding of the complete stress-strain curve of permeable concrete is essential for rational design, as structural designers are unable to take full advantage of the material with insufficient information about this behaviour.

A number of researchers (Carreira & Chu 1985; Kumar 2004; Lokuge, Sanjayan & Setunge 2004; Lokuge, Sanjayan & Setunge 2005; Mander, Priestley & Park 1988 a, 1988 b; Popovics 1973; Sandor 1973; Sargin, Ghosh & Handa 1971; Tasnimi 2004; Van & Taerwe 1996; Wang, Shah & Naaman 1978; Wee, Chin & Mansur 1996) have studied the stress-strain behaviour of unconfined and confined conventional concrete under uni-axial compressive loading in the last few years. Complete stress-strain curves were developed in some of these studies on the basis of easily measured conventional concrete material parameters such as peak stress f'_c, the corresponding strain εo and the initial modulus of elasticity *Eit*. It was found that the stress-strain behaviour of the conventional concrete for all strength levels is dependent on two major parameters-the testing conditions and the concrete characteristics. Tasnimi (2004) and Carreira and Chu (1985) listed some sub-influential factors on the stress-strain behaviour as:

- Stiffness of the testing machine and the frictional resistant between the loading platen and the specimens
- Strain rate, type of strain gauge and gauge length
- The type of loading (preloading, cycling, etc) and loading rate
- The shape, age and size of the test specimens
- The maximum aggregate size in relation to the specimen size
- The concrete homogeneity
- The water to cement (W/C) ratio and the mechanical and physical properties of the cement used
- The weaker top layer of the specimens

- The strain gauge length compared with the specimens' length and slenderness
- The specimens' diameters for the given slenderness ratio

5.2 Review of previous models for conventional concrete

Investigations into the stress-strain behaviour of unconfined and confined conventional concrete under uni-axial compression strength has been a topic for research for several decades. This behaviour plays an important role in the analysis and design of any concrete type, whether it is permeable or conventional concrete, when used in structural applications. The stress-strain models for both confined and unconfined conventional concrete can be divided with few exemptions into three categories according to their experimental forms. A number of researchers (Wang, Shah & Naaman 1978; Van & Taerwe 1996) used a form of equation previously proposed by Sargin, Ghosh and Handa (1971). Other researchers (Kent & Park 1971) proposed the utilisation of a second-order parabola for the ascending branch and a straight line for the descending branch of the stress-strain curve. The others researchers (Tomaszewicz 1984; Carreira & Chu 1985; Hsu & Hsu 1994; Wee, Chin, & Mansur 1996) developed stress-strain relationships based on earlier equations suggested by Popovics (1973). In all these models, selected parameters were included in the stress-strain curves and the models calibrated using the test data.

5.2.1 The empirical model of Sargin, Ghosh and Handa (1971)

The first model category uses a form of an equation first proposed by Sargin, Ghosh and Handa (1971) and modified later by (Wang, Shah & Naaman 1978; Van & Taerwe 1996) as represented in table 5.1. The stress-strain curves of the unconfined and confined concrete suggested by Sargin (1971) are illustrated in figure 5.1.

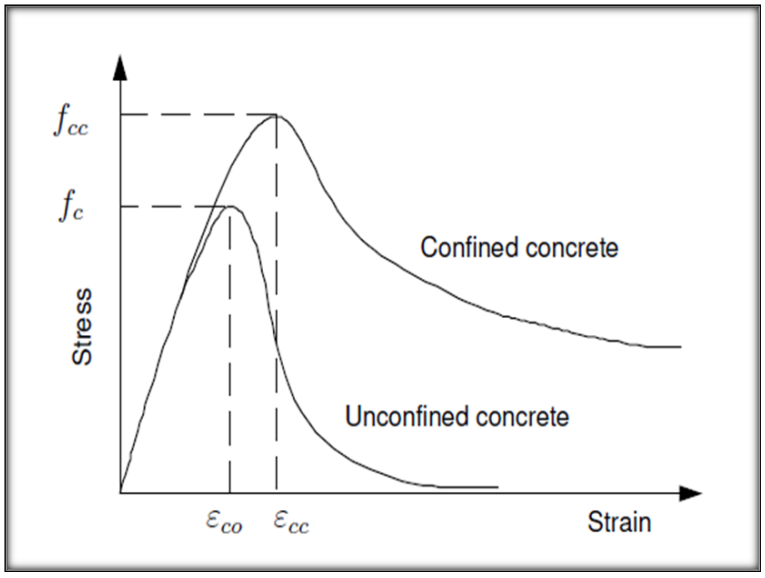

Figure 5.1 Typical stress-strain curves for confined and unconfined concrete (Sargin, Ghosh & Handa 1971)

Table 5.1 Stress-strain behaviours based on the model by Sargin (1971)

References	Equations
(Sargin, Ghosh & Handa 1971)	$fc = f^{'}c\left[A\left(\frac{\varepsilon}{\varepsilon_o}\right) + (\mathrm{D}-1)\left(\frac{\varepsilon}{\varepsilon_o}\right)^2\right] / \left[1 + (A-2)\left(\frac{\varepsilon}{\varepsilon_o}\right) + \mathrm{D}\left(\frac{\varepsilon}{\varepsilon_o}\right)^2\right]$ $A = E_{it}\,\varepsilon_o f^{'}c;$ $D = 0.65 - 7.25 f^{'}_{c} * 10^{-3}; E_{it} = 5975\left(f^{'}_{c}\right)^{\frac{1}{2}};$ $\varepsilon_o = 0.0024$
(Wang, Shah & Naaman 1978)	$fc = f'c\left[A\left(\frac{\varepsilon}{\varepsilon_o}\right) + \mathrm{B}\left(\frac{\varepsilon}{\varepsilon_o}\right)^2\right] / \left[1 + \mathrm{C}\left(\frac{\varepsilon}{\varepsilon_o}\right) + \mathrm{D}\left(\frac{\varepsilon}{\varepsilon_o}\right)^2\right]$ Two different sets of coefficients are used for the ascending and descending branches.
(Van & Taerwe 1996)	$0 \leq \varepsilon \leq \varepsilon_{max}$ $fc = f'c\left[\left(\frac{E_{it}}{E_o}\right)\left(\frac{\varepsilon}{\varepsilon_o}\right) - \left(\frac{\varepsilon}{\varepsilon_o}\right)^2\right] / \left[1 + \left(\frac{E_{it}}{E_o} - 2\right)\left(\frac{\varepsilon}{\varepsilon_o}\right)\right]$ $\varepsilon > \varepsilon_{max}$ $fc = f'c / \left\{1 + \left[\left(\frac{\varepsilon}{\varepsilon_o}\right) - 1 / \left(\frac{\varepsilon_{max}}{\varepsilon_o}\right) - 1\right]^2\right\}$ $\varepsilon_{max} = \varepsilon_o \left\{\frac{\left[\frac{E_{it}}{2E_o} + 1\right]}{2} + \frac{\left[\frac{E_{it}}{2E_o} + 1\right]^2}{4} - \frac{1}{2}\right\}^{1/2}$ $E_{it} = 21{,}500\,\alpha_E \left(\frac{f'_c}{10}\right)^{\frac{1}{3}};\ \varepsilon_{o=} 700\left(f'_c\right)^{0.31} * 10^{-6}$

5.2.2 The empirical model of Kent and Park (1971)

The second model category uses a form of an equation proposed by Kent and Park (1971). It consists of a parabolic ascending branch, a linear descending branch followed by a constant residual strength as illustrated in figure 5.2.

These authors generalised the equation of Hognestad (1951) to more completely describe the post-peak stress-strain by replacing 0.85 f'_c by f'_c and ε_{co} by 0.002. Table 5.2 details the model equations of Kent and Park (1971).

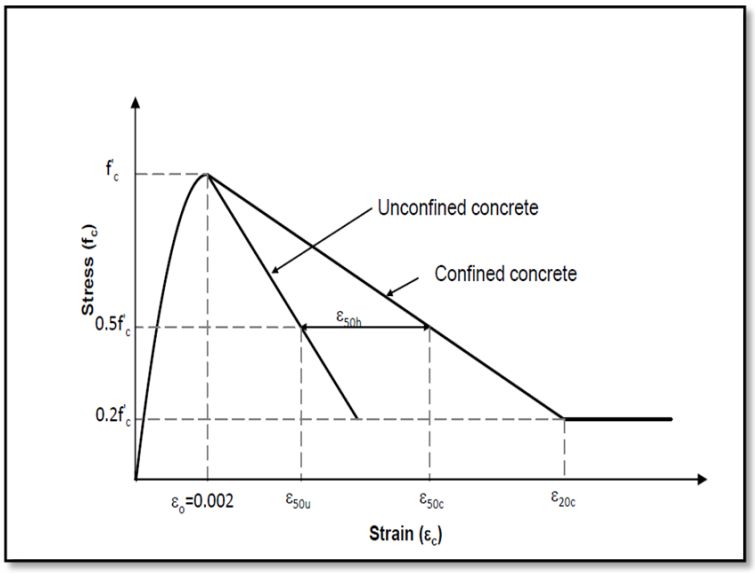

Figure 5.2 Typical stress-strain curves for confined and unconfined concrete

(Kent & Park 1971)

Table 5.2 Stress-strain behaviour based on model by Kent (1971)

References	**Equations**
(Kent & Park.1971)	$\varepsilon \leq \varepsilon_{co=0.002}$, $fc = f'_c[2(\frac{\varepsilon}{0.002}) - (\frac{\varepsilon}{0.002})^2]$ $\varepsilon \geq \varepsilon_{co}$, $fc = f'_c[1 - Z - (\varepsilon - 0.002)]$ $Z = \frac{0.5}{\varepsilon_{50u} - \varepsilon_{co}}, \varepsilon_{50u} = \frac{3 + 0.29 f'_c}{145 f'_c - 1000}$

5.2.3 The empirical model by Popovics (1973)

The third model follows the work by Popovics (1973) who proposed a single equation to describe the complete unconfined and confined concrete stress-strain behaviour. Three parameters are required to describe the full pre and post-peak behaviour. The variables are the peak compressive strength f'_c, the corresponding strain $\varepsilon_{o,}$ and the initial tangent modulus of elasticity E_{it}. The Popovics model works well for most normal-strength concrete (f'_c <55 MPa), but it lacks the necessary control over predicting the slope of the post-peak branch for high-strength concrete (Reddiar 2009). This model has been modified by different researchers (Tomaszewicz 1984; Carreira & Chu 1985; Hsu & Hsu 1994; Wee, Chin, & Mansur 1996) and additional parameters have been added in order to make it suitable for all concrete strength levels. Table 5.3 provides a summary of the modifications made to the Popovics model by these researchers. The typical stress-strain curves for unconfined and confined concrete are illustrated in figure 5.3.

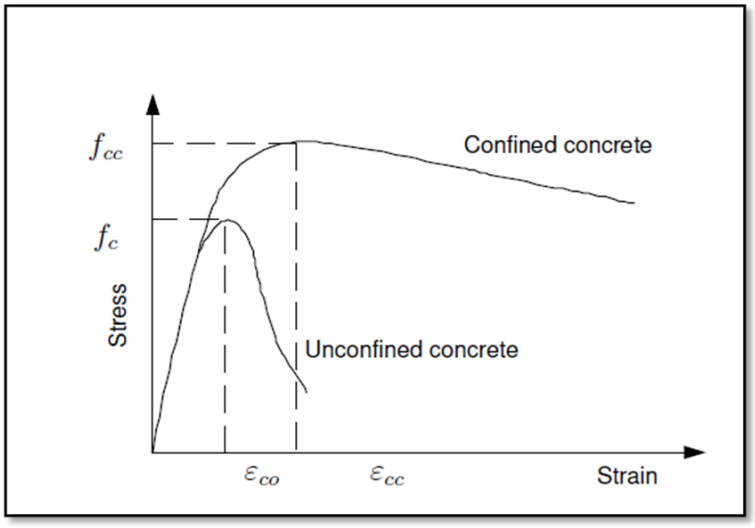

Figure 5.3 Typical stress-strain curves for confined and unconfined concrete (Popovics 1973)

Table 5.3 Stress-strain behaviour based on the model by Popovics (1973)

References	**Equations**
(Popovics 1973)	$fc = f'_c \beta (\frac{\varepsilon}{\varepsilon_o})/[\beta - 1 + (\frac{\varepsilon}{\varepsilon_o})^{\beta}]$ $\varepsilon_o = 735\,(f'_c)^{0.25} * 10^{-6}; \beta = 1 + 0.058 f'_c$
(Tomaszewicz 1984)	$0 \leq \varepsilon \leq \varepsilon_o$ $fc = f'_c \beta (\frac{\varepsilon}{\varepsilon_o})/[\,(\beta - 1 + \left(\frac{\varepsilon}{\varepsilon_o}\right)^{\beta}]$ $\varepsilon < \varepsilon_0$ $fc = f'_c \beta (\frac{\varepsilon}{\varepsilon_o})/[\,(\beta - 1 + \left(\frac{\varepsilon}{\varepsilon_o}\right)^{k\beta}]$ $\varepsilon_o = 700 f'^{0.31}_c * 10^{-6};\ \beta = \frac{8.32}{[8.32 - f'^{0.475}_c]}; k = \frac{f'_c}{20}$
(Carreira & Chu 1985)	$fc = f'_c\, \beta (\frac{\varepsilon}{\varepsilon_o})/[\beta - 1 + \left(\frac{\varepsilon}{\varepsilon_o}\right)^{\beta}]$ $\beta = \frac{1}{\left[1 - \left(\frac{f'_c}{\varepsilon_o E_{it}}\right)\right]}; E_{it} = 0.0736\ \rho^{1.51} (f'_c)^{0.3}$; $\varepsilon_0 = \left(1{,}680 + 7.1 f'_c\right) * 10^{-6}$
(Hsu & Hsu 1994)	$0 \leq \varepsilon \leq \varepsilon_d$, $fc = n f'_c \beta (\frac{\varepsilon}{\varepsilon_o})/[n\beta - 1 + \left(\frac{\varepsilon}{\varepsilon_o}\right)^{n\beta}$ $\beta = \left(\frac{f'_c}{65.23}\right)^3 + 2.59$ For $0 \leq \varepsilon \leq \varepsilon_o$ n=1 if $0 < f'_c < 62$ MPa, n=2 if $62 \leq f'_c < 76$ MPa; n=3 if $76 \leq f'_c < 90$ and n=5 if $f'_c \geq 90$MPa $\varepsilon > \varepsilon_d$ $fc = 0.3 f'_c \exp\,[-0.8 \left(\frac{\varepsilon}{\varepsilon_o} - \frac{\varepsilon_d}{\varepsilon_o}\right)^{0.5}$

(Wee, Chin, & Mansur 1996)	$0 \leq \varepsilon \leq \varepsilon_0$, $fc = f'_c \beta \left(\frac{\varepsilon}{\varepsilon_o}\right) / [\beta - 1 + \left(\frac{\varepsilon}{\varepsilon_o}\right)^{\beta}]$ $\varepsilon > \varepsilon_0$, $fc = k_1 f'_c \beta \left(\frac{\varepsilon}{\varepsilon_o}\right) / [k_1 \beta - 1 + \left(\frac{\varepsilon}{\varepsilon_o}\right)^{k_2 \beta}$ $\varepsilon_o = 780 \left(f'_c\right)^{\frac{1}{4}} * 10^{-6}$; $E_{it} = 10{,}200 \left(f'_c\right)^{\frac{1}{3}}$; $\beta = \frac{1}{\left[1 - \frac{f'_c}{\varepsilon_o E_{it}}\right]}$; $k_1 = \left(\frac{50}{f'_c}\right)^3$ and $k_2 = \left(\frac{50}{f'_c}\right)^{1.3}$

5.3 A mathematical stress-strain model for permeable concrete

The information about the stress-strain behaviour of the permeable concrete is still limited and the only research paper that provides useful information was based on experiments conducted by Deo and Neithalath (2010). The authors found that the stress-strain behaviour of the permeable concrete was approximately similar to that of the conventional concrete. They also found that there were many parameters, both of the materials and of the test method, that were related to stress-strain behaviour, including such as aggregate size, porosity ratio, and the pore structural features. While the strain rate has a minor effect on the stress-strain response, these authors observed that there is an increase in the peak stress and the slope of the ascending curve together with a decrease in the strain corresponding to peak stress with increasing strain rate. Deo and Neithalath (2010) proposed a mathematical stress-strain model for the permeable concrete that was related to the response of the features of

the pore structure. These authors employed the model proposed by Carreira and Chu (1985) for the conventional concrete but with some modifications. Figure 5.4 illustrates the typical stress-strain curve for the permeable concrete with different porosity ratios reported by Deo and Neithalath (2010).

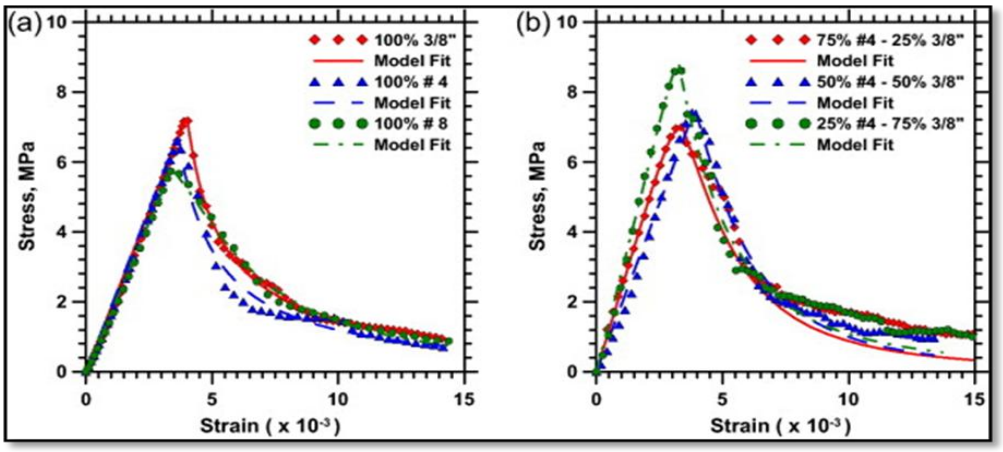

Figure 5.4 Experimental data and model fits for the stress–strain response of permeable concrete made using (a) single-sized aggregates, and (b) blended aggregates

(Deo & Neithalath 2010)

The model expression incorporating the modified terms is given below in equation (5.1).

$$f'_c{}^{\lambda} = \propto_0 + \propto_1 + [\ln(d_{MFS}) / \ln d_n] + \propto_2 \left(\frac{\emptyset_A}{S_p}\right)^{-1} + \propto_3 \ln(\Gamma_{3D}) \qquad (5.1)$$

Where:

λ =Power transformation

f'_c =Compressive strength

d_n =Number averaged pore size

$\emptyset_A$ =Area fraction of pores

d_{MFS} =Mean free spacing of pores

S_p =Specific surface area of pores

Γ_{3D} =Three-dimensional of pore distribution density

α_0, α_1 =Parameters

α_2 =Parameters

(Deo & Neithalath 2010)

The proposed empirical model was found to agree satisfactorily with the Deo & Neithalath 2010 test results but it required extensive computations to determine the essential parameters. It is very empirical and cannot be used to represent the stress-strain behaviour of a different strength of permeable concrete that is prepared under different conditions. However, the ascending branch of the stress-strain curve is well–represented by the model; and most discrepancies between the actual and the predicted curve were observed in the descending branch. This could be related to an increase in the heterogeneity and to a high degree of asymmetry in the pore structure features of blended aggregate mixtures (Deo & Neithalath 2010).

5.4 Proposed stress-strain relationship

There are some conditions that must be considered when proposing an equation to represent the stress-strain relationship of any concrete type (Hus & Hus 1994; Carreira & Chu 1985). These conditions are as follows:

1.The equation should be correlated roughly with experimental data.

2.Both ascending and descending branches of the stress-strain curve should be represented by the proposed equation.

3.The model should be as simple as possible and easily determined.

4.The equation should best be based on physically significant parameters that can be determined experimentally, such as the peak compressive strength f'_c, the initial tangent modulus of elasticity E_{it}, and the corresponding strain at the peak stress ε_o.

Due to the complexity of these variables and their interrelationships, it is very difficult to find an unique mathematical formula that can predicate the experimental stress-strain relationship under different circumstances with the same level of accuracy (Almusallam & Alsayed 1995). Many of these models do not generate the full curve of the stress-strain relationship, that is both the ascending and descending portions. Some researchers (Wang, Shah & Naaman 1978; Van & Taerwe 1996; Kent & Park.1971; etc.) have thus proposed two different formulas-one for the ascending portion and the other for the descending portion, to overcome this difficulty.

In an effort to develop a simple mathematical model that can represent the stress-strain curve of permeable concrete with different compressive strengths and porosity ratios, it was found that the model developed by Carreira & Chu (1985) and later modified by different authors such as Tasnimi (2004) appears suitable for adoption to explain the stress-strain relationship of permeable concrete. The advantages of this model are:

- It performs well for the low strength and normal strength concrete, which are both in the same range as the permeable concrete's compressive strength.

- It is simple and has the same general equation for use in both the ascending and the descending branch.
- Its parameters are easy to find from the experimental data.

Equations (5.2) and (5.3) represented the model proposed by Carreira and Chu (1985)

$$fc = f'_c \beta(\frac{\varepsilon}{\varepsilon_0})/[\beta - 1 + \left(\frac{\varepsilon}{\varepsilon_0}\right)^{\beta}] \quad (5.2)$$

$$\beta = \frac{1}{\left[1-\left(\frac{f'_c}{\varepsilon_0 E_{it}}\right)\right]} \quad (5.3)$$

Where:

β =Material parameter

f_c =Concrete stress

ε =Concrete strain

f'_c =The maximum stress

ε_0 =The strain corresponding with the maximum stress

E_{it} =Initial tangent modulus

(Carreira &Chu 1985)

5.4.1 The effect of the porosity on the stress-strain curve

As expected, the stress-strain curves for the permeable concrete are similar in shape to those of the conventional concrete as shown in figure 5.5. These experimental stress-strain relationships form part of the outcomes of this research project. It can be observed that the stress-strain behaviours of the permeable concrete for different aggregate sizes and sand ratios follow similar

trends. The porosity ratio showed a direct effect on the shape and descending branch of the stress-strain curve of the permeable concrete. With the reduction of the porosity ratio, the compressive strength, corresponding strain and modulus of elasticity increased. Moreover, the descending branch showed more ductile behaviour and gradual cracks with increasing porosity ratio. Figure 5.5 shows that equation (5.2) should be modified to reflect the effect of porosity, especially for the descending branch.

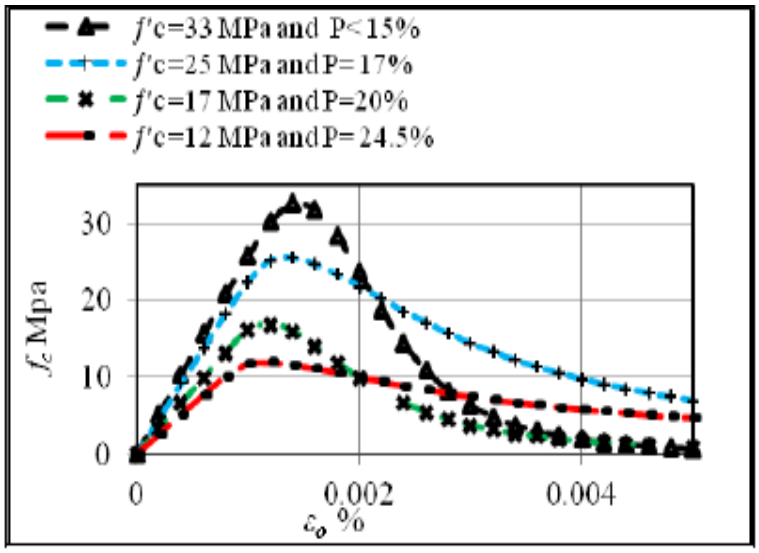

Figure 5.5 Stress-strain curves for permeable concrete.

5.4.2 Estimating strain at peak stress (ε_o)

One of the most important parameters affecting the ascending and descending portions of the concrete stress-strain curve is the corresponding strain at peak stress. Appendix C provides the values of the corresponding strain at peak stress for the various specimens in this project. The maximum and minimum values of ε_o for the permeable concrete specimens in this research varied from 0.0009 to 0.00189 for a strength range from 9MPa to 38MPa and porosity

range from 25% to 15%. The tests results indicated that, on average, strain corresponding to peak stress was increasing as compressive strength increased and the porosity ratio decreased.

Several authors reported a linear relationship between the peak compressive stress and the corresponding axial strain (Almusallam & Alsayed 1995, Carreira & Chu 1985), while Tasnimi (2004) reported a polynomial function. These relationships are shown in equations (5.4), (5.5) and (5.6), respectively:

$$\varepsilon_o = \left(0.398 f'_c + 18.147\right) * 10^{-4} \tag{5.4}$$

(Almusallam &.Alsayed 1995)

$$\varepsilon_o = \left(7.1 f'_c + 1{,}680\right) * 10^{-6} \tag{5.5}$$

(Carreira & Chu 1985)

$$\varepsilon_o = \left(65.57 f'^{0.44}_c - 6.748\right) * 10^{-5} \tag{5.6}$$

(Tasnimi 2004)

The experimental and estimated ε_o that were found according to these equations were plotted against the compressive strength for comparison and are shown in figure 5.6

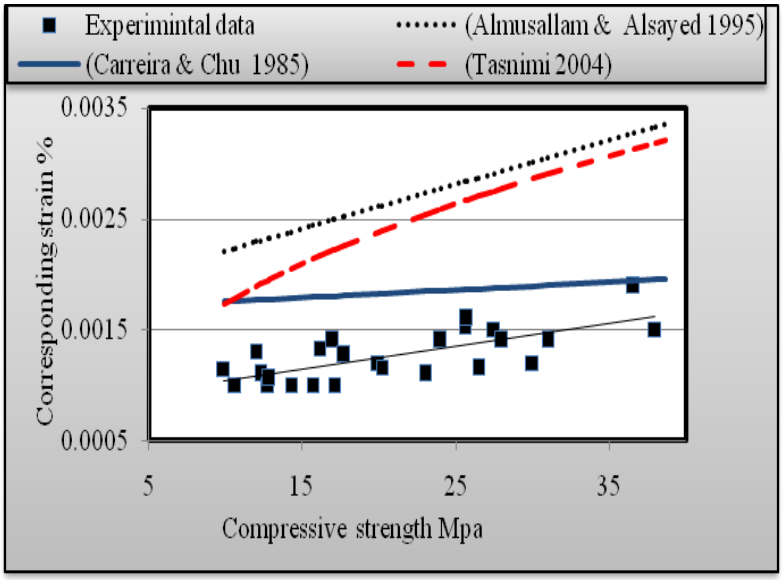

Figure5.6 The experimental and calculated ε_o versus the compressive strength

From figure 5.6, a linear relationship was found between the compressive strength and the corresponding strain based on the permeable concrete experimental data. It is also clear that equation (5.5) developed by Carreira & Chu (1985) gives a more accurate estimation for ε_o when compared with other equations. In the current research, a linear relationship similar to equation (5.5) has been proposed as shown in equation. (5.7).

$$\varepsilon_o = \left(2f'_c + 80\right) * 10^{-5} \qquad (5.7)$$

5.4.3 Estimating the initial modulus of elasticity (E_{it})

Twenty six cylinders with different compressive strengths (f'_c) and porosity ratios were tested using the strain gauge method. Results from Goede (2009) using the compressometer method were adopted to determine the $E_{it.}$

Appendix C details the values for the f'_c, unit weight ρ and the E_{it} for the present research and from existing literature.

Different theoretical relationships that can be used for the design of any type of concrete including permeable concrete, when the modulus of elasticity has not yet been determined by the laboratory tests, are presented in the literature. The Australia Standard AS-3600(2009) specified the following equation (5.8) for estimating the E_{it} of the plain concrete as a function of its unit weight ρ and of the compressive strength when $f'_c \leq 40$MPa.

$$E_{it} = 0.043(\rho)^{1.5}\,(fc)^{0.5} \tag{5.8}$$

(AS-3600 2009)

Similarly, the Architectural Institute of Japan AIJ (1985) has specified equation (5.9).

$$E_{it} = 21000\left(\frac{\rho}{2300}\right)^{1.5}\left(\frac{f'_c}{20}\right)^{0.5} \tag{5.9}$$

(AIJ 1985)

Pauw (1960) has specified equation (5.10) for determining the E_{it} for the conventional concrete.

$$E_{it} = 0.0736 * (\rho)^{1.51} * \left(f'_c\right)^{0.3} \tag{5.10}$$

(Pauw 1960)

Tasnimi (2004) specified equations (5.11) and (5.12) to determine E_{it} for low strength concrete and normal strength concrete, respectively.

$$E_{it} = 2.1684\, f'^{0.535}_{c} \quad (5.11)$$

$$E_{it} = 2.25 \ln\left[\frac{f'^{2.8}_{c}}{\rho^{0.2}}\right] + 0.05 f'_{c} \quad (5.12)$$

(Tasnimi 2004)

Ghafoori and Dutta (1995) derived equation (5.13) to find the E_{it} of the permeable concrete as a function of the unit weight and the compressive strength. The authors proposed equation (5.14) to find the E_{it} as a function of the compressive strength

$$E_{it} = 4.258 * 10^{-5} (\rho^{1.5})(f'^{0.5}_{c}) \quad (5.13)$$

$$E_{it} = 0.7134 * f'_{c} \quad (5.14)$$

(Ghafoori & Dutta 1995)

Where:

E_{it} = modulus of elasticity

f'_c = max compressive strenght

ρ = dry unit weight

In order to find the most suitable equation for predicting E_{it} of permeable concrete, the values of the initial tangent modulus of elasticity, which were obtained experimentally using the strain gauges, were combined with the results obtained by Goede (2009) using the compressometer. The comparative results are shown in figure 5.7. A comparison was then made between the experimental and the calculated E_{it} according to the equations proposed by Ghafoori and Dutta (1995) (Eq. 5.13), AS-3600 (Eq. 5.8) and AIJ (Eq. 5.9),

against the ($\rho^{1.5}\times f'_c{}^{0.5}$) to demonstrate the good agreement of the these equations with the experimental data.

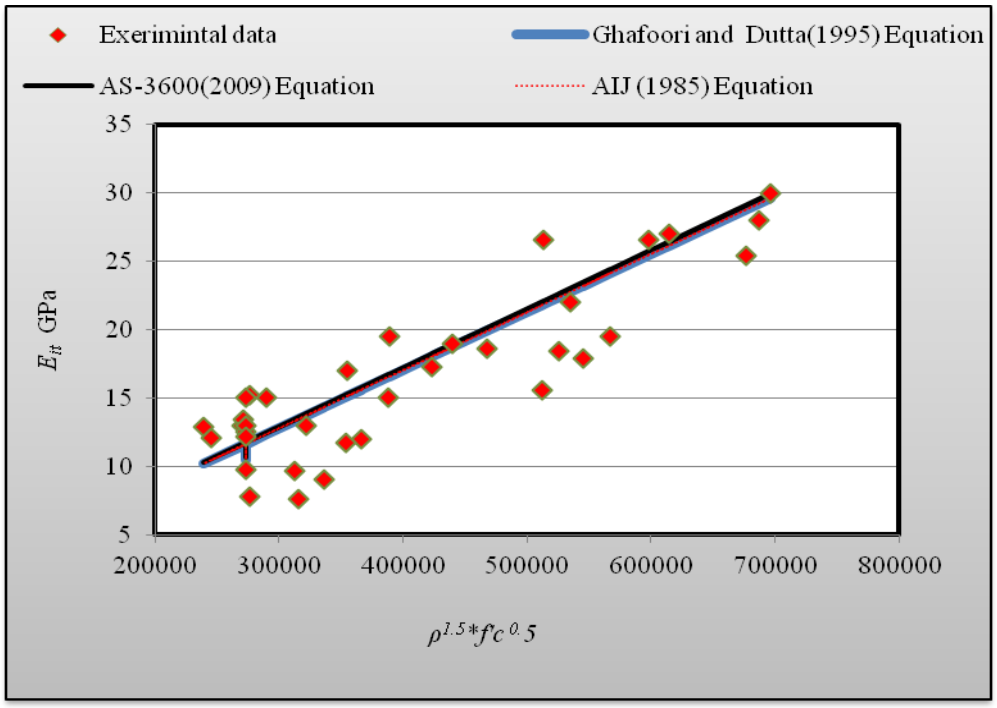

Figure 5.7 The relationship of experimental and calculated E_{it} versus $\rho^{1.5}\times f'_c{}^{0.5}$.

It can be observed from figure 5.7 that all of the equations proposed by various researchers gave a close approximation of the experimental data obtained in this study. The conclusion is that the modulus of elasticity of the permeable concrete is similar to that of the low strength concrete and normal strength concrete. This is not unexpected and is observed in other materials such as the various grades of steel where modulus remains at around 200GPa regardless of strength The equation proposed by Ghafoori and Dutta (1995) will be used to determine the E_{it} of the permeable concrete in the proposed model.

5.4.4 Proposed stress-strain relationship

A complete stress–strain curve for permeable concrete that satisfies the boundary conditions can be represented by the following equation (5.15) as proposed by Carreira and Chu (1985). This equation is suitable if the parameters are correctly evaluated as fitting the permeable concrete characteristics with different porosity ratios.

$$y = \beta x/[\beta - 1 + x\hat{}\beta] \quad (5.15)$$

Where:

$$y = \frac{f_c}{f'_c}$$

$$x = \frac{\varepsilon_c}{\varepsilon_o}$$

The first derivative of the equation $d(fc)/d\varepsilon_o$ gives the initial tangent modulus of elasticity for the ascending branch of the stress–strain curve, which is given by equation (5.16).

$$E_{it} = f'c/\varepsilon_o \left\{\frac{\beta}{\beta-1}\right\} \quad (5.16)$$

For the ascending part up to the maximum strength, the concrete parameter β is derived by equation (5.17)

$$\beta = \frac{1}{\left[1-\left(\frac{f'_c}{\varepsilon_0 E_{it}}\right)\right]} \quad (5.17)$$

(Carreira & Chu 1985)

Since the descending part of the stress-strain curve of the permeable concrete is directly affected by the porosity ratio, an additional parameter (*n*) will be added to equation (5.15). Equation (5.18) will thus be used for the descending part. Figure 5.8 illustrates the relationship between *n* and the porosity ratio (*P*). The relationship between the compressive strength and the porosity were proposed in equation 4.7 in Chapter 4. It will thus be a simple matter to calculate the porosity even if it is not tested in the laboratory.

$$f_c = \begin{cases} \dfrac{f'_c\,\beta(\frac{\varepsilon}{\varepsilon_o})}{[\beta - 1(\frac{\varepsilon}{\varepsilon_o})^{\beta}]} & \text{if} \quad \varepsilon \le \varepsilon_o \\ \dfrac{f'_c\,n\beta(\frac{\varepsilon}{\varepsilon_o})}{[n\beta - 1(\frac{\varepsilon}{\varepsilon_o})^{n\beta}]} & \text{if} \quad \varepsilon > \varepsilon_o \end{cases} \tag{5.18}$$

Where

n= parameter affected by the porosity ratio

$$f'_c = 142.03 * e^{-0.098*p} \tag{4.7}$$

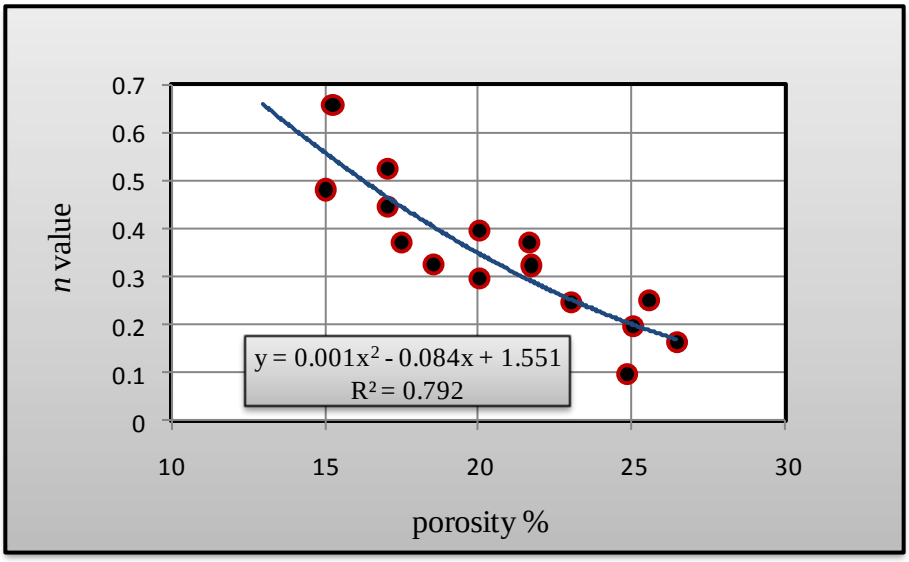

Figure 5.8 The relationship between the porosity ratio and *n* value

It can be observed from figure 5.8 that there is inverse relationship between the value of *n* and the porosity ratio (*P*) as represented by equation (5.19).

$$n = 0.001 * (P)^2 - 0.084 * (P) + 1.551 \quad (5.19)$$

5.4.5 Examination of the proposed model

In order to check the validity of the proposed empirical stress-strain model for unconfined permeable concrete under uni-axial compression strength, the stress-strain curves that were predicted using the empirical model for different compressive strengths and porosities are shown in figure 5.9 (A-E).

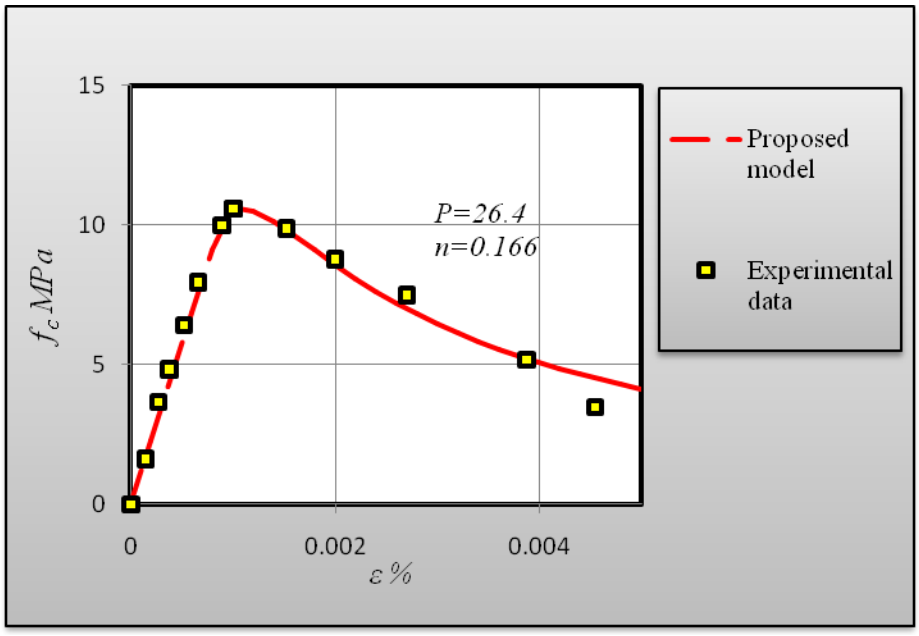

Figure 5.9A

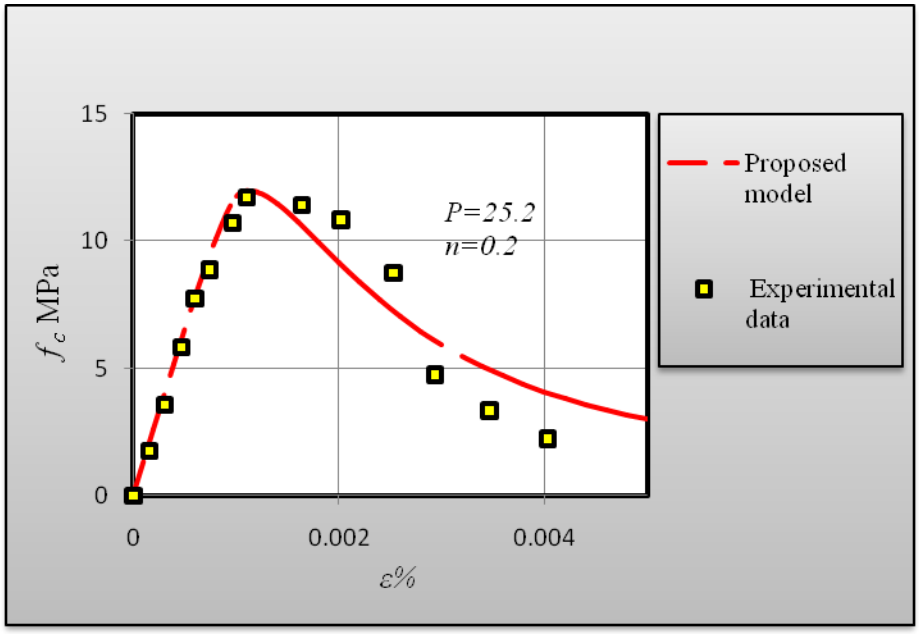

Figure 5.9 B

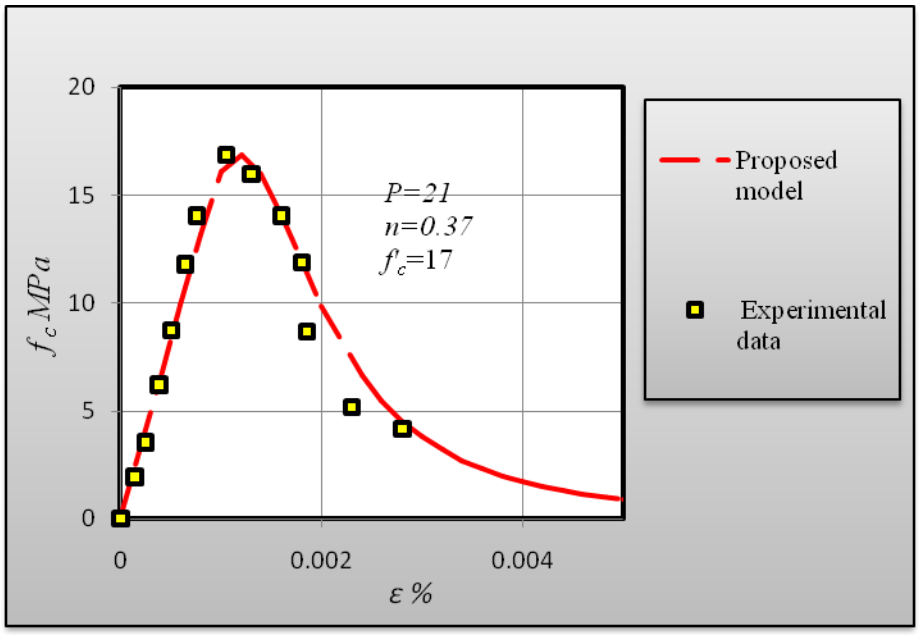

Figure 5.9 C

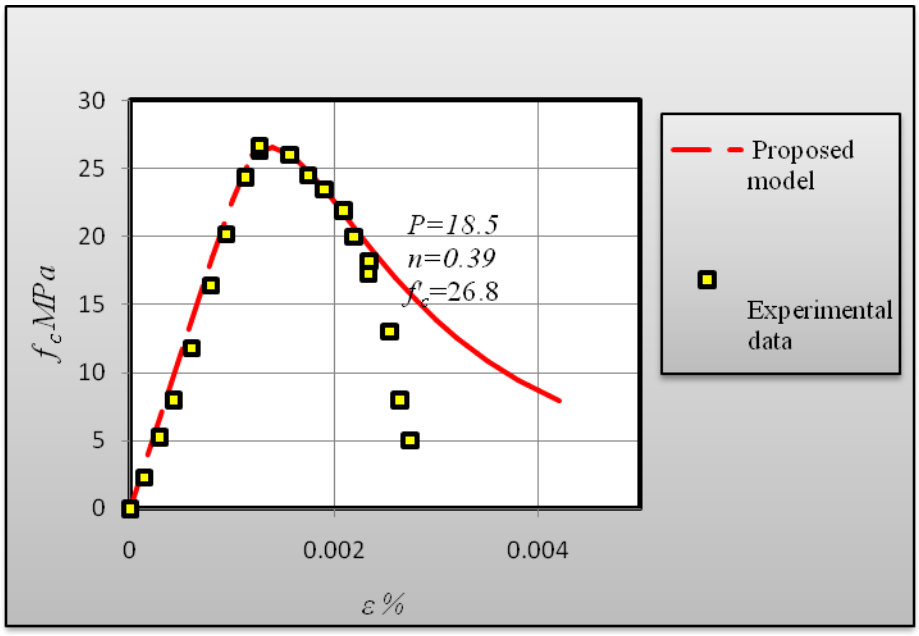

Figure 5.9 D

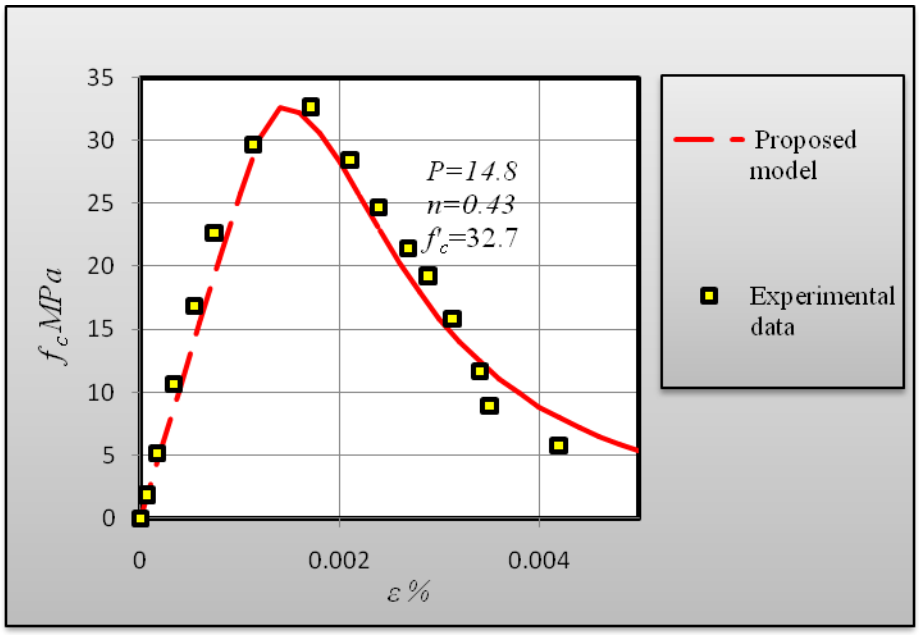

Figure 5.9 E

Figure 5.9 (A-E) Model predictions

It can be observed from figure 5.9 that the new proposed empirical model adequately represents the behavior of the permeable concrete (with different compressive strength and porosity ratio) for both the ascending and the descending branch. The model is also mathematical simple and the parameters are generally easy to find; the only parameters that needs to be known are the compressive strength and the density. The proposed equations can then be employed to find the other parameters.

5.5 Conclusion

The major conclusions that can be drawn from this chapter are outlined in point form below:

1. Existing equations used to predict the initial modulus of elasticity of low strength concrete and normal strength concrete can also be used for permeable concrete.
2. The proposed semi-empirical equation is able to generate complete-stress-strain curve for unconfined permeable concrete under uni-axial compression. This is applicable to permeable concretes having different porosity ratios and compressive strengths.
3. The stress-strain relationships are controlled by a few controlling parameters and the empirical expressions for these parameters based on f'_c and ρ are derived so that these relationships can be used in the absence of accurate experimental results.

CHAPTER 6
CONCLUSIONS AND RECOMMENDATIONS FOR FUTURE RESEARCH

6.1 Conclusions

Based on the results from this investigation on permeable concrete mixtures, the following conclusions are made:

6.1.1Effect of the composition materials on the fundamental properties

The experimental testing results illustrated that the fundamental properties of the permeable concrete such as compressive strength, stress-stain behaviour and modulus of elasticity are slightly lower than the same properties of conventional concrete. This can be attributed to the porosity characteristics, the pore distribution and the degree of connectivity inside the permeable concrete specimens.

The influence of the composition materials such as aggregate size, sand ratio and aggregate to cement ratio of several permeable concrete mixtures on the fundamental properties were investigated in this research. It was demonstrated that the use of a combination of 4.75mm and 9.5mm aggregates in 75%-25% proportions produced permeable concrete with acceptable mechanical and hydraulic properties.

An increase in the ratio of large (9.5mm) aggregates in the mixtures led to an improvement in the mechanical properties of compressive strength and modulus of elasticity (although there was a reduction in porosity and

permeability). The improvement in the mechanical properties can be attributed to the fact that the larger aggregate size reduced the contact area between the particles; these contact areas were considered the weakest zone inside the permeable concrete where the failure usually happened. The reduction in porosity and permeability occurred because the small aggregate (4.75mm) filled the voids between the larger aggregates.

The mechanical properties of the permeable concrete improved whilst the hydraulic properties reduced with an increase in the sand ratio and with a reduction in the aggregate to the cement ratio for the two aggregates combinations.

An analysis of the distribution of the pore areas throughout the permeable concrete specimens using ERDAS IMAGINE 2011 software showed that the pore areas changed from section to section within the same specimen due to the use of vibration during the casting procedure. This change in the pore areas of each section of the specimens initiated a change in the local strain and in the modulus of elasticity from section to section. A substantial reduction in the pore areas was also observed in the bottom part of the permeable concrete specimen, which was prepared using a combination of 4.75mm and 9.5mm aggregates in 50%-50% proportions. This can be attributed to the fact that the 4.75mm aggregates combined with the cement paste and sand ratio to fill most of the voids in the bottom part of the specimen because of using the vibration during its preparation. The permeability of this combination was thus significantly reduced despite the reasonable porosity, which was due to an increase in the unconnected pore area in the bottom part of this mixture.

Different relationships and equations were proposed between the fundamental properties of the permeable concreter using the experimental testing results. The compressive strength were expressed as a function of a density, porosity and MOE, whilst the water permeability was expressed as a function of the volumetric porosities.

6.1.2 Stress-strain behaviour and modulus of elasticity

A significant difference was found between the local strain and the modulus of elasticity, which was measured using the strain gauge, and the global strain and the modulus of elasticity for the permeable concrete specimens, which was measured using the platen-to-platen method. This was due to the effects of the sulphur capping on the global strain, the differences in porosity between the bottom and the top sections and from the effects of the Avery 500kN hydraulic power machine, which was used during the compression test.

The stress-strain curve of the permeable concrete followed a similar trend as the stress-strain curve for conventional concrete, but the curvature became more pronounced as cracking initiated in permeable concrete with a lower porosity. The descending branch of the stress-strain curve was also directly affected by the porosity ratio and showed a ductile behaviour with an increase in the porosity. The modulus of elasticity also increased with an increase in the compressive strength and with a reduction in the porosity; this was the same behaviour as, and followed the same trend for, the low and normal strength conventional concrete. As a result, the modulus of elasticity of the permeable concrete can be calculated using the equations previously reported for the low

and normal strength conventional concrete; these are based on the unit weight and compressive strength.

6.1.3 Proposed stress-strain model

One of the objectives for this research was to propose semi-empirical equations to represent the complete stress-strain behaviour for unconfined permeable concrete with compressive strength ranging between 10MPa-38MPa and porosity ranging between 25%-15%, made with different combinations of aggregate size and sand ratios. Various existing models for low strength concrete and normal strength concrete were used and compared with the experimental data. It was found that the model proposed by Carreira and Chu (1985) for the low and normal strength conventional concrete is suitable for adoption in the stress-strain relationship of permeable concrete. The parameters for the proposed model are also easy to find since the same equation can be used for both the ascending and the descending branches of the stress-strain curve.

Various parameters such as the peak stress f'_c, the corresponding strain at peak strength ε_o, the modulus of elasticity E_{it}, the density ρ and the porosity ratio P were studied and their relationships were experimentally determined.

The proposed stress-strain relationships in this research are controlled by a few controlling parameters and the empirical expressions for these parameters based on f'_c and ρ are derived so that these relationships can be used in the absence of accurate experimental results.

The validity of the proposed empirical stress-strain model for unconfined permeable concrete under uni-axial compression strength was checked with actual cylinder tests results under axial compression. It was observed that the model adequately represents the behaviour of the permeable concrete (with different compressive strength and porosity ratio) for both the ascending and the descending branch.

An important relationship was found between the MOE which were determined using the strain gauge (sg), and the platen-to-platen (p-to-p) methods. This relation would enable the designer to use the p-to-p method and then to apply a simple relationship for finding a much more representative MOE of the permeable concrete.

6.2 Limitations of this research

1. Permeable concrete is a relatively new material and all of the previous research concerned its strength and hydraulic properties. The effect of the sulphur capping and composition materials on the stress-strain behaviour and on the MOE of the permeable concrete had been discussed previously. The effects of the testing conditions and the testing equipment such as the testing machine or strain gauging types on this behaviour and on the MOE were thus not investigated due to the time constraints on this research.
2. The positive benefits of adding Alkali-Resistant Glass Fibre to conventional concrete to improve its strength and durability is well–recognised. This research did not examine the use of glass fibre in permeable concrete since

time constraints put this avenue of research beyond the scope of the current study.

6.3 Recommendations for future research

Suggestions for future research work can be summarised as follows:

1.The effect of the testing conditions and the testing equipment on the stress-strain behaviour and on the modulus of elasticity of the permeable concrete should be investigated.

2.New and simpler technologies for measuring the displacement in the permeable concrete rather than in the strain gauge should be sought due to the difficulty of affixing the strain gauge onto the rough surface of the permeable concrete.

3.Since the excellent ability of the permeable concrete in dampening road noise from tyre-pavement interactions has previously been recognised, a similar investigation into the suitability of using the permeable concrete in noise barrier walls is also needed.

4.It is known from the literature that the addition of the Alkali-Resistant Glass Fibre to conventional concrete improves both the mechanical properties and the durability. The effects of the possible addition of this fibre to permeable concrete also need to be investigated.

APPENDICES

Appendix A

Porosity test experimental data

Table A.1 Porosity for GA permeable concrete specimens at the room temperature

	S.No	M_{dry} gm	M_{sub} gm	L^* cm	D^* cm	V_t cm^3	ρ^* gm/cm^3	V_v cm^3	V_f cm^3	V_f/V_t	P^* %
GA15%	1	3150	1906.5	18.3	10	1437.3	0.999	1243.5	1243.7	0.865	13.5
	2	3140	1910.8	18.4	10	1445.1	0.999	1229.2	1229.5	0.85	14.9
	Average										14.2
GA10	1	3110	1915	18.4	10	1445.13	0.995	1195	1200.2	0.83	17
	2	3100	1885	18.4	10	1445.13	0.995	1215	1220.24	0.84	15.6
	Average										16.3
GA5%	1	3000	1850	17.5	10	1374.4	0.998	1150	1152.3	0.83	16.2
	2	3015	1850	18	10	1413.7	0.998	1165	1167.3	0.82	17.4
	Average										16.8

L^* = length cm
D^* = diameter cm
P^* = porosity
ρ^* = water density

Table A.2 Porosity for GB permeable concrete specimens at the room temperature

	S.No	M_{dry} gm	M_{sub} gm	L cm	D cm	V_t cm^3	ρ gm/cm^3	V_v cm^3	V_f cm^3	V_f/V_t	P %
GB15%	1	3220	2025	18.8	10	1476.54	0.999	1195	1195.2	0.81	19.1
	2	3240	2010	18.9	10	1484.43	0.999	1230	1230.2	0.83	17.1
	Average										18.1
GB10%	1	2800	1780	16.5	10	1295.91	0.999	1020	1020.2	0.78	21.3
	2	2850	1795	16.5	10	1295.97	0.999	1055	1055.2	0.81	18.6
	Average										20
GB5%	1	3120	1962.7	19	10	1492.25	0.999	1157.3	1157.55	0.77	22.4
	2	3190	1991.2	19.5	10	1531.52	0.999	1198.8	1199.06	0.78	21.7
	Average										22.1

Table A.3 Porosity for GC permeable concrete specimens at the room temperature

	S.No	Mdry gm	Msub gm	L cm	D cm	Vt cm^3	ρ gm/cm^3	Vv cm^3	Vf cm^3	Vf/Vt	P %
GC1	1	2860	1800	18.1	10	1421.5	0.998	1060	1062.1	0.747	25.3
	2	2910	1816	18.4	10	1445.1	0.998	1094	1096.2	0.758	24.1
	Average										24.7
GC2	1	2850	1722	19	10	1492.2	0.998	1128	1130.3	0.757	24.3
	2	2810	1750	18	10	1413.7	0.998	1060	1062.1	0.751	24.9
	Average										24.6

Table A.4 Porosity for GA permeable concrete specimens after storing them in the oven

	S. No	M_{dry} gm	M_{sub} gm	L cm	D cm	V_t cm^3	ρ gm/cm^3	V_v cm^3	V_f cm^3	V_f/V_t	P %
GA15%	1	2953	1906	18.3	10	1437	0.996	1046	1051	0.731	26.9
	2	3017	1911	18.4	10	1445	0.996	1107	1111	0.769	23.1
	Average										25.0
GA10%	1	2939	1915	18.4	10	1445	1	1024	1025	0.709	29.1
	2	2960	1885	18.4	10	1445	1	1075	1075	0.744	25.6
	Average										27.4
GA5%	1	2832	1850	17.5	10	1374	0.998	982	984	0.716	28.4
	2	2857	1850	18	10	1414	0.998	1007	1009	0.714	28.6
	Average										28.5

Table A.5 Porosity for GB permeable concrete specimens after storing them in the oven

	S. No	M_{dry} gm	M_{sub} gm	L cm	D cm	V_t cm^3	ρ gm/cm^3	V_v cm^3	V_f cm^3	V_f/V_t	P %
GB15%	1	3070	2025	18.8	10	1477	1	1045	1045	0.708	29.2
	2	3090	2010	18.9	10	1484	1	1080	1080	0.728	27.2
	Average										28.2
GB10%	1	2660	1780	16.5	10	1296	1	880	880	0.679	32.1
	2	2700	1795	16.5	10	1296	1	905	905	0.699	30.1
	Average										31.1
GB5%	1	2980	1962.7	19	10	1492	1	1017	1018	0.682	31.8
	2	3010	1991.2	19.5	10	1532	1	1019	1019	0.665	33.5
	Average										32.6

Table A.6 Porosity for GC permeable concrete specimens after storing them in the oven

	S.No	Mdry gm	Msub gm	L cm	D cm	Vt cm^3	ρ gm/cm^3	Vv cm^3	Vf cm^3	Vf/Vt	P %
GC1	1	2790	1800	18.1	10	1421.57	0.998	990	991.98	0.697	30.2
	2	2800	1816	18.4	10	1445.13	0.998	984	985.97	0.682	31.8
	Average										31
GC2	1	2730	1722	19	10	1492.25	0.998	1008	1010	0.676	32.3
	2	2700	1750	18	10	1413.71	0.998	950	951.9	0.673	32.7
	Average										32.5

Appendix B

Permeability test experimental data

Table B.1 Permeability of GA permeable concrete specimens

	S.No	Time sec		Specimen Length mm	K mm/sec
GA15%	1	T_1	179	185	
		T2	177	184	
		T3	178	183.5	
		Average	178	184	1.5
	2	T1	156.5	183	
		T2	156.8	184.5	
		T3	156.7	184	
		Average	156.6	184	1.67
	Average				1.6
GA10%	1	T1	167.6	183	
		T2	167.6	185.5	
		T3	167.5	183	
		Average	167.6	184	1.55
	2	T1	130.27	174	
		T2	127.38	175	
		T3	127.99	175	
		Average	128.5	175	1.935015
	Average				1.75
GA5%	1	T1	124	171	
		T2	122.5	172	
		T3	125	173	
		Average	123.8	172	1.97
	2	T1	134.5	179	
		T2	131.37	181	
		T3	130.6	180	
		Average	132.1567	180	1.94
	Average				1.95

Table B.2 Permeability of GB permeable concrete specimens

	S.No	Time sec		Specimen Length mm	K mm/sec
GB15%	1	T1	67.5	188	
		T2	66.2	187	
		T3	68.2	189	
		Average	67.3	188	3.97
	2	T1	91.29	188	
		T2	105.8	187	
		T3	97.54	189	
		Average	98.2	188	2.7
GB10%	Average				3.5
	1	T1	59.24	165	
		T2	52.4	166	
		T3	52.8	164	
		Average	54.8	165	4.27
	2	T1	79.58	165	
		T2	65.33	166	
		T3	58.96	164	
		Average	67.95	165	3.45
	Average				3.8
GB5%	1	T1	35.13	190	
		T2	33.85	191	
		T3	36.11	190	
		Average	35.03	190	7.7
	2	T1	38.52	195	
		T2	39	195	
		T3	40.56	195	
		Average	39.36	195	7.04
	Average				

Table B.3 Permeability of GC permeable concrete specimens

	S.No	Time sec		Specimen Length mm	K mm/sec
GC1	1	T1	47.77	184	
		T2	47.48	184	
		T3	47.4	184	
		Average	47.55	184	5.5
	2	T1	35.53	188	
		T2	39.62	188	
		T3	38.53	189	
		Average	37.89	188	7.05
	Average				6.3
GC2	1	T1	18.9	185	
		T2	18.9	185	
		T3	20	186	
		Average	19.3	185	13.7
	2	T1	27.18	180	
		T2	28.29	180	
		T3	28.29	176	
		Average	27.92	179	9.1
	Average				11.38

Appendix C

Compressive strength, corresponding strain ,modulus of elasticity and densities of the permeable concrete specimens

Table C.1 Compressive strength, corresponding strain, modulus of elasticity and densities values of the permeable concrete specimens

S.No	f'_c MPa	ε_o %	ρ kg/m^3	E_{it} GPa
1	9.89	0.001146	1976.7	7.8
2	10.62	0.001002	1991.8	15
3	12	0.0013	2050	13
4	12.3	0.0011	2095	9
5	12.77	0.00091	1984.95	7.6
6	12.86	0.001059	1965.9	9.7
7	14.28	0.001	2068.2	12
8	15.69	0.001	2046	12
9	16.15	0.001333	1981.3	11.7
10	17	0.0014	2070	15
11	17.1	0.0009	2068	19.55
12	17.7	0.00127	2220	19
13	20	0.0012	2080	17.25
14	20	0.00116	2211	18.6
15	23	0.0011	2255	26.6
16	24	0.001575	2220	15.6
17	25.6	0.0014	2235	22
18	25.7	0.0016	2208	18.4
19	26.5	0.00115	2298	19.5
20	27.5	0.0015	2210	17.88
21	28	0.0014	2267	13.6
22	30	0.0012	2285	26.6
23	31	0.0014	2300	27
24	36.6	0.00189	2321	25.4
25	38	0.0015	2315	28
26	38	0.00152	2323	30
27*	11.35		1861.4	12.99
28*	9.25		1834.1	12.86
29*	11.45		1880.6	15.19
30*	11.52		1854.9	13.44
31*	9.67		1837.3	12.06
32*	11.34		1875.7	12.57
33*	9.81		1838.9	9.81
34*	11.14		1856.5	14.99
35*	10.69		1893.4	12.99
36*	9.95		1843.1	12.1

*Goede (2009) test results

References

1.Alexander, MG & Milne, TI 1995, 'Influence of cement blend and aggregate type on stress-strain behavior and elastic modulus of concrete', *ACI Materials Journal*, vol. 92, no. 3, pp. 227-35.

2.Almusallam, TH & Alsayed, SH 1995, 'Stress-strain relationship of normal, hight and lightweight concrete ', *Magazine of Concrete Research*, vol. 47, no. 170, pp. 39-44.

3.Aoki, A 2009, 'Development of pervious concrete', MA thesis, University of Technology. Sydney.

4.Bean, EZ, Hunt, WF& Bidelspach, DA 2007, 'Field Survey of Permeable Pavement Surface Infiltration Rates', *Journal of Irrigation and Drainage Engineering*, vol. 133, no. 3, pp. 249-55.

5.Beshr, H, Almusallam, AA & Maslehuddin, M 2003, 'Effect of coarse aggregate quality on the mechanical properties of high strength concrete', *Construction and Building Materials*, vol. 17, no. 2, pp. 97-103.

6.Brinson, HF & Brinson, LC (eds) 2008, *Polymer Engineering Science and Viscoelasticity An Introduction*, Springer-Verlag US, Boston, MA

7.Brown, D. P. D 2003, 'Pervious Concrete Pavement: A Win-Win System', *Concrete Technology Today*, vol. 24, no. 2.

8.Burland, JB, Standing, JR, Jardine, FM (eds) 2001, *Building response to tunnelling: Case studies from the construction of the Jubilee Line Extension*, Volume 1: projects and methods, Thomas Telford Publishing, London.

9.Carreira, DJ & Chu, KH 1985, 'Stress-Strain Relationship for plain concrete in compression ', *Journal of the American Concrete Institute*, vol. 82 no. 6, pp. 797-804.

10.Chindaprasirt, P, Hatanaka, S, Chareerat, T, Mishima, N & Yuasa, Y 2008, 'Cement paste characteristics and porous concrete properties', *Construction and Building Materials*, vol. 22, no. 5, pp. 894-901.

11.Choi, S & Shah, S 1997, 'Measurement of deformations on concrete subjected to compression using image correlation', *Experimental Mechanics*, vol. 37, no. 3, pp. 307-13.

12.Chopra, M & Wanielista, M 2007, *Performance Assessment of Portland Cement Pervious Pavement*, University of Centeral Florida

13.Chun-Qing, L & Jian-Jun, Z 2007, 'Closed-Form Solution for Predicting Elastic Modulus of Concrete', *Aci Materials Journal*, vol. 104, no. 5, pp. 539-46.

14.Crouch, LK, Pitt, J & Hewitt, R 2007, 'Aggregate effects on pervious Portland cement concrete static modulus of elasticity', *Journal of Materials in Civil Engineering*, vol. 19, no. 7, pp. 561-8.

15.Deo, O 2011, 'Influence of material structure on the structural and environmental properties of pervious concretes', PHD thesis, CLARKSON UNIVERSITY. New York

16.Deo, O & Neithalath, N 2010, 'Compressive behavior of pervious concretes and a quantification of the influence of random pore structure features', *Materials Science and Engineering: A*, vol. 528, no. 1, pp. 402-12.

17.Duckworth, W 1953, 'Discussion of Ryshkewitch Paper ', *Journal of the American Ceramic Society*, vol. 36, no. 2, pp. 68-.

18.Dudley, N, Higgins, ZL, Hockings, M, MacKinnon, K, Sandwith, T & Stolton, T 2011, 'National Parks with Benefits: How Protecting the Planet's Biodiversity Also Provides Ecosystem Services', *Solutions Journal*, vol. 2, no. 6, pp. 87-95.

19.Ferguson, BK 2005, *Porous pavements*, CRC Press, Hoboken viewed <http://ezproxy.usq.edu.au/login?url=http://www.USQ.eblib.com.au/EBLWeb/patron?target=patron&extendedid=P_264219_0>.

20.Ghafoori, N & Dutta, S 1995, 'Pavement Thickness Design for No-Fines Concrete Parking Lots', *Journal of Transportation Engineering*, vol. 121, no. 6, p. 476.

21.Goede, WG 2009, 'Pervious concrete: Investigation into Structural Performance and Evaluation of the Applicaticability of Existing Thickness Design Methods',MA thesis, Washington State University.

22.Goodier, JN 1933, 'Concentration of stress around spherical and cylindrical inclusions and flaws.', *Transactions of the ASME*, vol. 55, no. APM-55-7, pp. 39-44.

23.Griffiths, AA 1921, 'The Phenomena of Rupture and Flow in Solid', *Phil. Trans. R. Soc*, vol. 221 no. 582-593, pp. 163-98.

24.Harber, PJ 2005, 'Applicability of No-Fines Concrete as a Road Pavement', BE dissertation, University of Southern Queensland. Queensland.

25.Haselbach , LM & Freeman, RM 2007, 'Effectively Estimating In situ Porosity of Pervious Concrete from Cores', *Journal of ASTM International (JAI)*, vol. 4, no. 7.

26.Hognestad, E 1951, *Study of combined bending and axial load in reinforced concrete members* Nov.1951 edn, 22, University of Illinois at Urbana Champaign.

27.Hsu, LS & Hsu, C-TT 1994, 'Complete stress-strain behaviour of high-strength concrete under compression', *Magazine of Concrete Research*, vol. 46, no. 169, Dec 1994, pp. 301-12.

28.Huang, B, Wu, H, Shu, X & Burdette, EG 2010, 'Laboratory evaluation of permeability and strength of polymer-modified pervious concrete', *Construction and Building Materials*, vol. 24, no. 5, pp. 818-23.

29.Hussin, M, Zhuge,Y, Bullen ,F & lokuge, W 2012, 'Investigation of Some Fundamental Properties of Permeable Concrete', *Advanced Materials Research*, vol. 487, pp. 869-73,www.scientific.net/AMR.487.869

30.Jin, X & Li, Z 2000, 'Investigation on mechanical properties of young concrete', *Materials and Structures*, vol. 33, no. 10, pp. 627-33.

31.Kent, DC & Park, R 1971, 'FLEXURAL MEMBERS WITH CONFINED CONCRETE', *Journal of the Structural Division*, vol. 97 no. 7, pp. PP 1969-90.

32.Khan, SA & Wang, X 2000, *Strain Measurements and Stress Analysis*, Amazone .com.

33.Kevern, JT 2008, 'Advancements in pervious concrete technology', Iowa State University. Iowa.

34.Kumar, P 2004, 'A compact analytical material model for unconfined concrete under uni-axial compression', *Materials and Structures*, vol. 37, no. 9, pp. 585-90.

35.Larbi, JA 1993, 'Microstructure of the interfacial zone around aggregate particles in concrete', *Heron*, vol. 38, no. 1, pp. 1-69.

36.Li, CQ & Zheng, JJ 2007, 'Closed-Form Solution for Predicting Elastic Modulus of Concrete', *ACI Materials Journal*, vol. 104, no. 5, pp. 539-46

37.Lian, C & Zhuge, Y 2010, 'Optimum mix design of enhanced permeable concrete- An experimental investigation', *Construction and Building Materials*, vol. 24, no. 12, pp. 2664-71.

38.Lian, C, Zhuge, Y, Beecham, S 2011, 'The relationship between porosity and strength for porous concrete', *Construction and Building Materials*, vol. 25, no. 11, pp. 4294-8.

39.Lokuge, WP, Sanjayan, JG & Setunge, S 2004, 'Constitutive model for confined high strength concrete subjected to cyclic loading', *Journal of Materials in Civil Engineering*, vol. 16, no. 4, pp. 297-305.

40.Lokuge, WP, Sanjayan, JG & Setunge, S 2005, 'Stress–Strain Model for Laterally Confined Concrete', *Journal of Materials in Civil Engineering*, vol. 17, no. 6, pp. 607-16.

41.Mander, JB, Priestley, MJN & Park, R 1988a, 'Observed Stress-Strain Behavior of Confined Concrete', *Journal of Structural Engineering*, vol. 114, no. 8, pp. 1827-49.

42.Mander, JB, Priestley, MJN & Park, R 1988b, 'Theoretical Stress-Strain Model for Confined Concrete', *Journal of Structural Engineering*, vol. 114, no. 8, pp. 1804-26.

43.Marolf, A, Neithalath, N, Sell, E, Wegner, K, Weiss, J & Olek, J 2004, 'Influence of Aggregate Size and Gradation on Acoustic Absorption of Enhanced Porosity Concrete', *ACI Materials Journal*, vol. 101, no. 1, pp. 82-91.

44.Matsuo, Y, Morino K, & Iwatsuki, E 2005,' A Study on Porous Concrete Using Electric Arc Furnace Oxidizing Slag Aggregate', *Bulletin of Aichi Institute of Technology. Part B*, vol. 40, no. 40, pp. 167-17.

45.McMillan, T 2007, *Comaprsion Traditional Concrete to Permeable Concrete for a Community College Pavement Application*, Bellevue Community College, Washington.

46.McCain, G & Dewoolkar, MM 2009, *Strength and Permeability Characteristics of Porous Concrete Pavements*, Sponsors: Transportation Research Board Washington DC, 2009, DVD.

47.Mendes, AJ, Torres, MA & César , J 2000, 'Analysis of reinforced concrete with external composite strengthening', *Composites Part B: Engineering*, vol. 31, no. 6–7, pp. 527-34.

*48.*Montes, F, Valavala, S & Haselbach, L 2005, 'A new test method for porosity measurements of portland cement pervious concrete ', *Journal of ASTM international*

49.vol. 2, no. 1, pp. 1-13.

50.Neithalath, N, Weiss, J & Olek, J 2006, 'Characterizing Enhanced Porosity Concrete using electrical impedance to predict acoustic and hydraulic performance', *Cement and Concrete Research*, vol. 36, no. 11, pp. 2074-85

51.Neithalath, N, Sumanasooriya, MS & Deo, O 2010, 'Characterizing pore volume, sizes, and connectivity in pervious concretes for permeability prediction', *Materials Characterization*, vol. 61, no. 8, pp. 802-13

52.Neville, A 1997, 'Aggregate and bond modulus of elasticity of concrete ', *ACI Materials Journal*, vol. 94, no. 1, pp. 71-4.

53.Noguchi, T, Tomosawa, F, Nemati, K, Chiaia, BM & Fantilli AP 2009, 'A Practical Equation for Elastic Modulus of Concrete', *ACI Structural Journal*, vol. 106, no. 5, pp. 690-6.

54.Obla, KH 2010, 'Pervious concrete -An overview', *the Indian concrete journal*.

55.Offenberg, M 2008, 'Is Pervious Concrete Ready for Structural Applications?', *Structure magazine*, p. 48.

56.Oluokon, F, Burdette, EG & Deatherage, J 1991, 'Elastic Modulus,Possion's ratio,and compressive strenght relationships at early ages', *ACI Materials Journal*, vol. 88, no. 1, pp. 3-10.

57.Pauw, A 1960, 'Static Modulus of Elasticity of Concrete as Affected by Density', *ACI Journal*, vol. 57, no. 6 pp. 679-88.

58.Popovics, S 1973, 'A numerical approach to the complete stress-strain curve of concrete', *Cement and Concrete Research*, vol. 3, no. 5, pp. 583-99.

59.Ravindrarajah, RS & Aoki, Y 2008, *Environmentally Friendly Pervious Concrete*, International conference on advances in concrete and construction (ICACC), Hyderabad, Andhra Pradesh, India.

60.Reddiar, MKM 2009, 'Stress-strain model of unconfined and confined concrete and stress-block parameters', MA thesis, Texas A&M University. Texas.

61.Richardson, DN 1991,' Review of Varibles that influance Measured Concrete Compressive Strenght', *Journal of Materials in Civil Enginerring*, vol. 3, no.2,pp.95-112.

62.Sandor, P 1973, 'A numerical approach to the complete stress-strain curve of concrete', *Cement and Concrete Research*, vol. 3, no. 5, pp. 583-99.

63.Sargin, M, Ghosh, SK & Handa, VK 1971, 'EFFECTS OF LATERAL REINFORCEMENT UPON THE STRENGTH AND DEFORMATION PROPERTIES OF CONCRETE', *Magazine of Concrete Research*, vol. 23, no. 75-6, pp. 99-110.

64.Schaefer, VR, Wang, K, Suleiman, MT& Kevern, JT 2006, *Mix design development for pervious concrete in cold weather climates*, Center for Transportation Research and Education, Iowa State University.

65.Sumanasooriya, MS & Neithalath, N 2009, 'Stereology- and Morphology-Based Pore Structure Descriptors of Enhanced Porosity (Pervious) Concretes', *ACI Materials Journal*, vol. 106, no. 5, pp. 429-38.

66.Tasnimi, AA 2004, 'Mathematical model for complete stress-strain curve prediction of normal, light-weight and high-strength concretes', *Magazine of Concrete Research*, vol. 56, no. 1, pp. 23-34.

67.Tennis, PD, Leming, ML& Akers, DJ.2004, *Pervious Concrete Pavements*, EB302.02, Portland Cement Association, Skokie, Illinois, and National Ready Mixed Concrete Association,Silver Spring, Maryland.

68.Tomaszewicz, A 1984, *Stress-strain relationship for concrete*, Report No. STF65A84065, Cement and Concrete Institute (SINTEF div. FCB) Trondheim-NTH.

69.Van, GA & Taerwe, L 1996, 'Analytical formulation of the complete stress-strain curve for high strength concrete', *Materials and Structures*, vol. 29, no. 9, pp. 529-33.

70.Wang, PT, Shah, SP & Naaman, AE 1978, 'Stress-Strain Curves of Normal and Lightweight Concrete in Compression', *Journal of the American Concrete Institute*, vol. 75, no. 11, pp. 603-11.

71.Wang, K, Schaefer, VR, Kevern, JT& Suleiman, MT 2006, 'Development of Mix Proportion for Functional and Durable Pervious Concrete', *NRMCA Concrete Technology Forum: Focus on Pervious Concrete*, Nashville, TN

72.Wanielista, M, Chopra, M, Spence, J & Ballock, C.2007, Hydraulic Performance Assessment of Pervious Concrete Pavements for Stormwater Management Credit, University of Central Florida, Florida

73.Wee, TH, Chin, MS & Mansur, MA 1996, 'Stress-Strain Relationship of High-Strength Concrete in Compression', *Journal of Materials in Civil Engineering*, vol. 8, no. 2, pp. 70-6.

74.Wu, K, Chen, B, Yao, W & Zhang, D 2001, 'Effect of coarse aggregate type on mechanical properties of high-performance concrete', *Cement and Concrete Research*, vol. 31, no. 10, pp. 1421-5.

75.Yang, J & Jiang, G 2003, 'Experimental study on properties of pervious concrete pavement materials', *Cement and Concrete Research*, vol. 33, no. 3, pp. 381-6.

76.Šemberk, P& Kohoutková, A 2005, 'Image-analysis-based measuring of lateral deformation of hardening concrete', *Materials Science*, vol. 11, no. 3, pp. 292-6.

Standerds

1.Architectural Institute of Japan 1985, *Standard for structural calculation of reinforced concrete structures,* Chapter 4, AIJ-1985, pp.8-11

2.American Society for Testing and Materials 2002, *Standard Test Method for Static Modulus of Elasticity and Poisson's Ratio of Concrete in Compression,* ASTM C-469-2002, ASTM International, West Conshocken.

3.American Society for Testing and Materials 2012, *Standard Test Method for Density and Void Content of Freshly Mixed PerviousConcrete,* ASTM C-1688/C1688M-2012, ASTM International, West Conshocken.

4.Standards Australia 1994, *Method 2: Preparation of concrete mixes in the Laboratory*, AS 1012.2-1994, Standards Australia, Sydney.

5.Standards Australia 1997, *Determination of the static chord modulus of elasticity and Poisson's ratio of concrete specimens*, AS 1012.17-1997, Standards Australia, Sydney.

6.Standards Australia 1999, *Method 9: Determination of the compressive strength of concrete specimen*, AS 1012.9-1999, Standards Australia, Sydney

7.Standards Australia 2009, *Method 11.1: Particle size distribution-Sieving*, AS 1141.11.1-2009, Standards Australia, Sydney.

8.Standards Australia 2009, *Concrete structure*, AS-3600-2009, Standards Australia, Sydney.